Localization of Vertebrae and Deformity Analysis using Digital Spinal Cord Images

Joddat Fatima

01-284152-001

A thesis submitted in fulfilment of the
requirements for the award of the degree of
Doctor of Philosophy (Computer Science)

Department of Computer Science

BAHRIA UNIVERSITY ISLAMABAD

April 2023

PhD-15

APPROVAL FOR EXAMINATION

Scholar's Name: **Joddat Fatima**

Registration No: **01-284192-001**

Programme of Study: **PhD in Computer Science**

Thesis Title: **Localization of Vertebrae and Deformity Analysis using Digital Spinal Cord Images**

It is to certify that the above scholar's thesis has been completed to my satisfaction and, to my belief, its standard is appropriate for submission for examination. I have also conducted plagiarism test of this thesis using HEC prescribed software and found similarity index 15% that is within the permissible limit set by the HEC for the PhD degree thesis. I have also found the thesis in a format recognized by the BU for the PhD thesis.

Principal Supervisor's Signature: _____

Date: _07-04-2023

Name: Prof. Dr. Amina Jameel

Co-supervisor's Signature: _____

Date: _07-04-2023

Name: Prof. Dr. Muhammad Usman Akram

PhD-16A

AUTHOR'S DECLARATION

I **Joddat Fatima** hereby state that my PhD thesis titled

Localization of Vertebrae and Deformity Analysis using Digital Spinal Cord Images

is my own work and has not been previously submitted to this university

Bahria University

Or anywhere else in the country/world.

At any time if my statement is found to be incorrect even after my graduation the University has the right to withdraw/cancel my PhD degree.

Name of scholar: **Joddat Fatima**

Date: **07-04-2023**

PhD-16B

PLAGIARISM UNDERTAKING

I Joddat Fatima solemnly declare that research work presented in the thesis titled "**Localization of Vertebrae and Deformity Analysis using Digital Spinal Cord Images"** is solely my research work with no significant contribution from any other person. Small contribution / help wherever taken has been duly acknowledged and that complete thesis has been written by me.

I understand the zero tolerance policy of the HEC and Bahria University towards plagiarism. Therefore, I as an Author of the above titled thesis declare that no portion of my thesis has been plagiarized and any material used as reference is properly referred/ cited.

I undertake that if I am found guilty of any formal plagiarism in the above titled thesis even after award of PhD degree, the university reserves the right to withdraw / revoke my PhD degree and that HEC and the University has the right to publish my name on the HEC / University website on which names of scholars are placed who submitted plagiarized thesis.

Name of scholar: **Joddat Fatima**

Date: **07-04-2023**

DEDICATION

I dedicate this PhD thesis to my dear husband, Saqib, who has been a consistent source of help, encouragement, and support during the difficulties of PhD and life. I'm appreciative for having you in my life. This work is likewise dedicated to my beautiful mother and my loving father, who have consistently loved and cherished me unconditionally and whose genuine models have trained me to work hard for the things that I aim to achieve. To my Daughters, Miraal, and Manha, not a single day did you complain how busy I was, I appreciate your patience and understanding. My in laws encouraged me, without their blessings, I would not have been able to reach at this point in my life.

Abstract

The spinal cord is an fundamental structure that creates a connection between the brain and the rest of the body. The long thin cord is made up of twisted nerves and tissues in combination with the 33 separate bones stacked over one another. Curvature deformity causes an extra bend in the spinal curve. The curvature deformities are of three types Kyphosis (thoracic region); Lordosis (cervical and lumbar region) , and Scoliosis (sideways). Different imaging techniques clinically used to diagnose these deformities include X-Ray, Computed Tomography and Magnetic Resonance Imaging. Many researchers have worked on deformity analysis of spinal curvatures, and numerous competitions and workshops have produced labeled datasets and new approaches as well. Recently, few semi-automated systems have been proposed for vertebrae segmentation and Scoliosis Cobb estimation but a fully automated method that can differentiate all three categories, and identify severity levels among the disorders with multiple imaging modalities is still missing. In this research, we present a two-step automated system for localization of vertebrae, segmentation of the spinal column, and classification of diseases on the basis of their curvature shape and Cobb estimation. A recent approach to object detection is utilized for vertebrae localization, in parallel to this spine column is segmented. Both of these results are used for the extraction of the midline curvature profile. These results supported in feature-based shape analysis mechanism for reliable classification of curvature, respectively. The proposed system also involves a traditional Cobb estimation procedure for curvature analysis and validation provides reliability to our predicted results. The evaluation of both modules has been carried out, using available datasets. The localization results achieved mean Average Precision (map) up to 0.94 for AASCE19, 0.97 for the Mendeley's dataset and 0.95 for the CSI16 dataset. Segmentation of spine column attained dice score up to 0.971, 0.960 and 0.953 for Mendel's, CSI16 and AASCE19 respectively. The comparison of segmentation block with literature shows improvement in dice score. The results of shape analysis using Random Forest (RF) classifiers attained an accuracy of 94.69%. Considering the same problem as that of image classification, the proposed feature-set performed better as compared with deep features of Efficient-Net B4 with a 2% improvement in the accuracy. The Cobb estimation results in comparison with latest state-of-the-art reduced the Mean Absolute Error (MAE) by 2 degrees. The classification of Lumbar Lordosis on the basis of proposed methodology achieved an accuracy up to 98.04% for Mendeley's dataset and 81.25% for CSI16 dataset respectively.

Acknowledgments

First and foremost, I would like to thank "Allah The Almighty" the most merciful (forgiving) and the most beneficent (generous). Secondly, I would like to acknowledge the efforts of my supervisors Engr. Dr Amina Jameel and Engr. Dr. Muhammad Usman Akram worked tirelessly and made this research possible. Without their support, help, and guidance, this research would not have been complete.

I would like to mention the efforts of Engr. Mashood M. Mohsan and Engr. Malaika Mushtaq as well who were my research partners and helped me a lot. My friends Engr. Dr. Adeel M. Syed, Engr. Aleem Ahmed, Engr. Faisal Imran and Tahira Anwar have helped me throughout and I am thankful for their backing. I would like to thank my class fellow and dearest friend Zainab Yousuf, without her, this would have been much more difficult to achieve.

I would also like to recogize the support provided by my employers who gave me relaxation for my work. My Dean and HODs, over the years, who helped me with the schedule making and their help is noteworthy.

Table of Content

List of Figures

List of Tables

List of Symbols

Abbreviations		Description
DIP	-	Digital Image Processing
CNS	-	Central Nervous System
CAD	-	Computer Aided Diagnostic
AI	-	Artificial Intelligence
CT	-	Computed Tomography
MRI	-	Magnetic Resonance Imaging
ROI	-	Region of Interest
CNN		Convolutional Neural Network
VB		Vertebral Bodies
DSC		Dice Similarity Coefficient
CSI		Computational Spine Imaging
AASCE19		Accurate Automated Spinal Curvature Estimation
FCN		Fully Convolutional Network
IoU		Intersection Over Union
RCNN		Region-based Convolutional Neural Network
YOLO		You Only Look Once
RF		Random Forest
LLA		Lumbar Lordotic Angle
LSA		Lumbosacral Angle
HED		Holistic- Nested Edge Detection
mAP		mean Average Precision
MAE		Mean Absolute Error
MICCAI		Medical Image Computing and Computer Assisted Interventions

1 Chapter

Introduction

1.1 Introduction

Digital Image Processing (DIP) was initiated for the newspaper industry in early 1920's [1] which later emerges in the field of computer science. The Domain of DIP is based on the manipulation of digital images using different computer algorithms. It involves analysing, transforming, and enhancing digital images in order to extract useful information or improve their visual appearance. Digital image processing is used in a vast range of applications, including medical imaging, satellite imaging, video processing, and computer vision. In medical imaging, digital image processing is used to extract features from medical images to aid in diagnosis and treatment. With advancement in the field of computer sciences and the space race between the powerful countries of the world, DIP attained great heights. When stepping into the new millennium, the domain entered the world of medicine, and transformed the medical examination techniques and the ways in which diagnosis was carried out by professionals [1]. The domain includes the principal concepts and methods; for visual representation, information retrieval, image enhancement and restoration. Additionally, depth in domain includes image matching and classification, feature set extraction, segmentation of objects, and image recognition.

Bio-medical Imaging is one of the popular domains of DIP which provides necessary information about the patient, and assistance, to the medical specialist for clinical examination without any physical procedure. Bio-medical imaging reveals the whole anatomy, which lies under the skin and helps to locate abnormalities, while it also speeds up the diagnosis process. With all these positive aspects, the complex nature of this domain requires medical knowledge, along with the recognition of unusual structures and shapes of human anatomy. This domain involves availability of necessary information, regarding health so that in case of any error or mistake, in terms of diagnosis by physical examination can be mitigated and precious human lives can be saved. This field focuses on developing and evaluating new imaging techniques and methods, encompassing system development, novel approaches for image acquisition and reconstruction, synthesis of imaging contrast and therapeutic agents.

The non-invasive procedures have made digital diagnosis very popular. These procedures are conducted without any surgical tools or needles; the patient gets complete internal examination with a clear view of each nerve, bone, and muscle etcetera. The medical diagnosis is almost getting dependent on these images. The developers are trying to improve imaging techniques to get more information through medical images. Therefore, the process of health recovery gets faster. Additionally, an increase in interest has also increased the variety of imaging modalities and datasets for medical diagnosis. Figure 1-1 shows different types of medical imaging modalities being used around the world. These multiple techniques are then further used for analysis and recognition processes. The research in this domain brings together engineers, computer scientists, radiologists, and clinical biologist.

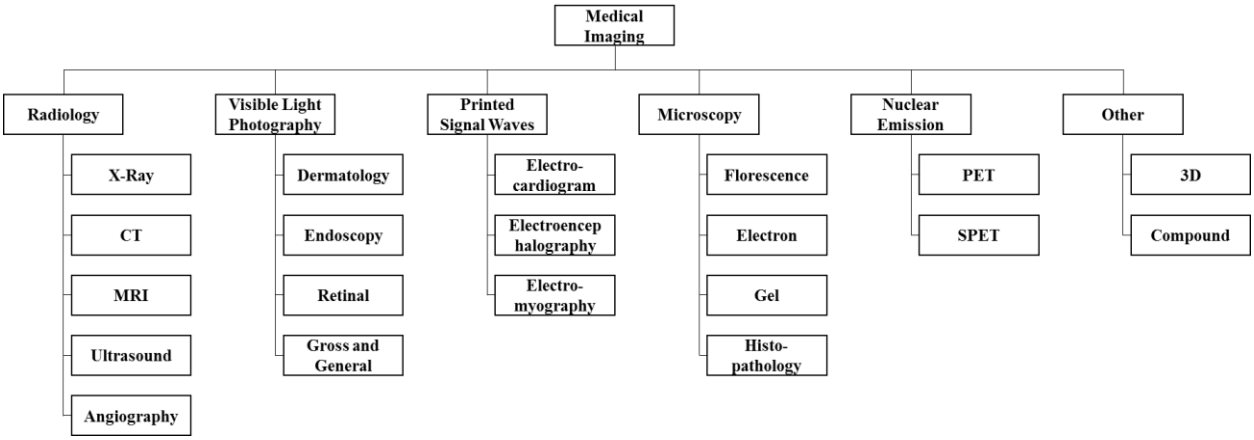

Figure 1-1 Different categories of medical imaging modalities used for differential diagnosis

1.2 Motivation

'*American Chiropractic Association (ACA)*' worldwide conducted a survey, they claimed that back pain is the single leading cause of disability. Experts in the medicine estimate that up to 80% of the population will encounter back pain at some point of time in their lives [2]. Back pain is considered as the third most common cause for patient visits to the doctor. Disability originated from pain in lower back pain has escalated by 54% between 1990 and 2015 [3]. From 1994 to 2005, MRI scans of the lumbar region increased by more than 300% in medicare beneficiaries. The '*Global Burden of Disease Study'* 2017 estimated the widespread of lower back pain. The study claimed that in 1990 was 377.5 million people suffering with LBP and shockingly it had increased up to 577.0 million in 2017 [4]. This research can benefit medical organizations having

a neurology department. A reliable diagnostic technique will be developed to help and analyse the severity level of posture issues. This research is applied in nature; the aim is to develop an application that will be adopted by medical field [5].

- Third world countries like Pakistan, require such kind of research area to be promoted since our country has a very low doctor to patient ratio. The use of advanced technology and algorithms in medical imaging can help diagnose and treat diseases more accurately and efficiently, improving healthcare outcomes for patients.
- The shortage of qualified neurologists in Pakistan is a serious issue that can have a significant impact on the health and well-being of its citizens. With a population of 180 million and only 120 qualified neurologists, the doctor to patient ratio is indeed alarming at 1:1.5 million people [6].
- The lack of an environment for active research in biomedical applications is a significant challenge faced by educational institutes in Pakistan. Without a robust research environment, it can be difficult for students and faculty to develop the skills and expertise needed to make breakthroughs in the field of biomedical applications.
- The scarcity of a reliable computer-aided diagnostic technique for the diagnosis and analysis of posture issues is a significant challenge faced by healthcare providers in Pakistan. Without accurate and reliable diagnostic tools, it can be difficult to identify and address posture issues, which can lead to long-term health consequences for patients.
- The ultimate goal is that the applied nature of this research would lead us to develop an application that can be accepted in the medical field. The focus of applied research is on creating tangible solutions that can have a real-world impact on patient health and wellbeing.

1.3 Problem Statement

The above mentioned facts motivated us to work on Computer Aided Diagnostic (CAD) system for reliable analysis of spinal deformities which will not only facilitate medical domain but it will also help to save the cost of going through the expensive procedure for evaluation of disease. Once spinal issues have been identified, treatment options may include medication, physical therapy, or surgical intervention, depending on the severity and type of condition. In some cases, emergency surgery may be required to prevent further damage to the spinal cord and prevent the onset of

paralysis. There is a need to develop a fully automated system using image processing, machine learning techniques that will support the clinician's manual diagnosis of postural spine diseases. To design an image processing and deep learning-based framework for analysis of different spinal imaging modalities for localization of vertebrae and spinal deformity analysis.

1.4 Objective

Biomedical image analysis for differential diagnosis is relatively a complex field; it can assist the radiologist and neurologists, in initial diagnosis in many ways. Artificial Intelligence (AI) based CAD systems are the need of the times that can help in mass screening of patients. The scope of this research domain is an applied-based diagnostic system for spine deformity analysis. The proposed system is a computer-based software application that will be fed with the vertebrae pattern images. The system will give a decision on the degree of level of deformity in spine structure collected features. The major objective of this research is to develop a reliable diagnostic system for localization of vertebrae that will be used for curvature deformity analysis using multiple imaging modalities. The sub objectives to achieve this main objective are:

- To develop a fully automated CAD system for analysis of spinal deformities. The system would provide healthcare providers with a tool to analyse medical images of the spine, and improve the accuracy and efficiency of diagnosis and treatment.
- To utilize robust localization algorithm for effective extraction of vertebrae even in the existence of noise and illumination changes. Noise and illumination changes can affect the accuracy of vertebrae detection by creating false positives or false negatives that can lead to misdiagnosis and inappropriate treatment.
- To apply best segmentation model through comparative analysis for segmentation of spinal column. The best-performing model can be selected based on its ability to accurately and efficiently segment the spinal column in medical images.
- To analyse spinal column and extracted vertebrae for calculation of clinical parameters being used for spinal deformities. This can reduce the time and cost required for manual measurement and analysis.

1.5 Contributions

Focusing above-mentioned objectives, the following research contributions, are made in this thesis:

- A novel automated framework is presented to handle different imaging modalities and clinical parameters related to spinal deformities. The proposed methodology has the potential to significantly enhance the diagnosis procedures and the treatment plan of spinal deformities.
- The annotation of all datasets in sagittal and coronal planes along with labels with the help of a radiologist is an essential step in developing accurate and reliable models for the analysis of spinal deformities.
- The object detection framework is utilized for vertebrae localization from different imaging modalities and the subsequent classification of their shapes using their centroids is an effective approach for analyzing spinal deformities.
- A new set of features is proposed for normal, C-Shape, and S-Shape analysis of the spine curve, which will be utilized as a decision support system. By developing this set of features, young radiologists can use them to diagnose and treat spinal deformities more accurately and efficiently.
- A comparative analysis of different classifiers and deep segmentation modes has been performed. By comparing the performance, researchers can determine which approach is the most accurate and reliable for analyzing spinal deformities.
- Clinical approaches are studied and made part of the proposed system for reliable Cobb angle estimation. Incorporating these clinical approaches into the proposed system can help to reduce the risk of errors and improve the accuracy.

This contributions are published in reputed journals and the list of publications is attached in Appendix A. The abstract of publications are also mentioned in Appendix D.

1.6 Hypothesis

The localization of vertebrae and deformity analysis using digital spinal cord images was planned to be achieved through several hypotheses, which include:

1. Spine segmentation: The first hypothesis is to accurately segment the spinal cord from the surrounding tissues, which would help us to localize the individual vertebrae. This can be achieved through various image processing techniques, such as thresholding, region growing, or edge detection.
2. Landmark detection: Once the vertebrae are localized, the next hypothesis is to accurately detect key landmarks that are centerpoints and corners on each vertebra. These landmarks will be used to accurately identify and track each spinal curvature profile.
3. Deformity analysis: With accurate localization and segmentation, deformity analysis can be performed to quantify the degree of spinal curvature or misalignment. This can be achieved through various techniques, such as computing the Cobb angle, which is the calculated from the angle between the top and bottom vertebrae in a curved section of the spine.
4. Classification of deformity: Finally, once the spinal curvature or misalignment is quantified, the type of deformity can be classified, such as scoliosis, kyphosis, or lordosis. This classification can provide important information for treatment planning and monitoring of the condition over time.

The hypotheses localization of vertebrae and deformity analysis using digital spinal cord images provides valuable information for diagnosis, treatment planning, and monitoring of spinal deformities.

1.7 Challenges

Localization of vertebrae and deformity analysis using digital spinal cord images can present several challenges, including:

1. Image quality: The quality of the digital spinal cord images can vary, depending on the imaging modality used and the parameters selected. Poor image quality can make it hard to accurately detect and localize the vertebrae, as well as detect subtle deformities.
2. Image artifacts: Artifacts can occur in digital spinal cord images due to various factors, including patient motion, hardware issues, and imaging protocol variations. These artifacts can interfere with accurate vertebrae localization and deformity analysis.
3. Variability in spinal anatomy: The spinal anatomy can vary significantly among individuals, making it challenging to develop a standardized approach for vertebrae

localization and deformity analysis. Furthermore, different types of deformities may require different methods of analysis, adding to the complexity of the process.

4. Time-consuming and labor-intensive: Localization of vertebrae required annotations and labelling with respect to the problem so it can be a time-consuming and labor-intensive process, requiring expertise knowledge in interpretation and analysis.
5. Inter-obsezver variability: There can be significant variability in the interpretation of digital spinal cord images, especially in cases of complex deformities. This can lead to inconsistencies in diagnosis and treatment planning.

To address these challenges, advanced image processing techniques, machine learning algorithms, and artificial intelligence were employed to assist with vertebrae localization and deformity analysis. Additionally, standardization of imaging protocols and training of healthcare professionals in image interpretation helped us to improve accuracy and reduce variability.

1.8 Dissertation Outline

The thesis document consists of six chapters. The problem statement and the motivation behind our research work are presented in Chapter 1 along with the objectives and contributions. In the upcoming chapters we will elaborate the discussions as follows:

- Chapter 2 gives a detailed introduction of the human spine, and its significance, along with its structural components and postural abnormalities. Details regarding types of common postural abnormalities include lordosis, which is an exaggerated inward curvature of the lumbar spine, kyphosis, which is an exaggerated outward curvature of the thoracic spine, and scoliosis, which is a lateral curvature of the spine are also presented.
- In chapter 3, we have discussed a vast and thorough literature review, with a detail section of the dataset used throughout the research study. In the final section of chapter a brief analysis on some of the key concepts and algorithms is also presented.
- In Chapter 4, we have discussed the vertebrae localization and spine segmentation procedure, using proposed algorithms are discussed in detail. The results of localization and segmentation are also illustrated.

- Chapter 5, presents the part of feature extraction and classification for deformity analysis for all three categories of the spine. The Cobb estimation is also discussed in detail along with their results.
- In chapter 6, the conclusion and future works in light of the proposed framework are discussed. The chapter explains the potential of proposed solution that can revolutionize the diagnosis and monitoring of spinal deformities, and future works can help improve the accuracy and applicability of the system in clinical settings.

2 Chapter

Spinal Cord: Deformity Diseases

The health of the human nervous system is directly proportional to the health of the spine. In this chapter, the anatomy of the human spine is introduced. The significance and structural details are also presented. Brief introduction about postural deformities of the spine, and a small overview regarding imagining technologies used for the diagnosis of these diseases is discussed.

2.1 Spinal Cord

Central Nervous System (CNS) is the utmost important processing unit in the human anatomy. It controls all the vital organs from breathing signals, eye blinking, and heart-pumping up-to-toe movement. The CNS is clinically bifurcated into two partitions, first and foremost is the brain and the second one is the Spinal cord. The CNS works like a human CPU, monitoring, and transferring information from the brain to the rest of the body, with the help of a spinal cord. The brain stem is the initial point of the spinal cord. The spinal cord is a longitudinal, fragile tube-like pipe with a soft texture, a bunch of nerves, and three-layered tissues. Nerves bundle are of two types, the information sensory known as sensory roots and signal transferring, that is, motor roots [7]. The spinal cord ends at cauda equina since it resembles the horsetail. In the field of neurosciences, the spinal cord is the major part of traumatic injury. The cross-sectional structure of the cord is considered of prime importance even in the skeleton study, which would be discussed in detail later.

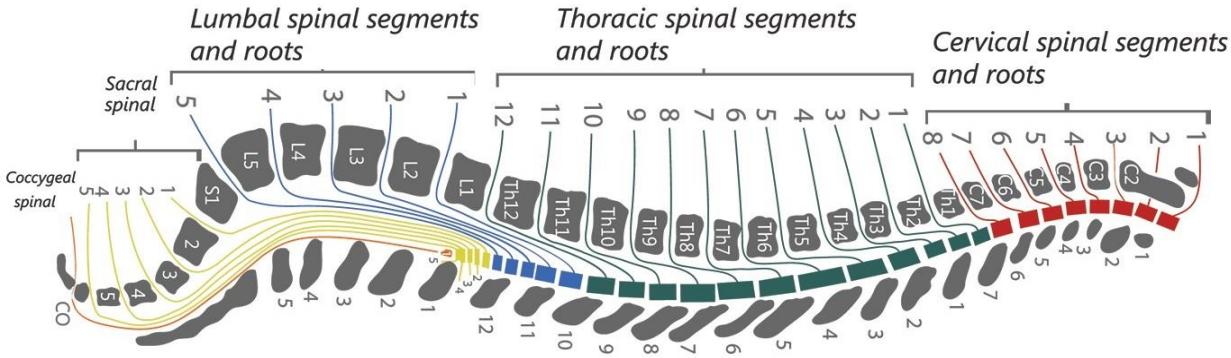

Figure 2-1 Anatomy of a human spine, Cervical (C1-C7), Thoraces (T1-T12), Lumber (L1-L5), Sacrum (S1-S5) and Coccyx (Co1) [8]

Spinal cord geometry starts with the brain station with approximate length of 40-50 cm and width of 1.0-1.5 cm. It ends at the hip bone. The spinal vertebral bone is one of the major sections of the spinal cord. It consists of 33 separates, yet connected bones, stacked together over one another [9]. These vertebrae are divided into five splits as shown in Figure 2-1.

1. Cervical spine: The cervical spine also known as neck region is the uppermost portion of the spine and consists of seven vertebrae, labeled as C1 through C7. This portion of the spine supports the head and allows for movement of the neck.
2. Thoracic spine: The thoracic spine also known as chest region is the middle portion of the spine and consists of 12 vertebrae, labeled T1 through T12. This portion of the spine is connected to the ribcage and provides support for the torso.
3. Lumbar spine: The lumbar spine also known as abdominal region is the lower portion of the spine and consists of five vertebrae, labeled L1 through L5. This portion of the spine is the largest and supports the weight of the upper body.
4. Sacral spine: The sacral spine also termed as pelvic region is a triangular-shaped bone placed at the base of the spine. It consists of five fused vertebrae bones, which are labeled S1 through S5.
5. Coccyx: The coccyx, also termed as the tailbone, is a tiny triangular bone placed at the very end of the spinal cord. It consists of four fused vertebral bones.

Each vertebra in the spine has a unique structure, but they share some common features. Each vertebra has a body, which is the large, solid portion of the bone. The vertebrae also have a neural arch, which surrounds and protects the spinal cord. Additionally, each vertebra has processes, which are bony projections that allow for muscle attachment and movement. Similar to the brain, the cord has three layers of tissues known as meninges that are termed as Pia the innermost layer, Arachnoid middle layer, and Dura outer firm layer shown in Figure 2-2. The small, structured bone, which are the building blocks of spinal architecture, are known as vertebra. These bones are attached adjacent with the help of a mushy soft disc, in series format, creating the exact shape and pattern of the whole cord. One of the essential medium connecting brain and cord for signal transmission to the rest of the body [9].

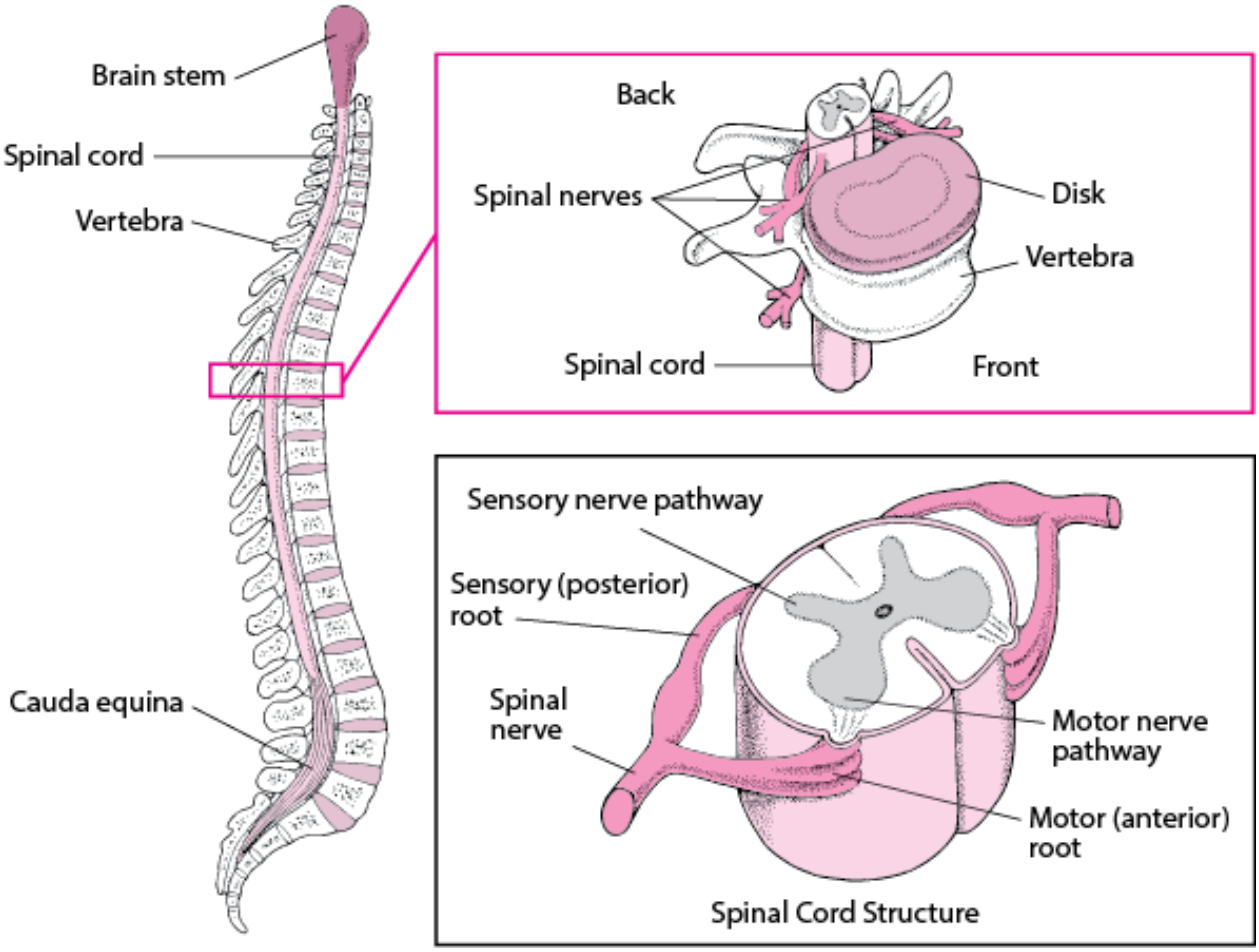

Figure 2-2 Components of spine showing three layers tissues, vertebrae-bone and disk [10]

2.2 Significance of Spinal Cord

The nervous system is a vital body phenomenon. Taking one of its major organ, the spinal cord, and describing its significance is a crucial task. The damage to the major information signal network can cause disruption in other vital organ's functionality [11]. Here are some of the key roles and functions of the spinal cord:

1. Transmitting sensory information: The spinal cord receives sensory information from the body, including touch, temperature, and pain. This information is sent to the brain for processing and interpretation.
2. Transmitting motor information: The spinal cord sends motor commands from the brain to the muscles and organs of the body. This allows us to move and control our bodily functions.

3. Reflexes: The spinal cord is responsible for many involuntary reflexes, such as the knee-jerk reflex, which help protect the body from injury.
4. Protection: The spinal cord is protected by the vertebrae of the spinal column and is surrounded by cerebrospinal fluid, which helps to cushion and protect it from injury.
5. Coordination: The spinal cord helps to coordinate movement and control of the body by transmitting information between the brain and the muscles.

Injury to the spinal cord can have significant consequences, including paralysis or loss of sensation in parts of the body. The spinal cord is a bunch of tangled nerves that travels from the brain through the spinal canal, and it is responsible for transmitting the brain messages and signals to the rest of the body organs. An injury to the spinal cord can damage or sever these nerve fibres, leading to a loss of sensation, movement, and bodily functions. Injuries to the upper part of the spinal cord can affect the ability to breathe, while injuries to the lower part of the spinal cord can cause problems with bowel and bladder control. Researchers are actively working on developing new treatments for spinal cord injuries, including stem cell therapy and other regenerative medicine approaches, to help restore function to those who have been injured [12]. Spine helps our body to twist, turn and bend as well as it helps in mobility of body. The prime importance of the spinal cord is its connectivity and movement functionality, which makes the human body strong enough for portability. Reflexes are automatic responses carried out by the body without conscious control. They are important for protecting the body from harm and for maintaining balance and coordination. The spinal cord plays a crucial role in carrying out reflexes [13].

In 2018, Global Digital Suite reported in '*Business Matters'*, the UK's leading business magazine, that 68% of the total population are digital system users [14]. A new terminology appeared '*Tech Neck'*, which is a growing concern and problem in this digital age. This term has emerged due to the growing use of technology in our daily lives, especially with the increased use of hand handheld gadgets such as mobile phones, pagers, PNDs and tablets. It refers to the strain and discomfort that can occur in the neck and upper back as a result of prolonged use of these devices. Our favourite posture and most comfortable office chairs might be causing long-lasting damage to the spine, without us even realizing it. It is hardly surprising but worth to mention that according to neurologist Dr Stacy Spivack [15], if you sit while slouched over, dropping your head and neck towards forward direction, you may be left with significant neck pain and spasms, your chest wall may become tight, causing pressure on ribs and compromises respiratory function. In a small study

in 2017, published in the '*Journal of Behaviour Therapy and Experimental Psychiatry'* [15], people who have mild to moderate depression and mood disorders are more likely to sit in a hunched position. These changes can lead to feelings of fatigue and decreased physical activity, which can contribute to poor posture and a sedentary lifestyle. Experts at the Harvard Health Letter wrote that sitting slumped after eating puts pressure on the abdomen that can trigger acid reflux and heartburn [15].

The tough and monotonous routine of our daily lives is affecting our posture and causing spinal deformity which, in extreme cases, may lead to total paralysis.

2.3 Diagnosis Techniques

There are several diagnosis methods for spinal deformities, including:

Physical Examination:

The of spinal curvature disorders can be done through physical examination which involves gait motion analysis, observation of posture, palpitation, and forward bend twist testing. A healthcare provider will assess the curvature of the spine, looking for any visible abnormalities or changes in posture. They may also measure the range of motion in the spine and check for any areas of tenderness or pain.

Neurological Evaluations:

Neurological evaluations are an important part of diagnosing spinal deformities, particularly those that may be related to neurological conditions or disorders. During a neurological evaluation, a healthcare provider will assess the functionality of the whole nervous system. It includs the assessment of brain signals, passage lines of spinal cord, and responses of nerves. Some of the specific tests and assessments that may be performed during a neurological evaluation for spinal deformities include:

- Reflex testing: This involves checking the body's reflexes, such as the knee-jerk, stretches or pinprick reflex, to assess the function of the nerves and spinal cord.
- Sensation testing: This involves checking for any areas of numbness or tingling in the body, which may indicate nerve damage or compression.
- Muscle strength testing: This involves assessing the strength and function of the muscles, which may be affected by spinal deformities or related conditions.

- Coordination testing: This involves assessing the ability to perform coordinated movements, such as walking heel-to-toe, which may be affected by neurological conditions. The most common and reliable method for a clear visual depiction of an organ is through digital images. It can also be used to analyse the severity of the disease.

Radiological Imaging:

Diagnosis of spine deformities often involves the use of radiographic images. These imaging tests can provide detailed images of the spine, allowing healthcare providers to evaluate the curvature and identify any underlying structural issues or abnormalities. When evaluating radiographic images of the spine, healthcare providers may look for several key features or parameters, including:

- Cobb angle: This is a measurement of the degree of curvature in the spine, typically measured on a lateral (side) X-ray image. The Cobb angle is an important parameter for determining the severity of spinal curvature and guiding treatment decisions.
- Sagittal balance: This refers to the alignment of the spine in the front-to-back direction, and is typically evaluated on a full-spine X-ray. Sagittal balance can affect a person's posture and gait, and can contribute to back pain or other symptoms.
- Vertebrae morphology: Healthcare providers may examine the shape and size of individual vertebrae on radiographic images to identify any abnormalities or signs of spinal deformities.
- Intervertebral disc height: Disc height can be evaluated on radiographic images to assess the health of the spinal discs, which act as shock absorbers between the vertebrae.

2.4 Imaging Techniques for Spine Analysis

Several imaging options are available for spinal analysis and diagnosis. The cheapest and most popular one is radiography or radio-graphical images. Due to advancements in technology and for detailed analysis, following techniques are commonly used for the evaluation of spinal issues. Among these, X-Ray is the most common and cheapest imaging modality as compared to other options which are relatively expensive and are required to be prescribed by a medical specialist. Figure 2-3 depicts all mentioned categories of imaging modalities from left to right: X-Ray, CT, MRI, PET, and SPECT Scans of human Spine. The details regarding each imaging modality with

respect to spinal disease diagnosis are given below. These imaging techniques provide excellent macro-structural information regarding the magnitude of the disease and ligamentous injury, which is then combined with the clinical examination.

i) X-Ray Images

ii) CT (Computed Tomography)

iii) MRI (Magnetic Resonance Imaging)

iv) PET (Positron Emission Tomography)

v) SPECT (Single-Photon Emission Computed Tomography)

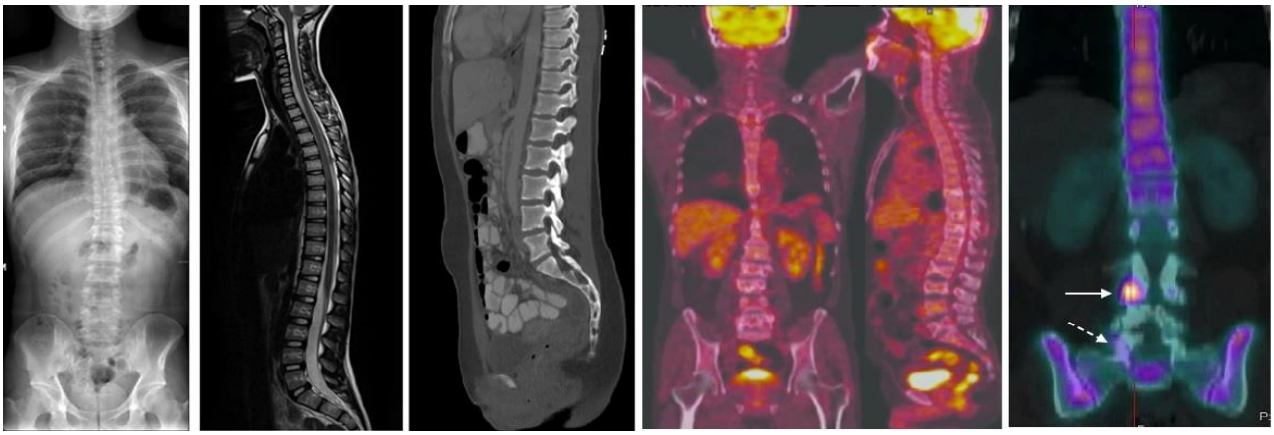

Figure 2-3 Different images, from left to right: X-Ray, CT, MRI, PET and SPECT scans of human spine [16-20]

2.3.1 X-Ray Images

X-ray images are a type of medical imaging technique that use high-energy electromagnetic radiation that helps to produce photograph of the body's internal structures. X-rays pass through the body and are absorbed in varying degrees by different tissues, with dense tissues such as bones appearing white on the resulting image. X-ray images are commonly used for diagnosing and monitoring a variety of spinal conditions and injuries, such as fractures, dislocations, scoliosis, and spinal tumours. X-rays can also be used to evaluate the alignment and stability of the spine, and to assess the extent of degenerative changes such as osteoarthritis or osteoporosis. To obtain an X-ray of the spine, the patient will typically lie down on a table or stand against an X-ray machine, and the technician will take images of the spine from various angles. The procedure is non-invasive

and usually takes only a few minutes to complete. While X-rays are useful for visualizing bony structures, they do not provide detailed information about soft tissues such as the spinal cord or nerves. In some cases, other imaging techniques such as MRI or CT scans may be needed to obtain a more complete picture of the spine and surrounding tissues [21].

2.3.2 CT Scans

Computed Tomography (CT) images are a type of medical scans that uses X-rays in combination with computer technology that produces detailed images of the internal structures of body, including the spinal cord. These scans presents cross-sectional illustrations of the body, allowing doctors to see the internal structures in greater detail than X-rays. To perform a CT scan of the spine, the inpatient will lie down on a bed that slides into a large, doughnut-shaped machine. The scanning machine spins around the patient, taking numerous X-ray scans from multiple angles. A system then merge these images to formulate a detailed 3D image of the spine. CT scans of the spinal cord can be utilize to diagnose a range of spinal conditions and injuries, including fractures, herniated discs, spinal stenosis, and spinal tumours. They can also be used to assess the extent of degenerative changes in the spine, such as osteoarthritis or osteoporosis. CT scans are normally harmless, but they do reveal patients to a trivial amount of ionizing radiation. The amount of radiation exposure is typically much lower than that of traditional X-rays, but doctors will still use caution when ordering CT scans, especially for pregnant women or children. In some cases, contrast dye may be used to enhance the images, which can cause an allergic reaction in some patients [21].

2.3.3 MRI Scans

Magnetic Resonance Imaging (MRI) scans are a type of medical radiography that require a magnetic field and radio waves to produce comprehensive scans of the internal structures of body, including the spinal cord. MRI scans bring highly precise, 3D images that allow medical specialist to view the internal anatomy of the spine in great detail. To perform an MRI scan of the spine, the patient will lie down on a bed that moves into a huge, cylindrical machine. The MRI apparatus produces a strong magnetic field around the patient, which causes the protons in the body's tissues to align in a certain way. Radio waves are then used to disrupt the alignment of the protons, and as they realign, they generate signals that are taken up by the detectors of machine. A system then

process these signals to formulate a detailed scan of the spine. MRI scans of the spine can be used to diagnose a variety of spinal conditions and injuries, including herniated discs, spinal stenosis, spinal tumours, and spinal cord injuries. They can also be used to assess the extent of degenerative changes in the spine, such as arthritis or disc degeneration. MRI scans are generally safe, but they are not recommended for certain types of patients who have some medical devices installed, such as cochlear implants or pacemakers, due to the strong magnetic field used during the procedure. In addition, some patients may feel claustrophobic inside the MRI machine, and sedation may be necessary to help them relax during the procedure [21].

2.3.4 PET

Positron Emission Tomography (PET) scan is a type of medical radiology that uses a tiny amount of radioactive material (tracer) to create images of the internal body organs and tissues, including the spine. The tracer is injected into the patient's bloodstream, where it travels to the area being studied. As the tracer decays, it beam (positrons) positively charged particles, these particals collide with (electrons) negatively charged particles in the body, triggering in the emission of gamma rays. These gamma rays are detected by a PET scanner, which produces a detailed 3D image of the area being studied. PET scans of the spine are commonly used to diagnose and monitor spinal tumours, as well as to assess the effectiveness of cancer treatments. PET scans can also be used to evaluate the metabolic activity of the spine, which can help doctors identify areas of inflammation or infection. PET scans are safe, but while conducting the scans patients is exposed to a small amount of radiation from the tracer. The amount of radiation exposure is typically low and is not considered harmful for most patients. However, women who are conciving baby or breastfeeding their child should clarify this to their doctor before undergoing a PET scan. The tracer can travel through the placenta or breast milk and this can potentially cause harm to the fetus or infant.

2.3.5 SPECT

Single Photon Emission Computed Tomography (SPECT) scan is a type of medical imaging that uses a small amount of radioactive material (tracer) to produce images of the body's internal structures, including the spine. The tracer is injected into the patient's bloodstream, where it travels to the area being studied. As the tracer decays, it emits gamma rays, which are detected by a

SPECT scanner. The scanner then produces a 3D image of the area being studied. SPECT scans of the spine are commonly used to diagnose and monitor spinal conditions such as herniated discs, degenerative disc, and spinal stenosis diseases. They can also be used to evaluate the blood flow to the spine and detect areas of inflammation or infection. SPECT scans are generally safe, but they do expose patients to a small amount of radiation from the tracer. The amount of radiation exposure is typically low and is not considered harmful for most patients. However, women who are expecting or breastfeeding should notify this to their doctor before undergoing for a SPECT scan. The tracer can travel through the placenta or breast milk and this can potentially cause harm to the fetus or infant.

2.5 Reference Body Planes

Reference body planes are imaginary planes that are used to describe the orientation and position of different parts of the body. There are three primary reference planes:

1. Sagittal plane: It is an anatomical term used to describe a vertical plane that divides the human body into two sections left and right. Movements of the body that occur in the plane include flexion and extension, as well as abduction and adduction to a lesser extent. For example, when patient bend forward to touch his/her toes, patient are flexing their body in the sagittal plane.
2. Frontal plane: It is an anatomical term used to describe a vertical plane that divides the human body into two sections front (anterior view) and back (posterior view) . Movements that takes place along this plane includes, abduction (moving away from the body's midline), adduction (moving toward the body's midline) , as well as lateral flexion. For example, when patient lift his/her arms out to the side, they are performing abduction in the frontal plane. When patient tilt his/her head to the side, they are performing lateral flexion in the frontal plane..
3. Transverse plane: It is an anatomical term used to describe a horizontal plane hat divides the human body into two halves upper (superior) and lower (inferior) half. Movements that appear along this plane typically involve rotation of the body. For example, when patient twist his/her torso from side to side, they are rotating their body in the transverse plane. Similarly, when patient turn his/her head to look to the side, they are rotating their head in the transverse plane.

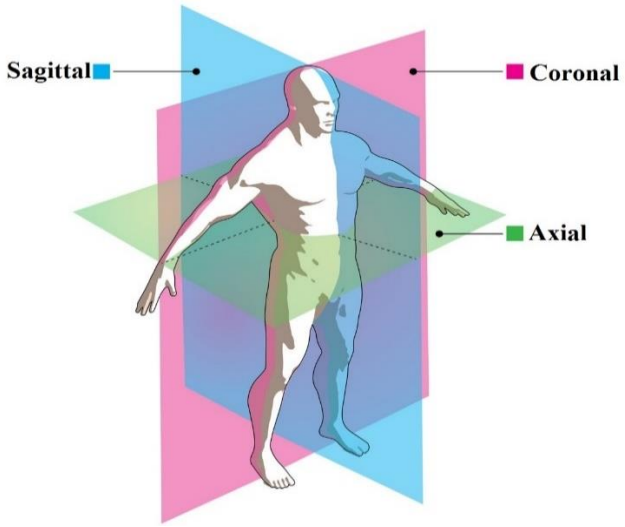

Figure 2-4 Reference planes for structural view of the normal spine: Coronal, Sagittal and Axial planes [22]

These reference planes are commonly used in medical imaging, such as MRI and CT scans, to describe the orientation and position of different structures within the body, including the spine. Figure 2-4 shows all three kinds of view planes. Spinal postural deformities can be assessed using Coronal and Sagittal planes.

2.6 Spinal Posture Disorder/Abnormalities

There are numerous medical issues that involve the spinal cord and therefore it is an extensive domain to discuss. However, the regular symptoms which indicate spine problems include back ache, immense sweating, and weakness, loses of senses; muscular numbness and swelling; change in bladder pattern, compromised reflexes and paralysis. These symptoms can narrow down the area of problem. So that the medical specialist can identify the region of the spine that is affected. These symptoms can appear due to any infectious bacteria, accidental trauma injury, vascular blockage, and fracture in spine bone, disk problems and tumours [23]. Our research focuses on deformity posture problems of the spine the regional based categorization is of three types that are Scoliosis, Kyphosis, and Lordosis, as shown in Figure 2-5.

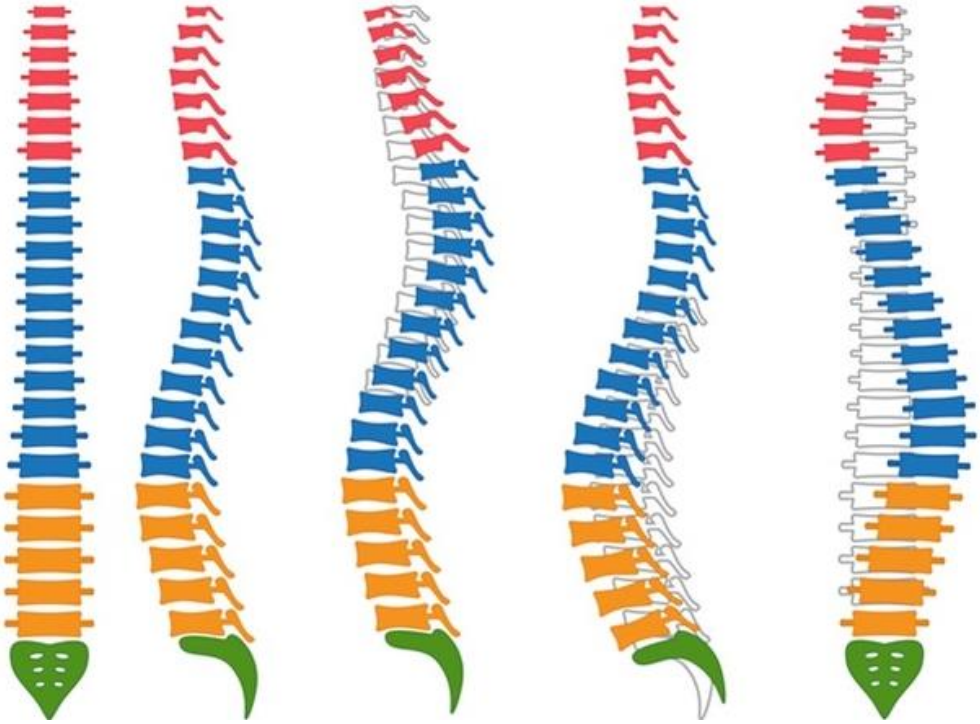

Figure 2-5 Spine deformities (a) Normal front view (b) Normal side view (c) Kyphosis (d) Lordosis (e) Scoliosis [25]

2.4.1 Scoliosis

Scoliosis is the three-dimensional deformity from the sideways. It is a rotated curvature of the spinal cord which commonly occurs during growing age and erupts before puberty. At the initial stage it is a deformity of approximately 10° and is considered to be a mild category. But, with the passage of time, it can get severe as the subject grows [24]. An increase in the severity of this deformity can lead to disability. Extreme curvature deformities decrease the space within the chest area. That may trigger breathing problems as it compromises the functionality of the lungs and the heart. The common symptoms of Scoliosis are chronic back pain, uneven hips, shoulders, and waist. The cause of this posture deformity is still unknown; the clinicians call this idiopathic [26]. There are different types of scoliosis based on the cause, age of onset, and severity of the curvature:

Idiopathic scoliosis:

Idiopathic scoliosis is a type of scoliosis that has no known underlying cause. It is the most common type of scoliosis and typically develops in children and adolescents between the ages of 10 and 18 years old. Idiopathic scoliosis affects girls more commonly than boys, and the severity of the curvature can vary widely from mild to severe. Although the exact cause of idiopathic

scoliosis is unknown, it is thought to be related to a combination of genetic, environmental, and biomechanical factors. In some cases, it may be associated with other medical conditions such as connective tissue disorders, neurological disorders, or spinal cord abnormalities. Diagnosis of idiopathic scoliosis typically involves a physical exam, medical history, and imaging tests such as X-rays or MRI to evaluate the degree and pattern of the curvature. Treatment options depend on the severity of the curvature and may include observation, bracing, or surgery. Observation may be recommended for mild cases of idiopathic scoliosis that are unlikely to progress. In more severe cases or in cases where the curvature is likely to progress, bracing may be recommended to help prevent further curvature. Surgery may be recommended for severe cases of idiopathic scoliosis that are causing pain or affecting the function of the lungs, heart, or other organs. The outlook for individuals with idiopathic scoliosis varies depending on the severity of the curvature and the response to treatment. With appropriate treatment and management, however, many people with idiopathic scoliosis can lead normal, active lives.

Regenerate response Idiopathic scoliosis is further divided into three subtypes based on the age of onset:

a. Infantile idiopathic scoliosis: Onset is before the age of 3 years.
b. Juvenile idiopathic scoliosis: Onset is between the ages of 3 and 10 years.
c. Adolescent idiopathic scoliosis: Onset is between the ages of 10 and 18 years.

Congenital scoliosis:

Congenital scoliosis is a type of scoliosis that is present at birth and is caused by an abnormal development of the spine. This can include abnormalities in the vertebrae, such as a failure of the vertebrae to form properly, or an abnormal fusion of the vertebrae, which can lead to a curvature of the spine. The exact cause of congenital scoliosis is not fully known, but it is suspected to be related to genetic factors and disruptions in fetal development. It can occur in isolation or as part of a larger syndrome or condition. Diagnosis of congenital scoliosis typically involves a physical exam, medical history, and imaging tests such as X-rays, CT scans, or MRI to evaluate the degree and pattern of the curvature and to identify any associated abnormalities. Treatment options depend on the severity of the curvature and may include observation, bracing, or surgery. Observation may be recommended for mild cases of congenital scoliosis that are unlikely to

progress. In more severe cases or in cases where the curvature is likely to progress, bracing or surgery may be recommended to help prevent further curvature and to correct the deformity. Treatment may also be necessary to address any associated abnormalities or medical conditions. The patients suffering with congenital scoliosis varies depending on the severity of the curvature and the presence of any associated abnormalities or medical conditions. With appropriate treatment and management, however, many people with congenital scoliosis can lead normal, active lives.

Neuromuscular scoliosis:

It is a type of scoliosis that develops as a result of a neuromuscular disorder, such as muscular dystrophy, cerebral palsy, spina bifida, or spinal muscular atrophy. The disorder affects the nerves and muscles that control the movement and alignment of the spine, leading to an abnormal curvature. Neuromuscular scoliosis can develop at any age, but it is most commonly diagnosed in children and adolescents. The severity of the curvature can vary widely, and it may progress rapidly or slowly over time. Diagnosis of neuromuscular scoliosis typically involves a physical checkup, patient's medical history, and radiological tests such as X-rays or MRI to evaluate the degree and pattern of the curvature and to identify any underlying neuromuscular disorder. Treatment options depend on the severity of the curvature and the underlying neuromuscular disorder and may include observation, bracing, or surgery. Observation may be recommended for mild cases of neuromuscular scoliosis that are unlikely to progress. In more severe cases or in cases where the curvature is likely to progress, bracing or surgery may be recommended to help prevent further curvature and to correct the deformity. Treatment may also be necessary to address the underlying neuromuscular disorder. The outlook for individuals with neuromuscular scoliosis varies depending on the severity of the curvature and the underlying neuromuscular disorder. With appropriate treatment and management, however, many people with neuromuscular scoliosis can lead normal, active lives.

Degenerative scoliosis:

Degenerative scoliosis, also known as adult-onset scoliosis, is a type of scoliosis that develops as a result of age-related changes in the spine, such as degeneration of the intervertebral discs, osteoarthritis of the facet joints, and spinal stenosis. These changes can lead to a loss of spinal stability and alignment, resulting in an abnormal curvature of the spine. Degenerative scoliosis

typically develops in individuals over the age of 50 and is more common in female gender than male. The severity of the curvature can vary widely, and it may progress slowly over time. Diagnosis of degenerative scoliosis typically involves a physical exam, medical history, and imaging tests such as X-rays or MRI to evaluate the degree and pattern of the curvature and to identify any underlying age-related changes in the spine.

Treatment options depend on the severity of the curvature and may include observation, physical therapy, pain management, or surgery. Observation may be recommended for mild cases of degenerative scoliosis that are unlikely to progress or cause symptoms. In cases where the curvature is causing pain or other symptoms, physical therapy or pain management techniques may be recommended to help alleviate symptoms and improve function. Surgery may be recommended in cases where the curvature is severe and causing significant pain or other complications. The individuals with degenerative scoliosis varies depending on the severity of the curvature and the presence of any underlying age-related changes in the spine. With proper treatment and planning, many patients with degenerative scoliosis can lead normal, healthy and active lives.

Traumatic scoliosis:

Traumatic scoliosis is a type of scoliosis that develops as a result of a traumatic injury to the spine, such as a fracture, dislocation, or ligamentous injury. The injury can cause the vertebrae to shift and become misaligned, leading to an abnormal curvature of the spine. Traumatic scoliosis can develop at any age, but it is most commonly seen in adolescents and young adults who have experienced a significant trauma to the spine, such as a car accident, sports injury, or fall from a height. Diagnosis of traumatic scoliosis typically involves a physical exam, medical history, and imaging tests such as X-rays or MRI to evaluate the degree and pattern of the curvature and to identify any underlying injury to the spine. Treatment options depend on the severity of the curvature and the underlying injury to the spine and may include observation, bracing, or surgery. Observation may be recommended for mild cases of traumatic scoliosis that are unlikely to progress. In cases where the curvature is causing pain or other symptoms, bracing or surgery may be recommended to help prevent further curvature and to correct the deformity. Treatment may also be necessary to address the underlying injury to the spine. The outlook for individuals with traumatic scoliosis depends on the severity of the curvature and the extent of the underlying injury

to the spine. With appropriate treatment and management, however, many people with traumatic scoliosis can lead normal, active lives.

The severity of scoliosis is also classified based on the degree of curvature, with mild scoliosis being less than 20 degrees, moderate scoliosis being between 20 and 40 degrees, and severe scoliosis being greater than 40 degrees. One can stop the increase in deformity by wearing a brace support while, on the other hand, surgery can stop the curve deformity from getting worse.

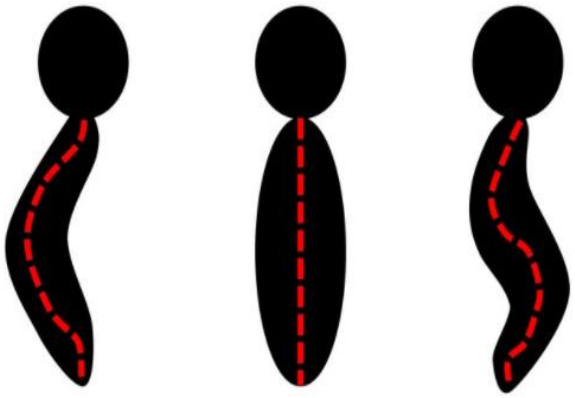

Figure 2-6 Scoliosis types (a) C-Shape, (b) Normal and (c) S-Shape [26]

Figure 2-6 shows the Scoliosis deformity has two shapes: ‘C’ and ‘S’. As the letter indicates, the shape of the spine curve forms the pattern of these alphabets. In the central canal of the spine, fluid gathering, and proliferation causes chronic pain in the neck area, which initiates feelings of fatigue and loss of sensation. Both C and S shape are two categories and the treatment procedures are back massage, brace belt of back, chiropractic and physiotherapy. To make it even more clear both curvature shapes treatment is very different; for example, the massage pattern, brace styling and exercises are different according to shape, the convex side muscles are weak and concave side muscles are tight. The C and S shape names indicate that S deformity has two convex sides making the class more server condition of scoliosis.

To describe it further, there are two types of C-Shaped scoliosis, that are, Dextro-scoliosis which is right-sided curve ‘Ɔ’ and Levo-scoliosis which is left-sided curve ‘C’. Whereas, S-shape is further classified into minor and major curves. As the name explains the major curve is the more significant and the minor curve is the smaller one. Both curvature shape define the massage pattern, brace styling, and exercises. The convex area of curvature needs to be identified for these treatments. The S shape has two convex which indicate more severe damage to the spine [27].

2.4.2 Kyphosis

The term Kyphosis is generally referred to the over-elaborated hunchback from the cervical region of the spinal cord [28]. In simple words, it is the slouching posture deformity from neck to shoulder. Kyphosis deformity mainly affects the starting vertebrae of the thoracic region along with the cervical region of the spine. Common symptoms include stiffness, fatigue, back ache, breathing difficulties, and chest pain and digestion problems. An increase in severity of Kyphosis can cause an increase in the chances of multiple diseases like vertebrae fracture, disk-generation, Osteoporosis, and cancer. Kyphosis can occur at any age, even in infants. But it is mostly common among older women.

There are several different types of kyphosis, which are classified based on the underlying cause and age of onset. Some of the most common types of kyphosis include:

Postural kyphosis:

Postural kyphosis is a type of spinal deformity that results in an excessive forward curvature of the upper back (thoracic spine). It is also sometimes called "round back" or "hunchback". Postural kyphosis can develop due to poor posture, especially in individuals who spend long periods of time sitting, hunching over electronic devices, or carrying heavy backpacks. In some cases, it may be a result of a sedentary lifestyle or lack of physical activity. Symptoms of postural kyphosis can include:

- Rounded or hunched appearance of the upper back
- Mild to moderate back pain or discomfort
- Stiffness or tightness in the upper back or shoulders
- Fatigue or muscle weakness in the upper back muscles

Treatment for postural kyphosis typically involves a combination of physical therapy, postural exercises, and lifestyle modifications to improve posture and strengthen the upper back muscles. In some cases, a brace may be recommended to help support the spine and encourage proper alignment. If postural kyphosis is severe or causing significant symptoms, surgery may be an option to correct the curvature.

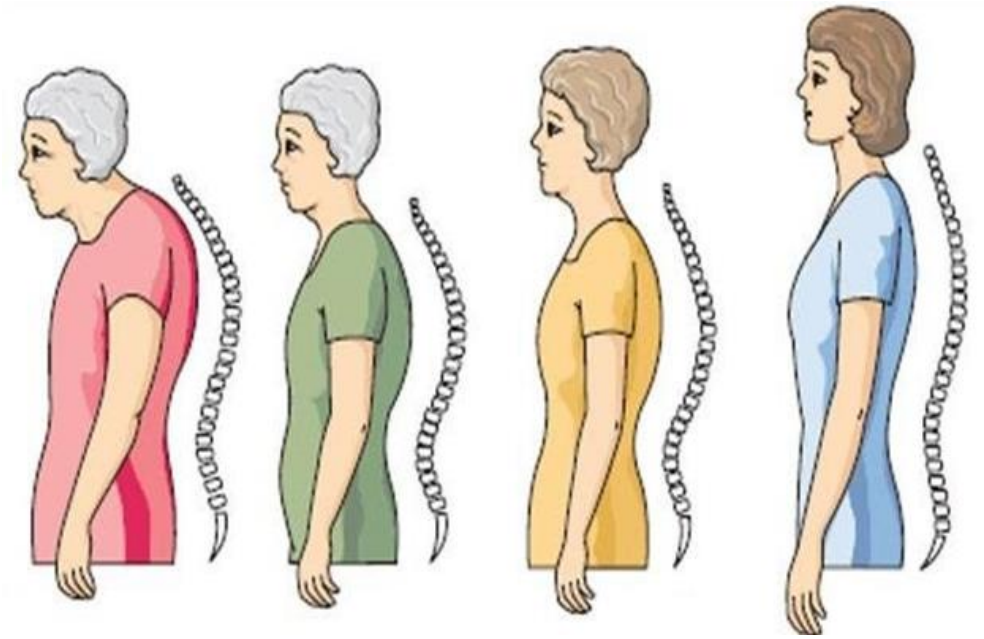

Figure 2-7 Development of a thoracic Kypohosis with age, showing increasing curvature of the spine [29]

Scheuermann's kyphosis:

Scheuermann's kyphosis is a type of kyphosis that typically develops during adolescence and is characterized by an excessive forward curvature of the spine in the upper back. It is also known as juvenile kyphosis or adolescent kyphosis. The condition is caused by abnormal growth of the vertebrae in the thoracic spine, which can lead to wedging of the vertebrae and a rounding of the upper back. The cause of the abnormal growth is not well understood, but it is thought to be a combination of genetic and environmental factors. Symptoms of Scheuermann's kyphosis may include a visible curvature of the spine, stiffness or pain in the upper back, fatigue, and poor posture. In severe cases, the curvature may compress the spinal cord or nerves, leading to neurological symptoms such as numbness, tingling, or weakness in the arms or legs. Diagnosis of Scheuermann's kyphosis typically involves a physical exam, X-rays, and sometimes other imaging tests such as MRI or CT scans. Treatment may include exercises to improve posture and strengthen the back muscles, bracing to prevent further curvature, and in severe cases, surgery to correct the curvature and stabilize the spine. Treatment for kyphosis will depend on the underlying cause and severity of the curvature. Mild cases may only require exercise and physical therapy, while more severe cases may require surgery to correct the curvature and stabilize the spine. Figure 2-7 shows the different stages of Scheuermann Kyphosis. Kyphosis is caused by a wedging, and it may contribute to the development of Scoliosis [28].

Congenital kyphosis:

Congenital kyphosis is a rare type of kyphosis that is present at birth and is caused by abnormalities in the development of the spine. The condition occurs when the vertebrae in the thoracic or lumbar spine do not form properly, leading to a curvature of the spine. The severity of congenital kyphosis can change widely, from a mild curvature that does not cause any symptoms to a severe curvature that can affect the function of the lungs, heart, and other organs. Congenital kyphosis is often diagnosed during infancy or early childhood, but in some cases, it may not be discovered until later in life. The condition is typically diagnosed through imaging tests such as X-rays, CT scans, or MRI. Treatment for congenital kyphosis depends on the severity of the curvature and the presence of any symptoms or complications. In mild cases, regular monitoring and observation may be sufficient. In more severe cases, treatment may involve bracing or surgery to correct the curvature and prevent complications such as spinal cord compression, respiratory problems, or neurological symptoms. With appropriate treatment and management, however, many people with congenital kyphosis can lead normal, active lives.

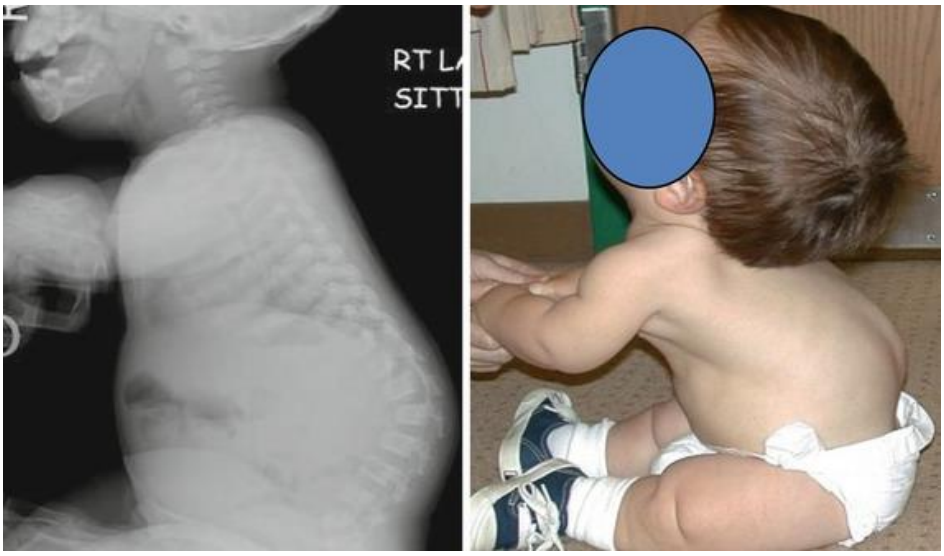

Figure 2-8 Patients with thoracolumbar Congenital Kyphosis [30]

Figure 2-8 shows young patients with thoracolumbar Congenital Kyphosis. Furthermore, Kyphosis can lead to other disorders like spinal arthritis, muscular dystrophy, and spine tumours. Congenital Kyphosis, occurs by birth when spinal vertebrae fail to develop normally. Surgery is the only treatment for this abnormality. Due to Kyphosis, the curvature change is more than 60° [28].

Though, early diagnosis and treatment can help to prevent its progression that may cause permanent damage.

Nutritional kyphosis:

Poor nutrition can contribute to the development of spinal problems such as osteoporosis, which can lead to kyphosis. Osteoporosis is a condition in which the bones of patient become weak and brittle, potentially making them more likely to break. A diet that is deficient in calcium, vitamin D, and other nutrients that are important for bone health can increase the risk of developing osteoporosis and kyphosis. Other risk factors for osteoporosis and kyphosis include aging, genetics, certain medical conditions, and lifestyle factors such as lack of exercise, smoking, and excessive alcohol consumption. To prevent nutritional deficiencies and promote good bone health, it is important to take a well-balanced diet that includes healthy rich food that contains calcium, vitamin D, minerals and other nutrients in them. Foods that contains good amount of calcium include green leafy vegetables, dairy products, and fortified food items such as cereal and orange juice. Vitamin D can be obtained through exposure to sunlight as well as through supplements and certain foods such as fatty fish and fortified dairy products. In addition to good nutrition, regular exercise, avoiding smoking and excessive alcohol consumption, and getting regular bone density screenings can also help to prevent osteoporosis and kyphosis.

Neuromuscular kyphosis:

Neuromuscular kyphosis is a type of kyphosis that is caused by neuromuscular disorders affecting the muscles, nerves, and/or the spinal cord. These disorders can result in a loss of muscle strength and control, leading to poor posture and spinal deformities. Some examples of neuromuscular disorders that can cause kyphosis include cerebral palsy, muscular dystrophy, spinal muscular atrophy, and spina bifida. These conditions can lead to a weakening of the muscles that support the spine and can cause the spine to curve abnormally. Neuromuscular kyphosis can cause a variety of symptoms, depending on the underlying disorder and the severity of the curvature. These may include back pain, muscle weakness, difficulty standing or walking, respiratory problems, and gastrointestinal problems. Diagnosis of neuromuscular kyphosis typically involves a physical examination, medical historyof patient, and radilogical tests which includes X-rays, CT scans, or MRI. Treatment may include exercises to strengthen the muscles and improve posture, bracing to

prevent further curvature, and in some cases, surgery to correct the curvature and stabilize the spine. The outlook for individuals with neuromuscular kyphosis varies depending on the underlying disorder and the severity of the curvature. With appropriate treatment and management, however, many people with neuromuscular kyphosis can lead normal, active lives.

2.4.3 Lordosis

When the lower lumber pelvic curve, which lies above the buttocks, excessively arches inwards, the deformity is termed as Lordosis. A small degree of swayback curve is normal, and even in the third trimester of pregnancy; it is well documented that there is an increase in lumbar Lordosis of the mother. This is the reason that women are more associated with this curvature deformity. The causes of Lordosis might be bad posture, spine surgery, genetics, congenital, injury, neuromuscular problems, pelvis, or hip illness. Lordosis symptoms indicate excess pressure on the whole spine structure, affecting movement of the body, causing severe lower back pain, discomfort, prominence of buttocks or changes in bowel and bladder. Treatment for Lordosis depends upon its severity. In mild cases, one can improve their condition with bracing the spine, physiotherapy, and exercises. Excess in the arches of the curve is treated with surgery [31]. There are different types of Lordosis

Postural Lordosis:

Postural lordosis refers to an excessive curvature of the lower back that is caused by poor posture. It is often seen in individuals who spend long hours sitting, particularly in a slouched position, or who have weak abdominal and hip muscles. In postural lordosis, the pelvis tilts forward, causing the lower back to curve inward. This can lead to lower back pain, stiffness, and muscle tension. Over time, postural lordosis can also lead to degenerative changes in the spine and increased risk of injury. Treatment for postural lordosis typically involves improving posture and strengthening the muscles of the core and hips. This may involve physical therapy, exercises to improve posture and strengthen muscles, and ergonomics modifications to workstations or seating. In some cases, bracing may be recommended to help support the spine and correct the curvature. In addition to these interventions, it is important to address any underlying factors contributing to poor posture, such as obesity, sedentary lifestyle, or certain medical conditions. By addressing these factors and improving posture and muscle strength, individuals with postural lordosis can often experience

significant relief of symptoms and improve their overall spinal health. Postural Lordosis shown in Figure 2-9, often comes due to over-weight and lack of muscle conditioning.

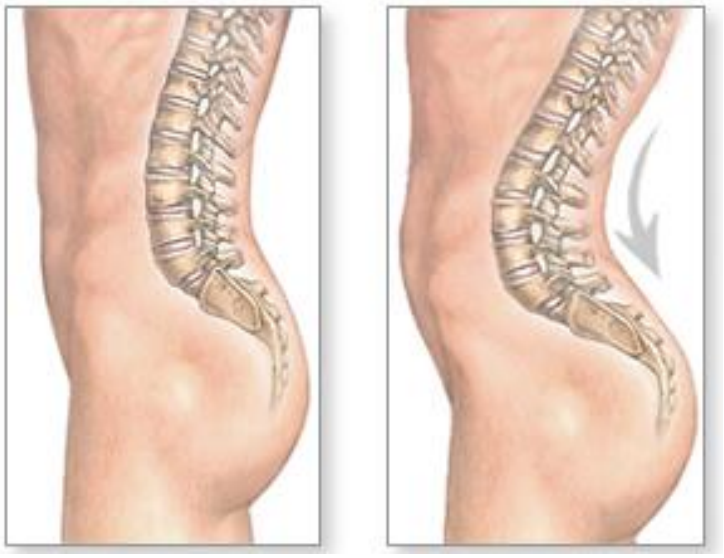

Figure 2-9 Normal vs Lumbar Lordosis in spine with exaggerated lumbar curve [32]

Congenital/Traumatic Lordosis:

Congenital lordosis is a rare form of lordosis that is present at birth and is caused by developmental abnormalities of the spine. This can include vertebrae that are malformed or fused together, resulting in an exaggerated or decreased curvature of the spine. Traumatic lordosis, on the other hand, is a type of lordosis that is caused by an injury to the spine. This can include fractures, dislocations, or ligament injuries that affect the curvature of the spine. Both congenital and traumatic lordosis can cause significant pain, discomfort, and functional limitations.

Treatment options for these types of lordosis depend on the severity of the curvature and may include physio-therapy, exercises to strengthen the muscles that are supporting the spinal cord, and bracing or casting to support the spine. In some cases, surgery may be necessary to correct the curvature and prevent further progression of the deformity. This may involve spinal fusion, in which vertebrae are permanently joined together, or other surgical procedures to correct the alignment of the spine. It is necessary to seek prompt medical attention if you suspect that you have congenital or traumatic lordosis, as early diagnosis and treatment plan can help to prevent further advancement of the deformity and boost outcomes.

Post-Surgical Laminectomy Hyper-Lordosis:

A laminectomy is a surgical procedure in which a portion of the bony arch of the vertebrae, known as the lamina, is removed to relieve pressure on the spinal cord or nerve roots. In some cases, this procedure may result in an increase in the Lordotic curve of the spine, known as post-surgical laminectomy hyper-lordosis. Post-surgical laminectomy hyper-lordosis can occur due to several factors, including the removal of supporting structures during surgery or a compensation response to a loss of stability in the spine. The condition can cause pain, discomfort, and functional limitations, and in some cases, may require further treatment.

Treatment for post-surgical laminectomy hyper-lordosis depends on the severity of the curvature and the symptoms experienced. In some cases, physical therapy and exercises to strengthen the muscles supporting the spine may be recommended. In other cases, bracing or casting may be necessary to support the spine and prevent further progression of the deformity. In severe cases, surgery may be necessary to correct the curvature of the spine. This may involve a spinal fusion procedure, in which the vertebrae are permanently joined together to stabilize the spine and correct the curvature. In some cases, additional surgical procedures may be necessary to correct any other underlying issues contributing to the hyper-lordosis. It is necessary to work along with your medical specialist that will help to develop a suitable approach of treatment for post-surgical laminectomy hyper-lordosis, as early intervention can aid to prevent additional progression of the deformity and improve results.

Neuro-muscular Lordosis:

Neuro-muscular lordosis is a type of lordosis that is caused by underlying neuromuscular disorders. These disorders can affect the muscles and nerves that support the spine, leading to an exaggerated curvature of the lumbar spine. Conditions that can cause neuro-muscular lordosis include cerebral palsy, muscular dystrophy, spina bifida, and other neuromuscular disorders. In some cases, the condition may be present at birth, while in others, it may develop later in life.

Neuro-muscular lordosis can cause pain, discomfort, and functional limitations, and in some cases, may require treatment to manage symptoms and prevent further progression of the condition. Treatment options may include physical therapy and exercises to strengthen the muscles supporting the spine, bracing or casting to support the spine, and in some cases, surgery to correct the curvature of the spine. The patient needs to work closely with a healthcare provider to develop

an appropriate treatment plan for neuro-muscular lordosis, as early intervention can help to prevent further progression of the deformity and improve outcomes.

Hip Flexion Contracture Lordosis:

Hip flexion contracture lordosis is a type of lordosis that is caused by a tightness or shortening of the muscles in the front of the hip, known as the hip flexors. This tightness can cause the pelvis to rotate forward, increasing the curvature of the lumbar spine. Hip flexion contracture lordosis is commonly seen in individuals who sit for prolonged periods of time, such as those with desk jobs or individuals who use wheelchairs. The condition can also occur as a result of injury or surgery to the hip. Hip flexion contracture lordosis can cause pain, discomfort, and functional limitations, and in some cases, may require treatment to manage symptoms and prevent further progression of the condition. Treatment options may include physical therapy and exercises to stretch and lengthen the hip flexor muscles, bracing to support the spine, and in some cases, surgery to correct any underlying hip issues contributing to the condition. Early intervention can help to prevent further progression of the deformity and improve outcomes.

2.7 Summary

In this chapter, we have discussed the anatomy of the human spine and its significance. Later on, we elaborated details regarding imaging modalities that are used for assessment of spine. The explanation on postural deformities, its types, causes and symptoms have been presented. The scope of this research is limited to curvature deformities. The above explained spinal curvature deformities are addressed in our methodology and the related literature regarding these deformities is discussed in the following chapter.

3 Chapter

Literature Review

Chronological based evaluation along with the analysis of previous research is integrated in this chapter. We have tried to present a thorough review of the existing literature and provide a comparison among the techniques as well. In the first section the literature discussed is from ancient times, regarding how spine curvature deformities were addressed. In the second and third section, recent approaches were segregated on the basis of technical aspects.

3.1 Classical Literature

Spine curvature deformity was assessed by evaluation of the pattern formulated in vertebral column, and the calculation of angles in that pattern gives the orientation idea about deformity. So, in order to analyse the severity of disproportionality, it was considered important to extract vertebrae regions from the whole image. Researchers have worked on this aspect and presented methods for localization and segmentation. Before starting this, firstly, we will discuss the earliest research papers for evaluation of spine deformity. Cobb[1] angle calculations by Flint [33], carried out a study on 31 female college students of age 19-22. The purpose of the study was to measure significance of abnormality of back muscles on lumber posture. Two images of the subject standing behind a mesh of a 2x2 screen in a relaxing position were obtained. With the help of previous studies, the plumb lines for both images were dropped to measure the line of gravity. The radiologist helped in detecting the focal point. By placing 4 landmark points, first two on the sacral and lumber junctions, third and forth over the upper surface and the dorsal surface of the sacrum. The first line was drawn from the dorsal to the apex which intersects the line from the sacrum pointers. The STL[2] angle at the intersection was the reading. Second reading was taken from the angle taken from the intersection of the lines parallel to the pointers on the inner-lumbar surface. This L-angle was taken to measure Lordotic Curve. A larger value of the angle reading indicates a smaller curve and vice versa. Figure 3-1 explains the methodology of manual Cobb estimation.

[1] Cobb was used as a standard measurement to quantify the magnitude of deformity in spinal cord. Dr John Cobb invented this method in 1948.

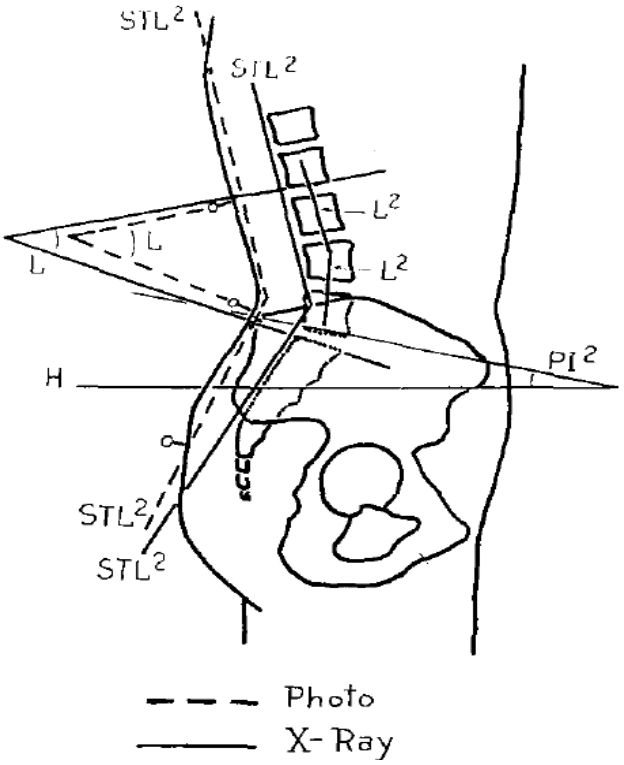

Figure 3-1 M. Marilyn Flint Cobb calculation technique [33]

Loebl presented a technique [34] for measurement of normal spine posture using Rheumatology images. Dataset used was of 176 spine images of patient's age 15-84 years from Westminster Hospital and Queen Mary's Hospital, Roehampton. The position of subjects for the images were sitting, standing, and bent. As shown in Figure 3-2, inclinometer was used with 9 cm gap and scale was set to degree. Keeping weight needle remain vertical, indicated the angle of spine inclination.

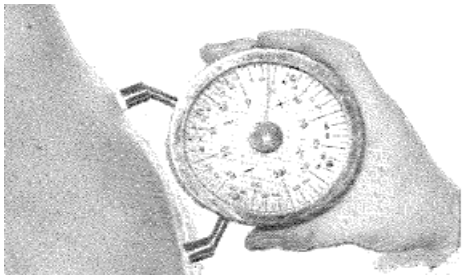

Figure 3-2 Loebl [34] Inclinometer was used to measure spine curvature

Mehta in [35] firstly analysed the spine deformity Scoliosis using radiographs. The convex side of the vertebrae was rotated in a clockwise direction through an arc of 90° with intervals of 15°. This produced a series of images with remarkable variation in appearance. On these composite images multiple landmarks were drawn and a transverse process was used to get a rotational difference. The study was carried out to determine the extent of curvature change. Levine and Leemet [36],

in their study proposed an edge detection procedure to determine where the spine was located after that vertical signature of the entire image was taken, and a smoothing method was applied to reduce noise. Later, after edge detection, least square polynomial fit was applied, the center line was calculated with the help of the median of both edges.

Chwialkowski et al. [37] in their research article produced a quantitative measuring strategy for lumbar disc evaluation. The proposed method utilized 12-15 sagittal images; Edge enhanced rectangular block was used to find the Region of Interest (ROI). A morphological model of vertebral structure was designed, to localize the vertebra. Intensity profiling of each estimated area of disc space was carried out, along with the bisection line. In [38], Smyth et al. described the usage of Active Shape Models (ASM) to locate vertebrae in DXA[2] images. All vertebrae in the image were marked manually with six points for each from thoracic T7-T12 and Lumbar L1-L4. ASM involves building a statistical model of the shape and appearance of the object of interest, and then using this model to deform an initial estimate of the object's location until it fits the object's actual location in the image. To simplify the co-variance matrix Point Distribution Model was applied in addition to Principal Component Analysis (PCA). It is used for reducing the dimensionality of data while retaining as much of the original information as possible Basically, ASM uses both shape-based and grey level appearances for detection of objects in an image. The results were characterized as a Gaussian distribution with the help of the Expectation Maximization (EM) algorithm.

3.1.1 Discussion

That early literature mostly focused upon enhancement and restoration of images. For the medical domain, image acquisition and dataset collection were the major issues for the researchers. The literature indicates problems such as low-quality images, and limited availability of imaging modalities. The immaturity in the domain was the key factor and a limited number of available techniques for segmentation and classification, was also one of the drawbacks. Roentgenographic [39] and X-Ray images were mainly used for differential diagnosis. Morphological processing was popular for the extraction of components from images. One of the secondary issues was the

[2] Dual-energy X-ray absorptiometry was an imaging scanner that was used for measuring bone mineral density.

limitations of the hardware, such as storage spaces, memory issues, and smaller cycles per second of the processor, leading to low capacity as a whole for complex processing. Table 3-1 shows the summary of the classical literature studies [40].

Table 3-1 Summary table of classical literature review

#	*Author*	*Year*	*Pre-Processing*	*Technique*	*Diseases*	*Image Type*	*Dataset*	*Results*
1	Flint [33]	1963	Mesh of 2x2 screen	Landmarks and angle formation	Pelvis Posture	Roentgenographic	31 women	No correlation of Lordosis and hip-trunk
2	Loebl [34]	1967	--	Inclinometer for curve measuring	Arthritis	Roentgenographic	176	10% within normal ranges
3	Mehta [35]	1973	Intervals of 15-degree rotation	Transverse process and Image matching	Scoliosis	Radiograph	--	Morphological Difference
4	Chwialkowski et al. [37]	1989	Edge Enhanced Rectangular Block with ROI	Candidate fitting vertebral disc space then intensity profiling	Lumbar Disc	MRI	12-15 sagittal images	Abnormality in correlation intensity distribution compared with clinical
5	Smyth et al. [38]	1997	Landmarks contour of T7-T12 and L1-L4	ASM starts with 3 points till convergence	Osteoporosis	X-Ray images	78 women	0.20 Precision

3.2 Localization and Segmentation

The localization or detection step finds the vertebrae or spine, which rather involves segmentation or pixel-wise classification of the object. This section of literature focuses on highlighting the work carried out in these areas. In [41] and [41] both research articles have proposed segmentation techniques using Hough transform. In [41] Brejl and Sonka have used 2D MRI with different dimensions; the training dataset has manual boundary tracing, in combination with landmark identification. Shape-variant Hough Transform, and Edge-based object segmentation were used for segmentation. In [42], the authors have used 50 NHANES[3] II X-Ray images. Every image landmarks were identified on the basis of morphometric points, with the assistance of an expert

[3] National Health and Nutrition Examination Survey

radiologist. The Generalized Hough Transform (GHT) was customized to provide shape information using its mean and corresponding templates. The GHT is an extension of the Hough Transform that allows detection of inconsistent shapes, not just predefined ones. GHT can be computationally expensive due to the high-dimensional parameter space. The average 72.06 out of 80 landmark falls in the boundary box and the orientation error was average 4.16°.

Gamio et al. in [43] and Peng et al. [44] proposed a novel research approach for localization using MRI scans. In [43], the localization of spine bone was done using normalized cut technique and after that Nystrom approximation method was implemented for vertebral body segmentation. On the other hand, researchers in [44] proposed two-staged algorithm; the first one was intervertebral disk localization and the second one was vertebral segmentation. In the first stage, localization was performed by a model-based search method, which gives clues regarding intervertebral disc spaces. The intensity profiling on polynomial function was used to refine and verify candidate disc spaces. The center point of the disc with extended profiling in the horizontal direction will provide a shape approximation. Later, a canny algorithm was used for the boundary extraction and re-calculation of disc space with the boundary values and repeat polynomial profiling identified inter-vertebral disc distances. Successful boundary extraction of 22 vertebrae for 5 datasets was approximately average 94%.

Xiaoqian et al. in [45], utilized 801 cervical and 972 lumbar X-Ray images from NHANES II. The researchers studied a nine-point landmark model, which clinical experts used to explain vertebral shapes. Xu et al. established an automatic system, which detects those nine-points on the basis of their semantic heuristics. To grab corner information author proposed Partial Shape Matching (PSM) using dynamic programming. The basic idea behind partial shape matching is to find the best correspondences between the points or features of the two shapes. To reduce the number of data points to 20 vertices, the technique of curve evolution was applied. Using Dynamic Programming (DP), each point set triangle data was saved, and for every classification matching was carried out. Dynamic Programming is a powerful technique for solving complex optimization problems efficiently. Unlike [44], Benjelloun and Mahmoudi in [46], conducted a detailed analysis for extraction of anterior left faces of vertebra contour. Their methodology relied upon Harris' interest point detector for key points. Contrast enhancement produced better results in corner recognition.

Klinder et al. in their research article [47] described a framework for vertebrae detection and segmentation using CT images. By using sophisticated GHT containing parameters of multiple shapes, and a number of objects. Vertebral coordinate system in combination with a seed point progressive adaptation method, were used for the location and coordinates of vertebra. For identification of vertebrae, average intensity information inside each vertebra bounding box was utilized. In the segmentation procedure, adapting triangulated shape model was applied. In [49], Larhmam et al. claimed 89% accuracy in their approach, where they studied 200 images. Out of these, 40 were healthy while 160 were not to validate the results. They have also used Hough Transformation based on modified template matching methodology. A reference template is created for each vertebra in the image by selecting a small region of interest (ROI) that includes the vertebra and its surrounding anatomical structures. The Hough Transform is applied to the preprocessed image to detect potential vertebra locations. In this step, the algorithm scans the image and detects potential vertebral shapes based on the template created. In segmentation, the first step was model construction on the geometry of an average of 25 vertebras. In the second step, canny was applied and Gaussian smoothing was used in combination with Sobel. Hough Transform was the third step of the segmentation process to reduce false positive edges. To identify vertebra potential centers authors used Contrast Limited Adaptive Histogram Equalization (CLAHE). CLAHE is particularly useful in situations where the image has low contrast works by spliting the input image into small portions, overlapping areas are called tiles. For every tile, a histogram equalization is performed, which redistributes the pixel values in the tile so that they span the entire available range of pixel values. This results in an increase in the contrast of the tile. In [48], Ribeiro et al. used 40 cases from which 19 were confirmed fractured bones and 22 normal spinal images. Gabor filter bank with 180 filters was applied to these grey-scaled images at angles $\theta = -\pi/2$. In the center of the vertebra, points were marked using a mouse for distance calculation and region splitting. Using the neural network, the logistic sigmoid function for more detailed analysis, along with morphological opening and closing was carried out for holes, noise and region filling. The accuracy of the proposed system was quoted to be in the range of 91-92%. Rasoulian et al. [50] suggested a novel shape pose segmentation technique. The dataset used for processing consist of 32 CT images acquired from Kingston General Hospital and Vancouver General Hospital. The proposed methodology used a groupwise Gaussian Mixture Model (GMM) to establish boundary. GMM is fit to the intensity distribution of the pixels within the ROI. The GMM

models the distribution of the image intensity values using a weighted sum of Gaussian probability density functions. The Expectation Maximization (EM) algorithm is used for estimating the parameters of a GMM. The EM algorithm iteratively updates the parameters of the GMM to maximize the likelihood of the observed data. To segment out EM registration algorithm was used. The estimated parameters of the GMM are used to perform vertebrae registration between the two input images. The registration process is conducted by transforming one image to align with the other using the estimated parameters. To smoothen CT scans, the Multivariate Gaussian kernel was utilized in fusion with a canny edge detector to produce boundary. For the results, the evaluation metric mean of point-to-surface distance error was computed to be 1.38 ± 0.56.

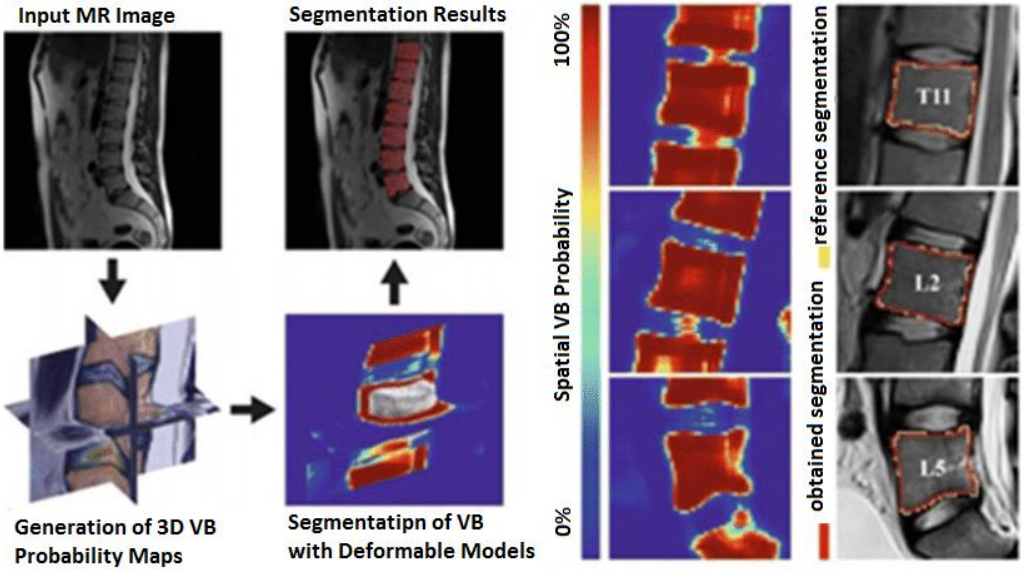

Figure 3-3 Spatial vertebral body and probability maps using 3D CNN [51]

The Convolutional Neural Network (CNN) was utilized in [51] and [52]. In a study [51], Korez et al. developed a semi-automated supervised segmentation methodology for vertebral bodies; in the study the dataset consisted of MRI scans of 23 subjects. 3D mesh of mean shape model of vertebral bodies was formulated. Later, CNN supported to provide generalized probability map of Vertebral Bodies (VB). Figure 3-3 shows their entire model. The actual novelty of the proposed technique was 3D spatial VB probability maps. For the evaluation of the proposed methodology, the Dice Similarity Coefficient (DSC) was calculated 93.4 ± 1.7%. Similar to this, to reduce misdiagnosis from Computer Aided Diagnosis (CAD) systems, Arif et al. [52] proposed a fully automated cervical segmentation framework using FCN. With the help of probabilistic spatial regression,

localization of the vertebrae was done. For segmentation, a dataset from Royal Devon and Exeter Hospital containing 124 X-Ray images in training and 172 in test data were utilized. Without any manual input, a shape-aware deep network was formulated. The evaluation metric achieved DSC of 0.84 and a shape error of 1.69 mm.

U-Net was used by authors in [53], [54] and [55], Shi et al. in [53] developed two-stepped methodology. In the initial step, spinal region extraction was carried out using 2D U-Net variants. Later, for each vertebra centroid localization, was done by applying M-methodology which resulted in producing a 3D ROI. With the help of inception, 3D U-net model was trained on 61 annotated CT images. The correct identification of 92% and error rate of 0.74 mm with 0.8mm of DSC was achieved. While in [54], Lu et al. described a fully automated approach for lumbar spinal stenosis grading. The research provides three major contributions: First NLP scheme to extract level-wise ground truth labelling from radiological reports. Second, disc-level vertebral segmentation and localization using the U-Net framework. Third, was usage of CNN for stenosis grading. Lumber MRI dataset of 22,796 disc-levels extracted from 4,075 patients, the proposed algorithm gave an accuracy of 94%. In [55], automatic landmark localization introduced a hybrid WHDV[4] method that includes U-Net architecture. For evaluation, a dataset of 1696 radiographical images of child hips, age 2-11, including both cases of normal and diseased was used. Experimental results accuracy showed significant improvements in comparison with the RFRV-CLM[5] method, having median error of 6.92% and 5.85% respectively.

Kim et al. in [56] presented a semi-automatic vertebrae segmentation technique using MRI scans of lumber region. After extraction of ROI for each vertebra, specify parameters with the help of a correlation map. Multiple ROI were tuned with Hough Transform along with Canny Edge Filtering. Later, segmentation was carried out via graph-based and line-based algorithms. Evaluations of algorithm are tested on lumbar sagittal MRI scans, DSC reached 90%, in comparison with the manual process.

Rehman et al. [57] discussed the CAD system for accurate vertebrae segmentation. Modified form of U-Net, and combination of shape prediction were applied, termed as FU-Net framework. The FU-Net framework is fomulated to enhance the connectivity between the blocks of encoder and

[4] Weighted Heatmap Displacement Voting

[5] Random Forest Regression-voting Constrained Local Models

decoder of the U-Net architecture. This is achieved by adding fully connected layers between the encoder and decoder blocks to allow information flow across different scales of the image. For all experiments, 2D sagittal slices were applied, data augmentation was compulsory to improve learning. The proposed methodology produced 96% DSC and 0.1 ± 0.05 absolute surface distance on two different datasets of CSI16 and CSI 2014. The details regarding dataset is given in Appendix B. In [58], vertebral segmentation has been done using an iterative segmentation model that combines 3D U-Net and DeconvNet. The authors have used the xVertSeg dataset. Cross-entropy was used as a loss function for multi-label classification.

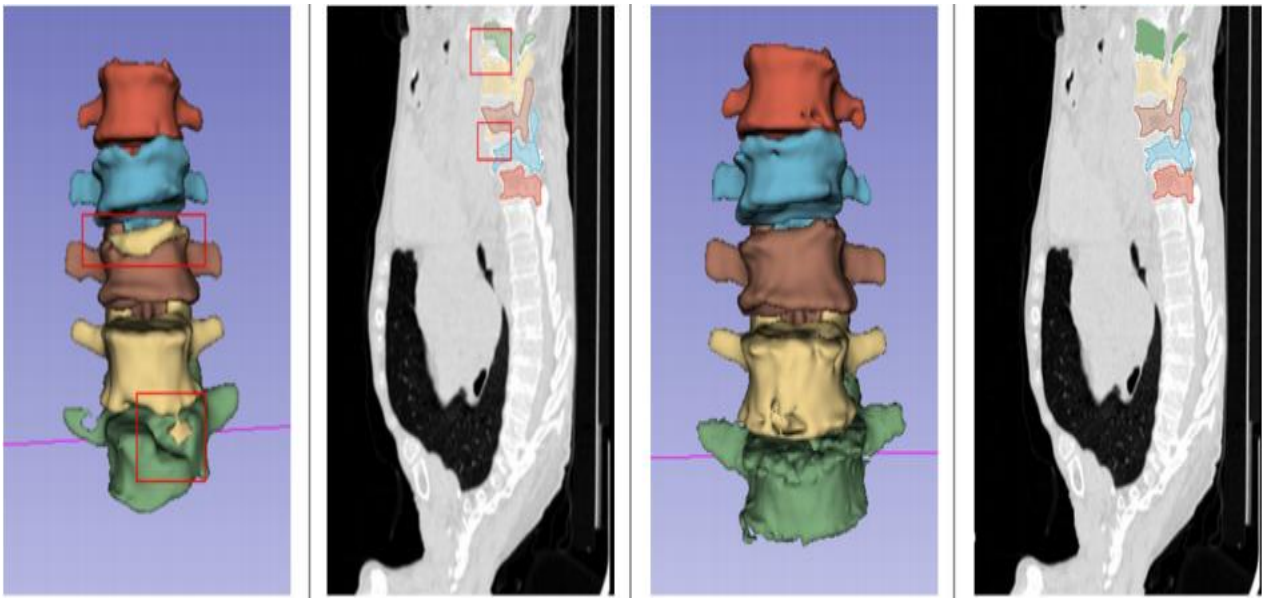

Figure 3-4 FCN segmentation results of Lessmann et al. [59]

Lessmann et al. [59] addressed vertebrae segmentation and identification of abnormalities with the help of FCN. Four major components of authors approaches are: 1. segments voxels from a 3D patch 2. Instance memory 3. Identification sub-network 4. Completeness classification sub-network. Dataset used was Computational Spine Imaging (CSI) 2014 of thoracolumbar spinal CT. DSC of segmentation 94.9 ±2.1% and 93% correct anatomical identification. Figure 3-4 presents some of their segmentation results.

In 2019, Chen et al. [60] used a 3D FCN in combination with Hidden Markov Model (HMM) for the localization of vertebrae. For accurate vertebral segmentation FCN architecture was applied and the HMM was utilized for modelling the temporal dependencies between adjacent slices. The

authors utilized 242 CT scans for training, in addition to 60 scans for evaluations from public a dataset of the MICAAI[6] Challenge. Initially, FCN was used for training and detection of vertebra centroids. Another FCN network was formulated for both local and global information from scans, this classification network handle indexing of vertebrae. The HMM is trained on the sequence of segmentation masks generated by the FCN. The HMM models the temporal dependencies between adjacent slices to improve the accuracy of the vertebrae localization. The authors proposed post-processing strategy to increase the robustness and to achieve high level optimization HMM. Experimental results on test data produced mean identification rate (MIR) of 87.97% and mean error distance of 2.56mm.

Hans Liebl et al. [61] and Liang et al. in [62] addressed the problem segmentation of vertebrae; both authors have used modified variants of –U-Net. In [61] Btrfly Net framework was used for labelling of the vertebrae. In order to segment each vertebra the U-Net architecture was applied. The VerSe19 dataset was used for training and the VerSe20 was used as test data achieving a mean DSI of 91.7%. In [62], MRI scans from SpineWeb's dataset of lumbar vertebrae were given to two major convolution modules, DAB depth-wise, and MC micro-codec convolutional module. To improve the accuracy, the author replaced DAB and MC modules with DABU-Net and MCU-Net and DSC reached up to 0.9185. DABU-Net stands for Dilated and Asymmetric Bottleneck U-Net. It is a modification of the popular U-Net architecture that uses dilated convolutions and asymmetric bottlenecks to improve the performance of the model. MCU-Net stands for Multi-Scale Context U-Net. It is a modification of the U-Net architecture that uses multi-scale context modules to capture contextual information at different scales.

In 2021, latest article by Liu et al. in [63], proposed an automatic algorithm for the segmentation of vertebrae using Deeplab V3+ . The dataset contains 157 x-Ray scans which are produced by Digital Image Group in London, Ontario, Canada. For the Cobb angle measurements the Smallest Distance Point (SDP) method was utilized. The performance in the DSI was 0.9379 ± 0.0286 and the correlation coefficient 0.95.

[6] The MICCAI Society is a professional organization for scientists in the areas of Medical Image Computing and Computer Assisted Interventions.

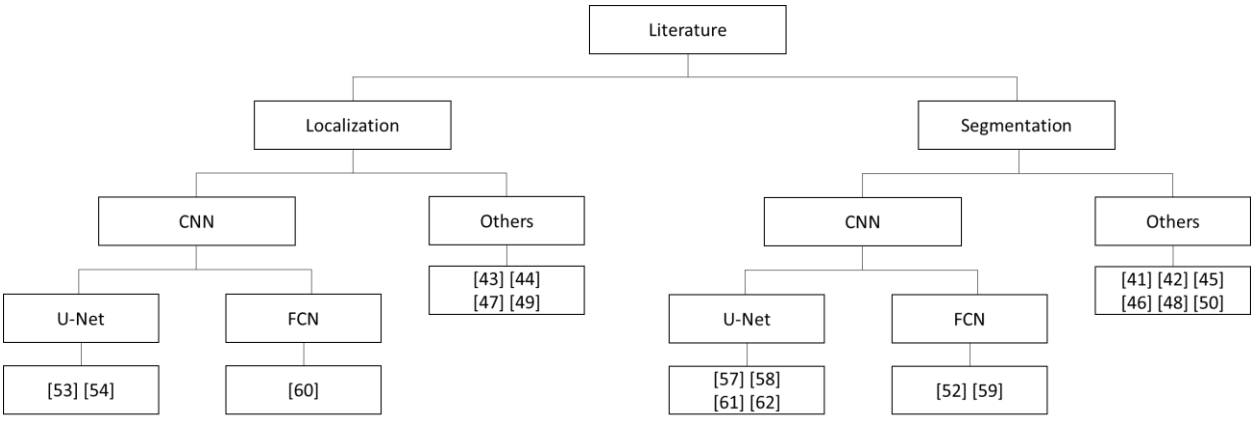

Figure 3-5 Overview of techniques used for localization and segmentation in literature

3.2.1 Discussion

In the second section, related research work on localization and segmentation was compared. The work in medical imaging was gaining popularity. Therefore, it increased the amount of research work carried out in this domain. The automated clinical assistance perspective attained acceptance and the image processing domain was growing day by day. AI became the apple of the eye. Huge funding and projects started and that, in turn, started a new wave of algorithms and techniques in applied research. In Figure 3-5 and Table 3-2, different research articles were mentioned, and we have summarized them with some highlighted points in those articles. For example, initially techniques like Hough Transform, Shape Matching, Curve Fitting, EM, Gabor, and Canny filters were prominent. They played a key role in almost every research article and gave reliable and improved results [40].

A new era of CNN, introduced multiple variants of deep learning frameworks. The research in this domain shifted their work that revolved around different architectures of CNN such as FCN, U-Net, FU-Net, and DeconvNet. Different articles have used variants and hybrid versions of these standard networks to improve their results. Using all kinds of imaging modalities with different CNN architectures literature shows good results in terms of spine segmentation and authors have used mainly mean DSC as an evaluation metric for results.

Table 3-2 Summary table of localization and segmentation literature review

#	Author	Year	Pre-Processing	Technique	Detection	Dataset	Results	Evaluation Metrics
1	Brejl and	2000	Manual contouring	Shape-variant Hough and	Thorax Localization	55 MRI Images	1.8 ± 0.6 1.0 ± 0.3 1.8 ± 0.5	Mean Error

	Sonka [41]		and landmarking	Edge-based object		(15 training)		
2	Tezmol et al. [42]	2002	Gaussian smoothed	Customize Hough Transform	Vertebrae Segmentation	50 X-Ray Images	72.06/80 average 4.16°	Mean Orientation Error
3	Xu et al. [43]	2008	9 landmark-point corner guided	DP and PSM	Vertebrae Segmentation	900 X-Ray Images	PSM 85%	Precision TP / (TP + FP)
4	Ribeiro et al. [47]	2010	Manually delineated plateaus setting	180 Gabor Filter Bank and ANN	Lumbar Vertebrae	41 X-Rays Images	0.91-0.92 High Overlap Success Rate	Accuracy
5	Larhmam et al. [49]	2012	Manual ROI Histogram equalization Canny and Sobel	Modified Hough, Template Matching and CLAHE	Cervical Spine Column Localization	200 X-Rays Images	89%	Global Accuracy
6	Rasoulian et al. [50]	2013	GMM and PCA	Cubic spline and polynomial curve	Lumbar Spine Segmentation	32 Images	Distance error 1.38 ± 0.56	Mean point-to-surface error
7	Korez et al. [51]	2016	3D Mesh Shape Model VB	CNN 3D spatial VB Probability Maps	Vertebrae Shape	23 subjects MRI Scans	93.4 ± 1.7 %	DSC
8	Arif et al. [52]	2018	Zero padding Image dimension 100x100	FCN Probabilistic Spatial Regression	Cervical Vertebrae segmentation	26 X-Ray	0.84	DSC
9	Shi et al. [53]	2018	Centerline. intensity	3D U-Net	Spine Localization	61 CT	0.80	Average DSC
10	Lu et al. [54]	2018	U-Net spine-curve fitting	multi-class CNN	Intervertebral Discs	4075 Patients MRI Scans	0.93	Mean DSC
11	Kim et al. [56]	2018	Hough and Canny Edge	Line based and graph cut method	Lumbar Spine	19 MRI Images	90%	DSC
12	Rehman et al. [57]	2019	--	FU-Net Region-based deep U-Net	Osteoporotic	20 CT 25 CT CSI14 & CSI16	92.8 ± 1.9% 95.4 ± 2.1%	DSC
13	Chuang et al. [58]	2019	--	3D U-Net and DeconvNet	Vertebral Lumbar	25 CT xVertSeg .v1	88.4%	DSC
14	Lessmann et al. [59]	2019	Gaussian smoothing	FCN	lumbar spine	15 CT 15 CT	94.9 ±2.1%	Average DSC

15	Chen et al. [60]	2019	--	FCN 3-D HMM	Vertebrae Localization	242+60 CT MICAAI	87.97% 2.56 mm	MIR
16	Liebl et al. [61]	2020	--	Btrfly Net and U-Net	Segmentation	VerSe20 20	91.7%	DSC
17	Liang et al. [62]	2020	--	DABU-Net and DenseMCW1-Net	Segmentation	MRI scans	91.85%	DSC
18	Jun Liu et al. [63]	2021	--	Multi-scale Deeplab V3+ (SDP)	Segmentation	X-ray images	0.93 ± .02	DSC

3.3 Shape Analysis and Cobb Estimation

Measuring the geometrical differences in spine was clinically important, this could provide information to segregate deformed spine from normal. The standard way to measure or track curvature disproportionality was through Cobb angle. Another way to assess spinal cord deformity was using clinical parameter which mostly helped to analyse the morphology of spine. In this section of literature we have selected the prominent work carried out in these two areas. Anitha and Prabhu in [64] proposed an automatic quantification of spinal curvature using 250 radiographs. Initially, they enhanced the input image, then Gradient Vector Field (GVF) Snake methodology calculated the boundary. GVF Snake, or Gradient Vector Flow Snake, is a type of active contour model used for image segmentation. It is an extension of the traditional snake model that uses the Gradient Vector Flow field to guide the contour towards the object of interest. To enhance the boundary morphological operations were used. Hough Transformation calculated the slope of the horizontal lines of boundary.

Sardjono et al. in [65] evaluated multiple techniques, to determine the Cobb angle. The authors underlined Jalba et al. [66] Charged Particle Method (CPM) from 2004, for vertebra edge detection. In CPM, the image is represented as a 2D or 3D grid of points, and each point is assigned a charge based on its intensity value. The charges are then allowed to move under the influence of an electric field generated by the image gradient. To identify S-curve, three parts of the spine in the vertical direction had determined two angles of Cobb, while for C-curve, two parts of the spine had identified a single Cobb angle. Piecewise linear curve fitting method, and polynomial function has determined Cobb angle apex of the curve are identified and marked on the radiographic image. A straight line is then drawn through the upper and lower endplates using a ruler or protractor. The angle between the two lines is measured using a protractor or angle measuring tool. This angle

represents the Cobb angle. In the polynomial curve fitting method, a polynomial function is fitted to the curve of the spine using regression analysis. The upper and lower endplates of the vertebrae at the apex of the curve are identified and marked on the radiographic image. A polynomial function of a specific degree (e.g. second or third degree) is then fitted to the curve of the spine using regression analysis. The angle between the upper and lower endplates of the vertebrae at the apex of the curve is then calculated using the coefficients of the polynomial function. On 36 X-Ray images, R2 was measured with different segments and steps providing satisfactory results.

In [67], [68] and [69] the authors have used different approaches for spine shapes analysis. Pasha et al. [67] have used 103 X-Rays of AIS patients and applied 3D spine model to measure clinical parameters. From T1- L5 vertebral centroids were connected to formulate 3D spine curves. To normalize spine heights Isotropic scaling was used. To merge similar kinds of spines into one cluster Agglomerative Hierarchical Clustering (AHC) was used. Almost 3 anatomical views of the spine were determined in each cluster. Where as in [68], Pastor et al. conducted a study on 232 CT scans with different arbitrary field views over a period of 12 months. The first stage, manual centroid annotation was done. In the second stage, a learning based decision forest method was implemented. Detection procedure was based on Random Regression Forest for localization and identification of vertebrae. A set of features are extracted from the input medical images. These features may include shape, texture, intensity, and gradient information. A set of training data is used to train the RRF model. The training data consists of labelled examples of vertebrae, with each example consisting of a set of features and a corresponding location of the vertebra in the image. At each node of the RRF, a random subset of the features is selected to be used for splitting the data. This helps to avoid overfitting and improves the generalization ability of the model. The RRF model is used to predict the location of the vertebra in the input image based on the extracted features. Voxel-wise operations were applied for the improvement in results achieving the identification rate of 79.6%. Unlike [67] and [68], Vergari et al. in [69] proposed classification technique for the automatic detection for Scoliosis. The dataset originally consisted of 796 radiographs and was augmented up to 2096 images. The classification method was inspired from the architecture of LeNet-5[7]. The LeNet-5 architecture consists of total seven layers, that includes three convolutional layers, two pooling layers, and two fully connected layers. The input to the

[7] Lenet-5 w one of the earliest pre-trained CNN models proposed by Yann LeCun in year 1998

network is a 32x32 grayscale image. The results were further processed through discriminant analysis which improved the accuracy level of correct classification rate up to 96.5%.

Bagus Adhi Kusuma [70] in his research study proposed the early detection of Scoliosis using digital X-Ray images. In pre-processing, X-Ray images were converted into grey scale and seed locations were marked. After that, the inpiut image was divided into 12 sub-images. The median filter and canny detection was used to exyract the boundary regions. Later, center point calculations were carried out using polynomial curve fitting. To calculate of Cobb angle gradient equation technique was applied. In the end, K-Mean clustering played a pivitol role to determine the Scoliosis. Average deviation of proposed procedure was less than 6°.

Pan et al. [71] used two Faster R-CNN models separately that helped in detection and segmention of the vertebral bones and spinal cord from 248 X-Rays images. The measurement of Cobb angle between (multiple superior and interior perpendicular) the cranial vertebrae and caudal vertebrae. Group of all possible angles were calculated, and a highest angle was selected to be the Cobb angle. For evaluations and assessment of system interms of reliability and accuracy, two experienced radiologists helped separately in measuring the Cobb angle manually. Results of these two Faster R-CNN models were compared with manual, achieving intraclass and interclass correlation coefficients of 0.941 and 0.887, respectively.

In [72], Safari et al. developed a semi-automatic approach for the estimation of Cobb angle. In the input X-Ray image ROI was extracted using contrast stretching. The complete spine curvature was determined with help of manual landmarking and then 5-th order polynomial curve fitting was applied. The Cobb-angle estimation is carried out by using a tangent equation. The equation is calculated at the inclination points, which are the angle between two perpendicular lines to the spinal curve. The paper claimed the correlation coefficient between the angle values was 0.81.

In [73], [74] and [75] all have used multiple variants of CNN models for assessment of scoliosis using different datasets of X-ray images. In [73] a new high-precision regression technique, Adaptive Error Correction Net (AEC-Net) was introduced that extracted boundary features which were supported in Cobb angle calculations. The encoder network takes the input image and processes it through a series of convolutional layers. These layers learn to extract features from the input image and encode them in a high-dimensional representation. A boundary prediction network is then applied to the output of the encoder. This network predicts the location of the boundary between different structures in the image. The boundary prediction network is trained to

minimize the difference between the predicted boundaries and the ground truth boundaries. The Angle-Net approach for Cobb calculation was used for curve feature set formulation. Finally, Error Correction Net was incorporated that estimates the output of both networks using extrapolation. The proposed framework attained MAE 4.90. The article [74] used ResNet50 for vertebrae bounding boxes and corner points. The ResNet50 architecture consists of 50 layers, including convolutional layers, batch normalization layers, and fully connected layers. It also includes residual connections, which allow for the efficient training of very deep networks. The input to the network is an image, and the output is a set of bounding boxes and corner points that identify the location and shape of the vertebrae. Cobb angle estimation was done through a tangent equation. Liu et al. in [75] used Deeplab V3+ for segmentation and smallest distance point method for Cobb angle measurements. The performance in the DSC was 0.9379 ± 0.0286 and the correlation coefficient 0.95.

In [76] and [77], both research articles have used Accurate Automated Spinal Curvature Estimation 2019 (AASCE19) dataset for the evaluations of results. In [76] Zhang et al. spinal landmark locations were predicted by using Fully Convolutional Network (FCN). Spinal Landmarks Segmentation Network was used for segmentation and to decrease the complexity, ShuffleNet structures were applied. Cobb estimation technique was selected from literature named as structured support vector regression. The evaluation results were MSE 0.0039 and Mean Correlation Coefficient 0.914 respectively. Cui et al. in [77] attained the Cobb results, Average Mean Absolute Error (AMAE) up to 9.2832° and the SMAPE till 21.675%. The authors utilized U-Net network for segmentation of target area in combination with a convex hull algorithm for corner detection. Cobb estimation was done using the traditional method, which is from determining the marginal vertebrae of Scoliosis.

Comparison of automated spinal curvature estimation algorithms using AASCE19 dataset Wang et al. in [78] evaluated top eight methods of the MICCAI Challenge from 12 teams. The best performing method achieved a Symmetric Mean Absolute Percentage (SMAP) of 21. 71%. In the first phase, PSPNet[8] was utilized to segment vertebral bodies and intervertebral space. The main innovation of PSPNet is the use of a pyramid pooling module to capture multi-scale contextual information. The pyramid pooling module applies pooling operations at different scales to the

[8] Pyramid Scene Parsing Network

feature map produced by the convolutional layers. By applying pooling at multiple scales, the network is able to capture contextual information at different levels of abstraction, which helps to improve its ability to recognize objects and distinguish between different classes. ResNet-101 was applied for feature extraction. In the second phase, Tencent team used almost all recent popular architectures, such as ResNet, DenseNet and EfficientNet to accomplish regression task, and with a combination of all the results generalization error was reduced.

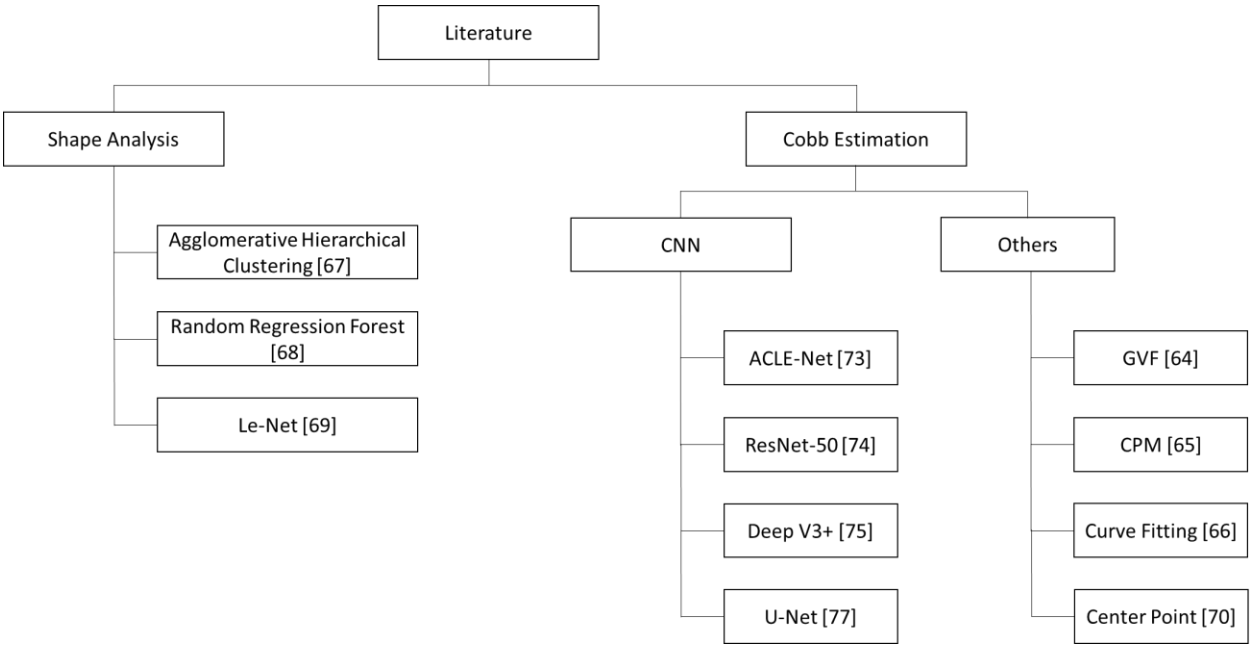

Figure 3-6 Overview of techniques used for shape analysis and Cobb estimation in literature

3.3.1 Discussion

The third section of our research consists on the papers of shape analysis from curvature extraction and Cobb estimation. Challenges and Workshops datasets were used and results evaluations on curvature were done through SMAPE and MAE as shown in Table 3-3. Figure 3-6 shows the overview of literature with techniques used for shape analysis and Cobb estimation. Different segmentation techniques were used to extract vertebrae or multiple regression methods were applied which were used for Cobb estimation. Here the point is worth mentioning that the most common deformity targeted for assessment was scoliosis. Cobb estimation is the main procedure

followed with different methodologies for deformity analysis. The illumination changes in images have yet to be catered for, and still there is room for improvement in results [40].

Table 3-3 Summary table of shape analysis and Cobb estimation literature review

#	***Author***	***Year***	***Technique***	***Diseases***	***Dataset***	***Results***	***Evaluation Metrics***
1	Anitha and Prabhu [64]	2011	GVF Snake and Hough Transform Providing Slope	Curve Extraction	250 X-Ray Images	--	inter/intra observer error.
2	Sardjono et al. [65]	2013	Auto Cobb angle by CPM Piece-Wise Linear Curve fitting	Scoliosis	36 X-Ray Images	0.9124 0.9175	R2 and MAE
3	Kusuma [66]	2017	Canny, Polynomial Curve Fitting and K-Means	Scoliosis	28 X-Ray	5.86°	Average Deviation
4	Pasha et al. [67]	2019	3D Reconstruction of Spine Curve, AHC	AIS	123 X-Ray	44% and 56%	hypo-thoracolumbar kyphotic
5	Pan et al. [71]	2019	Faster R-CNN	Scoliosis	248 X-Ray	2.20° and 2.94	MAD
6	Safari et al. [72]	2019	Manual Landmarking and Curve fitting Cobb Estimated	Scoliosis	14 X-Rays	0.81	Correlation Coefficient
7	Chen et al. [73]	2019	AEC-Net	Scoliosis	581 X-Ray	4.90	MAE
8	Pastor et al. [70]	2020	Decision Forest Morphological Operational Refinement	Vertebrae Identification	232 CT Images	79.6%	Identification Rate
9	Vergari et al. [69]	2020	CNN inspired by LeNet-5	Scoliosis	2096 Radiographs	96.5%	Average Accuracy
10	Alharbi et al [74]	2020	CLAHE, ResNet50	Scoliosis	243 X-Ray	90%	Accuracy
11	Liu et al. [75]	2021	Multi-scale Deeplab V3+ SDP	AIS	157 X-Ray	0.9379 ± 0.0286	DSC
12	Zhang et al. [76]	2021	FCN, SLSN and Heatmap	Challenge	AASCE19	0.0039 0.914	MSE MCC
13	Cui et al. [77]	2021	U-Net, Convex Hull	Scoliosis	AASCE19	9.2832°, 21.675%	AMAE SMAPE
14	Wang et al. [78]	2021	PSPNet, ResNetRegression DenseNet	Challenge	AASCE19	21.71%	SMAPE

3.4 Datasets

Multiple resources of labelled spine datasets are available on SpineWeb; most of their data is composed of X-Rays, MRI, and CT scans. The following datasets are used for evaluation, validation, and comparison of all the experiments.

CSI16

4th International Workshop and Challenge on Computational Methods and Clinical Applications for Spine Imaging, CSI16, held in Athens, Greece. The details regarding dataset is given in Appendix B. CSI16 dataset contains thoracolumbar spine scans which are acquired at a resolution of between 1 to 0.35 mm with Hologic Discovery A DXA scanner. The images are given in both .bmp format and. vtk format. The dataset has in total 303 scans, which are later divided into two partitions. Training set has 287 images, Test data contains 16 images [79]. Figure 3-7 shows a sample from this dataset.

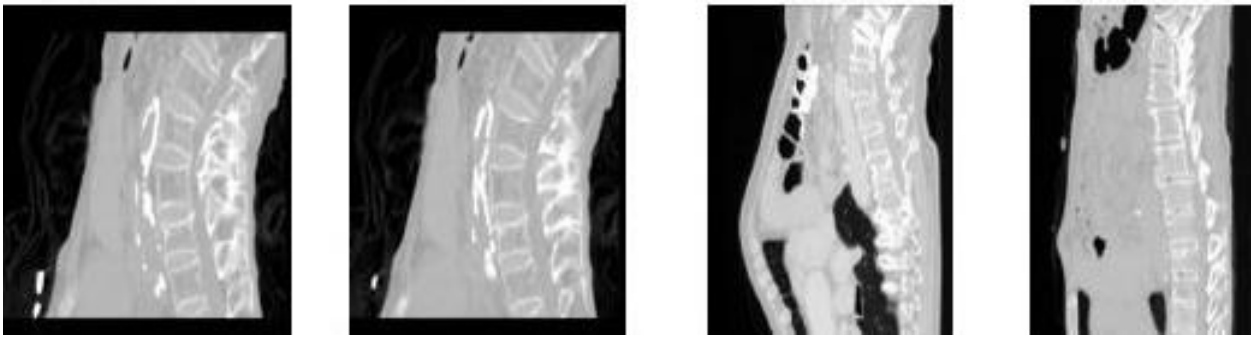

Figure 3-7 Sample images of CSI16 dataset containing CT Lumbar scan in sagittal plane.

AASCE19

The Accurate Automated Spinal Curvature Estimation Challenge was jointly conducted with the conribution of the 2019 MICCAI Workshop on Computational Methods and Clinical Applications for Spine Imaging. The details regarding dataset is given in Appendix B. The dataset provided has a total count of 609 anterior-posterior frontal plane X-Ray images. The publicly available dataset was divided into 3 splits, 477 training images, 70 validation images, and 62 testing images. The single image contains 17 vertebrae from are of thoracic and lumbar spine. Input images format is .jpg with size of 2048 x 1024 [80].

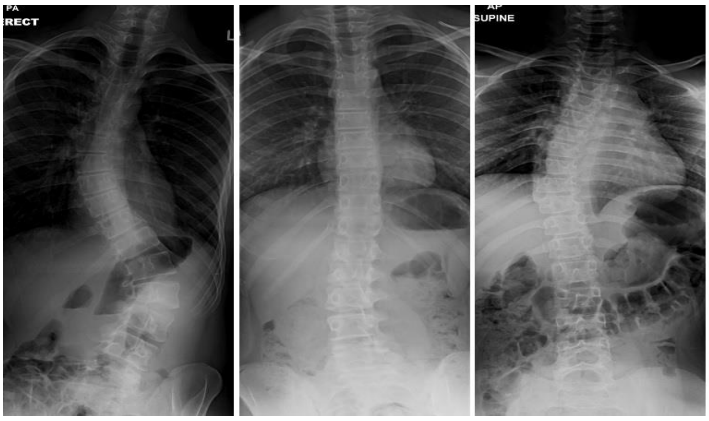

Figure 3-8 Sample images of AASCE19 dataset containing X-Ray images in coronal plane

Mendeley's Data

This data was published in 2019 with contribution of [81], a containing MRI scans of 515 patients who have symptomatic back pain. The dataset was provided with support from Universitas Multimedia Nusantara, Liverpool John Moores University. The details regarding dataset is given in Appendix B. There are a total 48,345 MRI slices in this dataset with image resolution of 320x320 and 320x310 respectively. The image format of MRI scans is .png.

Figure 3-9 Sample images of Mendeley's dataset containing MRI lumbar scan in sagittal plane

The details regarding each dataset is presented in tabular form with types of images, total number of images and the training/testing split that are used in our research are given in Table 3-4.

Table 3-4 Table of dataset

#	Name	Sponsor	Type	Format	Area	Images	Train/ Test
1	CSI16 [79]	Laboratory of Imaging Technologies (University of Ljubljana, Slovenia)	CT Scans	.bmp	Thoraco -lumbar	303	287 /16
2	AASCE19 [80]	London Health Sciences Center	X-Ray Image s	.jpg	Thoraco -lumbar	609	547 /62
3	Mendeley' s 2019 [81]	Universitas Multimedia Nusantara, Liverpool John Moores University	MRI Scans	.png	Lumber	1027	976 /51

3.5 Data Annotation & Labelling

Multiple datasets have been produced by different hospitals and there were multiple challenges conducted to diagnose spinal deformities. During the training phase, data annotation and labelling is required and all the datasets were annotated manually. The details regarding dataset annotation and labelling process are given in Appendix C. A collaborative team consisting of radiologists and researchers provided us with annotation in both coronal and mid-sagittal views. That annotation includes spine measurements, labels for ground truth along with pseudo-coloured ground truth images [82].

The AASCE19 dataset already provided labelled corner points for each vertebra. Further data labelling was carried out with the support of radiologists using Adobe Illustrator. The tool helped us to connect the given corner points and a polygon shape was formulated for mask generation. Data labelling is carried out with the support of an expert radiologist.[9] The details regarding experts and collaborators are given in Appendix C. The Adobe Illustrator tool is used for annotation of vertebrae, center pixel and spine masks. The dataset AASCE19 has input images of size 2048 x 1024. The details regarding tools used for dataset annotation and labelling process are given in Appendix C. Labelling, a cross-platform GUI tool is used to annotate this dataset which saves the file into VOC, XML and ImageNet formats. It is an object detection tool, which creates a rectangle bounding box that can label around the entire vertebrae.

[9] Dr Muhammad Talha, Consultant Spinal Surgeon and Dr Muhammad Babar Khan Consultant Radiologist at Combined Military Hospital, Rawalpindi (Appendex C)

3.6 Research gaps

To identify vertebrae correctly and segment the spine is a crucial part. Publicly available datasets provide clinically significant spinal measurements. The research will enable both medical specialists and researchers in image processing to decrease the variability being posed by manual and semi-automated methodologies. The spinal measurements are considered as one of most important procedure before any surgical intervention procedure hence, the manual or semi-automated approaches creates room to improve and explore this area. Furthermore, the development of an automated analysis tool that involves spinal measurements and disproportionality classification also requires to be necessitated, which can facilitate both radiologists and neurosurgeons. Addressing to bridge the gap, following efforts have been made in this research thesis:

- Most of the work in the literature is carried out on segmentation of each vertebrae
- Conventional methods failed to extract vertebrae in the presence of noise and low contrast.
- Deep learning-based methods mostly tried to segment each vertebrae, which tend to fail in presence of deformed regions.
- In addition to this, automated spinal deformity classification methodologies for all categories are absent in existing work.
- The shape analysis-based scheme, to classify the shape-based difference in scoliosis to assess normal, C and S shape of curvature is one of major gap that needs attention as both curvature shapes define treatment plan of the massage pattern, brace styling and exercises.
- To the best of our knowledge, there is no single framework which is proposed to handle different imaging modalities and clinical parameters related to spinal deformities

These research gaps require a basic framework that takes input images for localization of vertebrae in parallel with a segmentation technique for the spinal cord. In combination with the spinal Cobb measurements assessments and whole spine geometry shape analysis with help of feature set. To address spinal disorder diseases classification, an automated classification module is required that grades the severity of deformity from calculations and estimation of curvature.

3.7 Summary

In this chapter we have discussed the most recent and relevant approaches which are proposed in the literature for localization and segmentation of the spine and the deformity assessment. The literature is discussed in a group-wise manner same as our proposed framework. We get a clear picture from the above literature that mostly publicly available datasets are used for analysis of spinal disproportionality. Multiple types of spinal deformities and their diagnosis are explored through segmentation and regression methods. Similarly, most algorithms focused on segmentation of vertebrae and localization of the spine. Cobb estimation was a prominent method for the analysis of spine curves [40]. To the best of our knowledge, there is no system presented in the literature which addresses all imaging modalities and deformities. Shape based detailed analysis for curvature classification was missing; no feature-based analysis was done on scan level to classify scoliosis into C and S shape. In the light of clinical parameters discussed with radiologist, we decided to focus on morphology of spine for curvature features. The flip approach of vertebrae localization and spine segmentation was adopted as we required midline curvature for shape analysis.

4 Chapter

Vertebrae Localization and Spine Column Segmentation

In the previous chapter, as already mentioned, that the researchers have focused their research work on spinal deformities and their diagnosis through segmentation and regression methods. Commonly different deep learning architectures were used for segmentation of vertebrae. However, clinical parameters studied in the literature and the discussions carried out with domain experts enlightened us to shift the spotlight and focus on morphology of spine. The details regarding experts and collaborators are given in Appendix C. This strategy to upturn the entire procedure and instead of segmentation of vertebrae localization of vertebrae will provide better features in terms of its positioning and center points. For further assessment of curvature, a tidy midline center profile is extracted using segmentation of the whole spinal column. In this chapter, we present the first phase of our methodology for vertebrae and spine column segmentation. The chapter is divided into two sections; the explanation regarding these two parallel streams is elaborated in detail with various steps of the algorithm to be followed.

4.1 Overview

The complex structured interlocking bones that assemble over one another, formulating the spinal column are vertebrae. As discussed earlier in chapter 2, spine deformity may occur due to many reasons, but the increase in severity leads to paralysis. There are many forms of deformed spine; if it gets diagnosed at an early stage, it may revive to its normal form with physiotherapy, and exercise. The accurate localization and segmentation results are the basis for spine curvature deformity analysis. The shape analysis is performed by features extracted from localized vertebrae and segmented spine column. In sagittal plane Cobb estimation is used for deformity analysis. There are some limitations in Cobb estimation method, due to its dependence on vertebral structure and orientation of end plates. Thus, Scoliosis curves; C-shaped and S-shape are mainly focused and are classified using feature set. The proposed system produces an automatic platform, for not only localization, but also classify deformities. Figure 4-1 shows the abstract level of work carried out in the methodology. Details of Module-I are discussed in this chapter. Both streams of the Module-I then contribute for the next section of feature extraction that facilitate shape-based classification which is discussed in upcoming chapter 5.

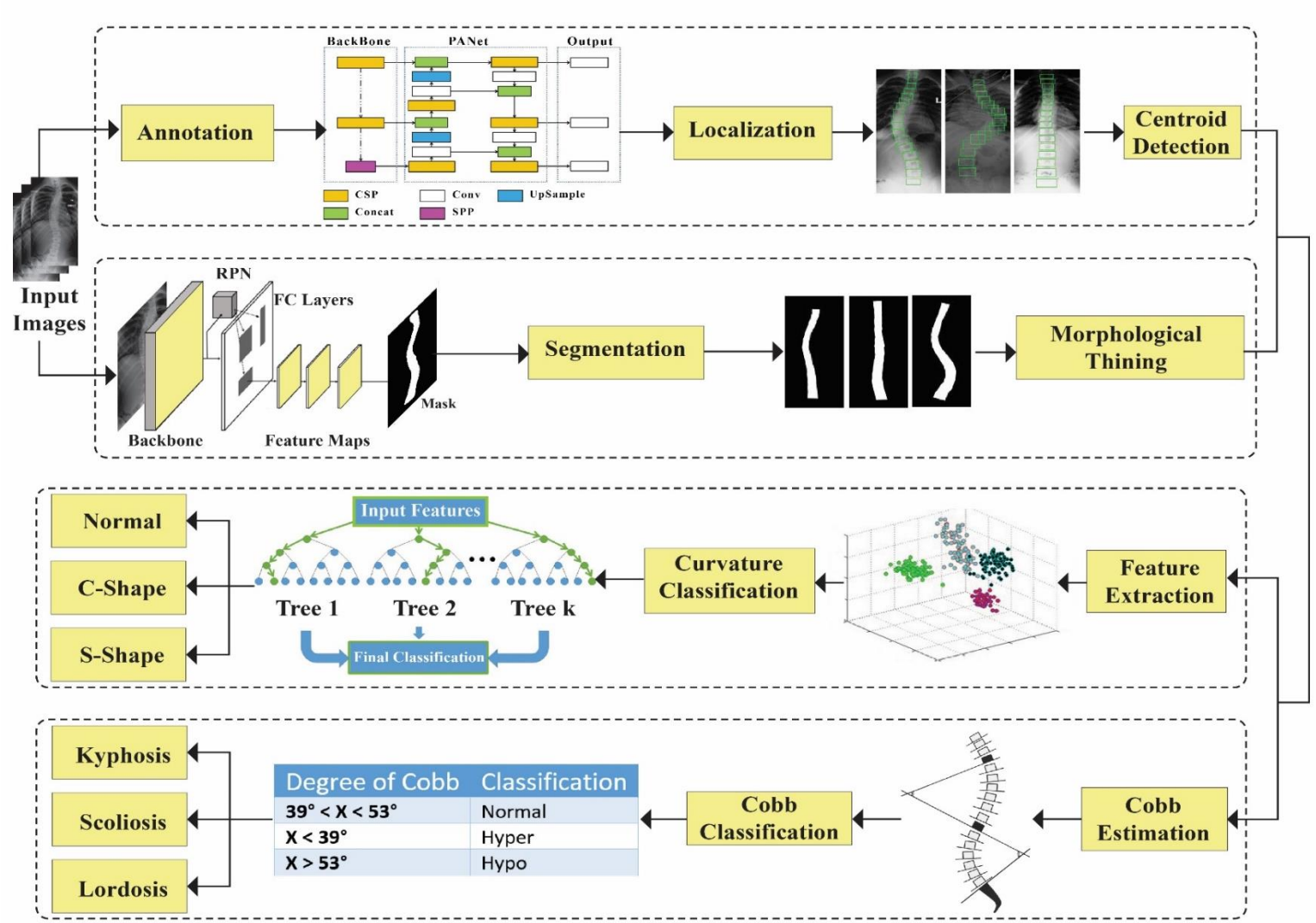

Figure 4-1 Abstract level illustration of our proposed framework

4.2 Proposed Framework

There are two main components of Module I. The first one is localization and segmentation, while the second is shape analysis. A block diagram in Figure 4-2 shows the first module of the methodology. Parallel two streams run in this component; in the localization module the objective is to extract the vertebral regions from the images. In the localization stream, a candidate window moves over the image to vote for vertebra patches. The next step involves an accumulation phase that converts the detected patches into a bounding boxes, these bounding boxes indicates the location of the vertebrae inside the input image. Later, these predicted vertebrae are passed for skeleton extraction. Parallel to localization of vertebrae is spine column segmentation section; the vertebral bones stacked over one another to form whole spine column. Instead of segmentation of each vertebra, we focused our work on segmenting the cord to the optimization level, as it is more effective in shape analysis. For these, multiple popular neural networks are opted from the literature, and a comparative study is carried out to identify the best possible results. The segmented masks are then passed through spine center profile. Both streams of Module-I produce centerline profile extracted images.

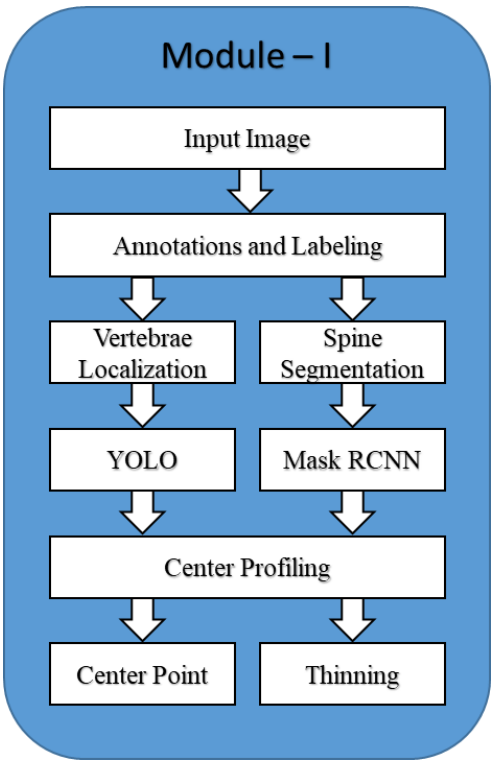

Figure 4-2 Stepwise detailed view of localization and segmentation streams of Module-I

4.3 Vertebrae Localization

Clinically, the precise localization and identification of vertebrae is crucial in digital spinal imaging. The initial spine assessment, disease diagnosis, surgical procedure planning and post-operative recovery analysis depend upon accurate localization. The prime difficulties for an automatic mechanism arise due to smaller ROI, infrequent presence of abnormal curvature, noise in images and surgical implantations. Previous methodologies relied on parametric models only. The performances of such models can significantly reduce for pathological cases. For vertebrae localization, we have opted for the recent approach of instance object detection described below.

4.3.1 Data Labelling & Annotations

In chapter 3, dataset labelling is already discussed for every dataset. For each image annotations were performed for vertebrae in cervical region 8, for thoracic region 12 and for lumbar region 5 and 1 for sacrum region in sagittal image view. The YOLO architecture performs inbuilt augmentation. YOLO format is text file of same naming convention as image, theses files contains the coordinates information of object, along with the height and width of object. Figure 4-3 shows the original image, the bounding mask, the plygon boundary formation for mask, and the binary mask created from the third image respectively.

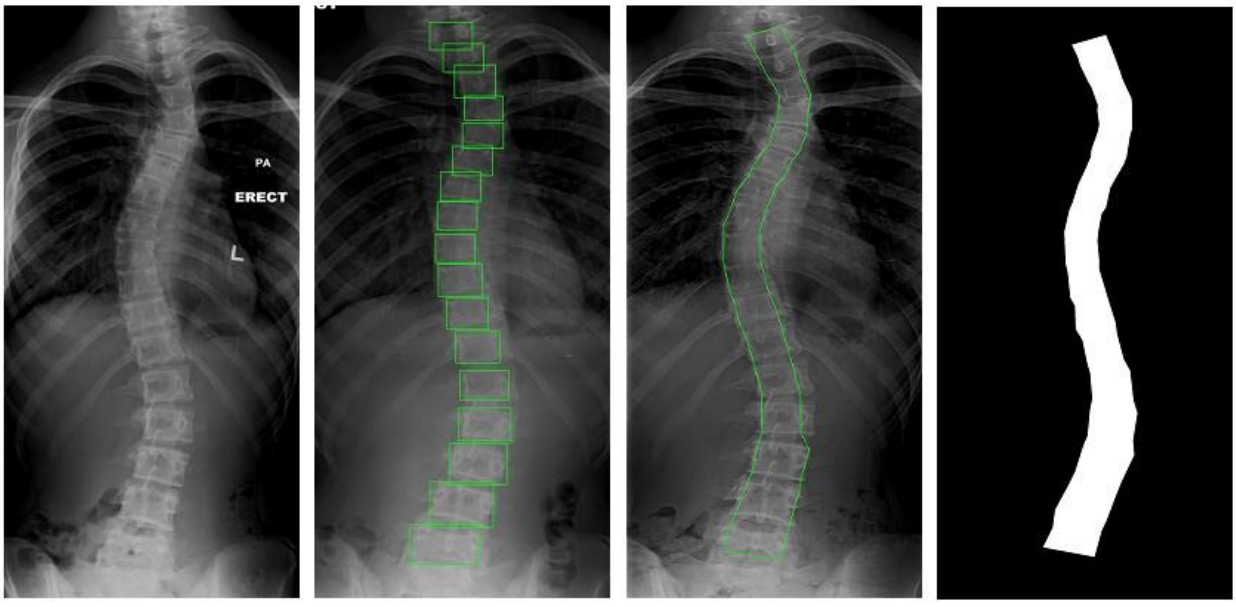

Figure 4-3 From left to right: (a) Original image (b) Bounding mask (c) Polygon boundary (d) Binary mask

4.3.2 Proposed Network Architecture

Joseph Redmon et al. [83] proposed a real time object detection algorithm named as YOLO "You Only Look Once", and it contains a clever concept of a convolution neural network. Unlike traditional object detection algorithms, YOLO does not rely on region proposal methods or sliding windows to detect objects. Instead, it divides the input image into a grid of cells and predicts the objectness score and bounding box coordinates for each cell. YOLO then applies non-maximum suppression to remove redundant detections and returns the final set of objects detected in the image. YOLO has several advantages over traditional object detection algorithms. It is fast and efficient, capable of processing images in real-time on a single GPU. It is also able to detect objects at different scales and aspect ratios within the same image, and can detect multiple objects in a single pass. Since its introduction, YOLO has gone through several updates and iterations, including YOLOv2, YOLOv3, YOLOv4 and YOLOv5, which have further improved its accuracy and speed. YOLO is widely used in various applications, including autonomous vehicles, security systems, and robotics.

The algorithm first explores the concept of image classification, explaining what is in the image. Object localization is a second stage, which allows to locate the objects in real-time that are present in the image. The final stage creates a bounding box around the object located, for instance segmentation. To predict bounding box the network extract features from the whole image. It can also predict multiple bounding boxes for different classes simultaneously in the same image. In YOLO architecture the input image is divided into S × S grids. For candidate Bounding box, if the object center lies into a grid cell, that grid cell is responsible for detecting that object. The bounding box contains 5 parameters of predictions that are x, y, w, h, and confidence score. The x and y are coordinates representing the center of the box. The w and h are width and height relative to the entire image. For each grid cell that predicts B bounding boxes, confidence scores are calculated. This confidence score explains how much the model is confident that the bounding box B contains an object.

In our research, we have adopted the YOLOv5 version, it is fifth variant of the YOLO family, which contains almost twenty-four convolutional layers, followed by two fully connected layers. The algorithm simply uses reduction layers of 1×1 accompanied by 3×3 convolutional layers. The initial learning rate is 0.01 reaching to the final one cycle learning rate of 0.2. The number of

anchors is 3 and the model adopted the pre-trained weights of YOLOv5s. Figure 4-4 describes the architectural view of YOLOv5. This newest version of YOLO was released by Glenn Jocher [81].

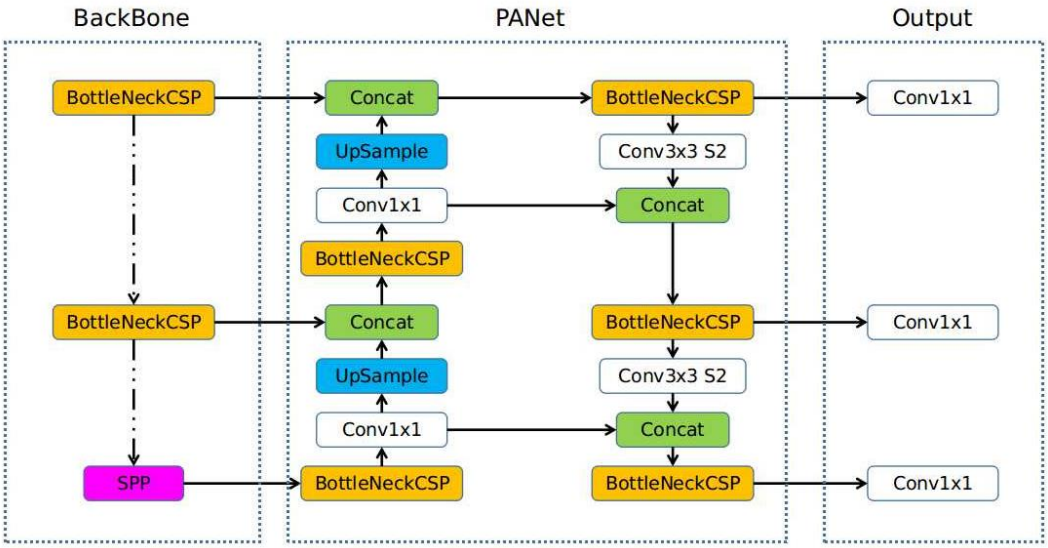

Figure 4-4 Detailed three-staged overview of localization algorithm of YOLOv5 architecture [84]

YOLOv5 is written in the PyTorch framework, very lightweight and easy to use. It introduces auto-anchoring step, which includes uploading a custom dataset and start training. To make it memory efficient, the image size remains the same and scaling augmentation is done through feed transformation. It creates. yaml format file for model configuration. This file specifies the different layers of the network and then it multiplies those by the number of layers in the block. There are three stages of this architecture.

1. **BackBone**: This stage is responsible for extracting feature maps from the input image. YOLOv5 uses a modified version of the CSPDarknet53 architecture as its backbone network, which consists of a series of convolutional layers with varying filter sizes and depths. includes cross stage partial network into darknet to reduce FLOPS[10]. This step not only decreases the model size but also makes sure to achieve speed and accuracy of inference.

[10] Floating point operations per second

2. **PANet**: The neck network is responsible for combining the feature maps from the backbone network into a set of higher-level feature maps that are more suitable for object detection. YOLOv5 uses a Feature Pyramid Network (FPN) as its neck network, which uses lateral connections to combine feature maps of different resolutions. In addition, with FPN[11] low level features are propagated. Adaptive pooling link-ups the feature grid and other features, the network selects the useful features.
3. **Output:** Head network: The head network is responsible for predicting bounding boxes and class probabilities for detected objects. YOLOv5 uses a novel anchor-free approach called YOLOv5 Head, which directly predicts the coordinates of the bounding boxes and the class probabilities without using predefined anchor boxes. The head network also includes a series of convolutional layers and upsampling layers that increase the spatial resolution of the feature maps before making the final predictions.

This three-stage architecture of YOLOv5 allows it to achieve high accuracy and speed for object detection tasks.

Table 4-1 Parametric values of YOLOv5 architecture

Parameters	**Values**
Learning Rate	0.01
Weight Rate Decay	0.0005
Momentum	0. 937
Batch Size	1
Number of Iterations	300
Number of anchors	3
Anchor size	[149,82, 160,104, 214,78] [207,105, 196,130, 265,110] [244,142, 338,132, 324,178]
IoU training threshold	0.20
Final One Cycle Learning Rate	0.2

[11] Feature Pyramid Network

In Table 4-1 we have presented the parametric values of YOLOv5s architecture. The parameters are selected empirically; learning rate of 0.01 is used in training, it decides the influence of current weights in the next step. On the other hand, to regularize the network value of weight rate decay is 0.0005. As the dataset was small so batch size was fixed to 1. The YOLOv5 architecture suggests some parameters for customize dataset, such as the number of iterations to be set as 300, no of anchors to be 3. Yolov5 has introduced an auto-anchoring step for customise dataset it will automatically check anchors and after comparing the algorithm will start training new anchors automatically. In YOLOv5 data augmentation using mosaic data loader is done. The self-augmentation block helps the network to work even for small datasets. The decrease in inference time of the models is due to PyTorch framework. The framework allows to reduce floating point precision in training and inference in half.

4.3.3 Experiments and Metrics

To evaluate vertebrae localization performance, a quantitative metric that is mAP is used (Eq 4.1). It is the average precision score for multiple classes, where precision is the fraction of true positive among all predictions for a given class, and recall is the fraction of true positive among all ground-truth objects for the class. Another evaluation metric is the Intersection Over Union (IOU) (Eq 4.2). It measures the similarity between the predicted bounding box/segmentation mask and the ground truth bounding box/segmentation mask by calculating the ratio of the area of intersection between the two and the area of their union.

$$mAP = \frac{1}{n}\sum_{i=1}^{n} APi \tag{4.1}$$

$$IOU = \frac{area(intersection)}{area(union)} \tag{4.2}$$

In the following Figure 4-5 on AASCE19 dataset, the YOLOv5 results are presented by calculating intersection over union of the ground truth compared with predicted bounding boxes. The figure clearly illustrates that there is minor difference in the predicted bounding box as compared to the ground truth.

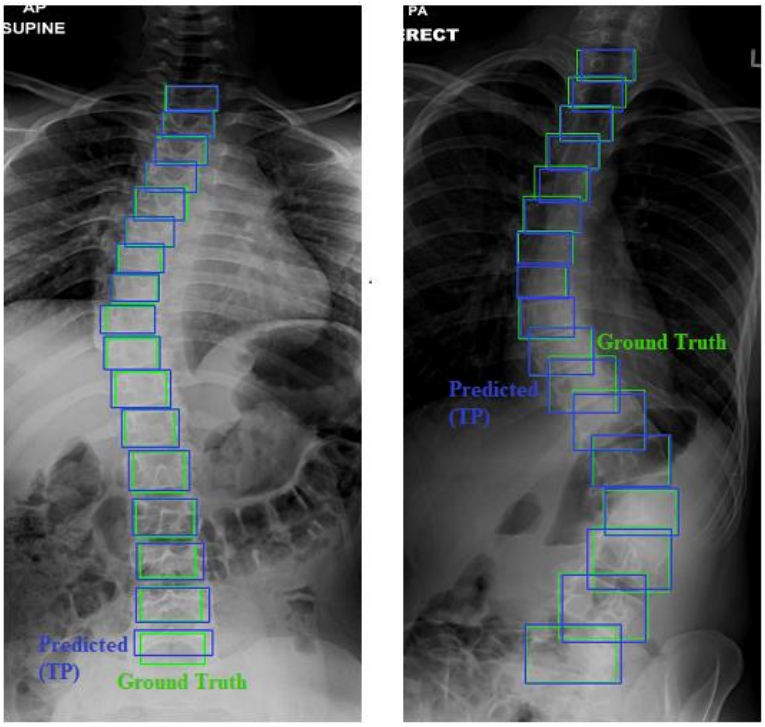

Figure 4-5 Comparison of YOLO results: ground truth vs. predicted vertebrae for AASCE19 dataset

4.3.4 Results

The experimental results show that the YOLOv5 has a high ability to detect vertebrae almost on all datasets. The speed of detection is higher, and the mean average precision metrics over the test dataset is 0.94 at the 0.5:0.9 IOU threshold reported for the YOLOv5 algorithms for AASCE19 dataset. The Mendeley's dataset has better results of mAp of 0.97 at the 0.5 IOU threshold and for CSI16 results of mAp of 0.95, respectively. If the same network/method is further improved, it can increase the accuracy at significant level. The training took approximately 30 to 36 hours on NVIDIA GeForce GTX 1060 6GB. The details regarding tools are mentioned in Appendix C. The following Table 4-2 shows the mAP results of YOLOv5 on all three datasets.

Table 4-2 mAP score of YOLOv5 on AASCE19 and Mendeley's dataset

#	Datasets	Image Type	mAP
1	AASCE19	X-ray	**0.94**
2	Mendeley's Data	MRI	**0.97**
3	CSI16	CT	**0.95**

In the Figure 4-6 the detail graphs on AASCE19 dataset is presented here (a) represents predicted Box that is bounding box regression loss (b) represents confidence of object presence termed as

objectness loss (between 0 and 1) (c) and (d) represent the Recall and Precision values of YOLOv5s during training with increasing epochs.

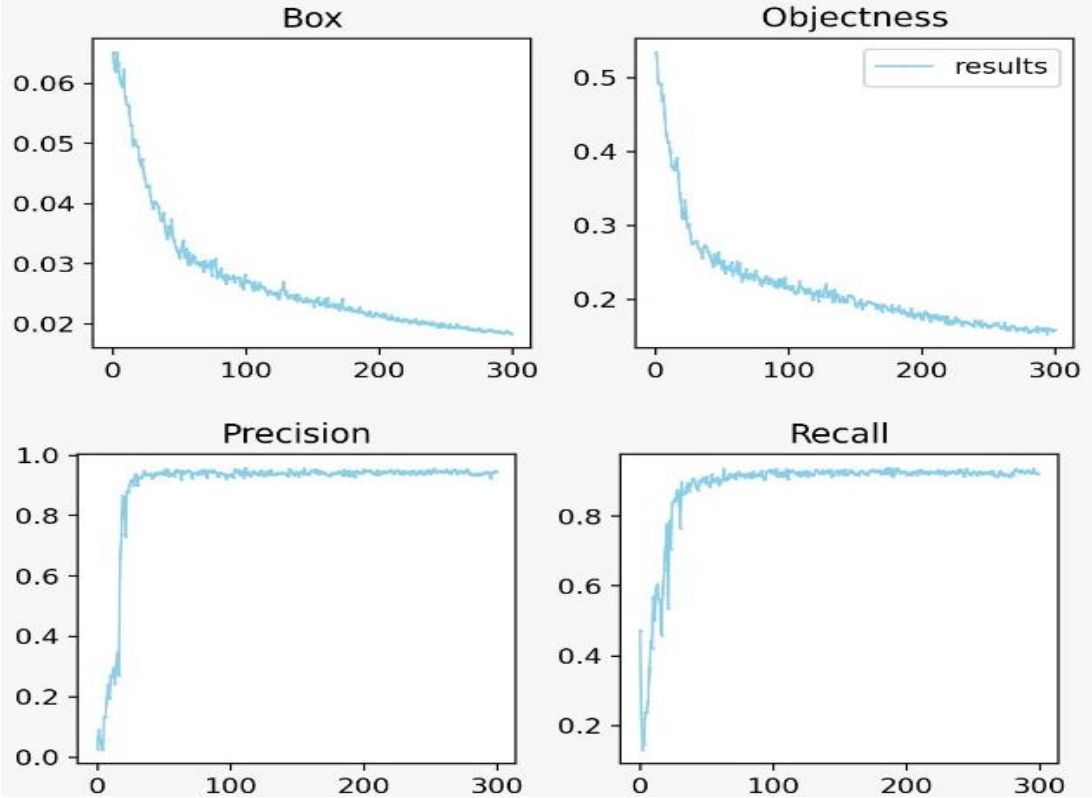

Figure 4-6 Graphs of YOLOv5 presnting box loss, objectness loss, precision and recall

The vertebra localization results on AASCE19 dataset in the form of image collage is presented in Figure 4-7. In the first column the original image is shown; the second column has ground truth, the third shows Heatmap, and in the last column predicted bounding boxes using YOLOv5 are shown. Here, the heatmaps show the confidence of proposed model for vertebrae localization. The figure clearly shows that the model is putting more attention towards the locations where vertebra exists. These are internally used by the model to further localize the vertebrae. Comparison of results of different models on Mendeley's Dataset is presented below in Table 4-3. This table illustrates the comparative analysis of different object detection models. Here, in results YOLOv5 has the highest value of mAp, which means it performace is better in comparison with other object detectors.

Table 4-3 Comparison of results of different models on Mendeley's Dataset

#	Object Detection Models	mAP
1	R-FCN	0.894
2	SSD513	0.925
3	FPN FRCN	0.942
4	YOLOv3	0.917
5	**YOLOv5**	**0.975**

The selection of YOLOv5 was not random we have compared YOLOv5 with other object detection models. Region-based fully convolutional network (R-FCN) In R-FCN, the input image is first passed through a convolutional network to generate a feature map. A Region of Interest (RoI) pooling layer is then applied to the feature map to generate fixed-size feature vectors for each object proposal. These feature vectors then generate class scores and refine the object proposals. It achieved 0.894 mAP value to detect the lumbar vertebrae. Single Shot MultiBox Detector with a 513x513 input image size (SSD513) is an extension of the original SSD architecture, which is a one-stage object detection framework that uses a single deep neural network to generate object proposals.

On Mendeley dataset it has achieved mAP up to 0.925.The mAP value of 0.942 is obtained by using the FPN FRCN, which is the second highest value in Table 4-3. FPN is a network architecture that aims to improve object detection performance by providing a multi-scale feature representation of the input image. FRCNN, on the other hand, is a two-stage object detection framework that uses a region proposal network (RPN) to generate object proposals, and then applies a separate classifier to each proposed region to predict the class and location of the object. YOLOv3 is the third version of the YOLO family, from the statistical evaluations it is believed that v3 is three times faster as compared to SSD and it has achieved 0.917 mAP in detecting the vertebrae.

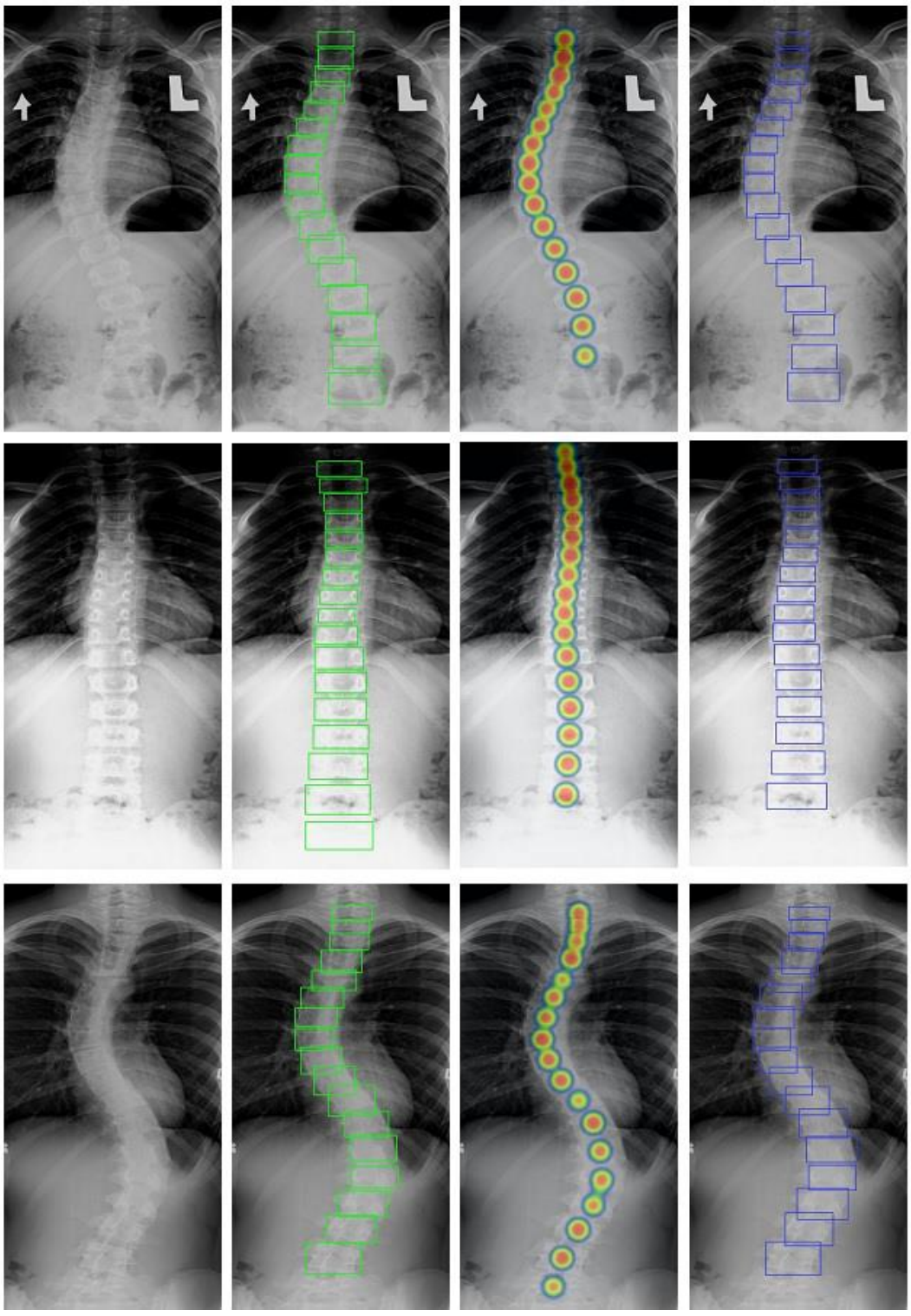

Figure 4-7 The vertebrae localization results. From left to right: a) Original image b) Ground truth c) Heatmap d) Predicted bounding boxes

In Figure 4-8 Mean and STD of Euclidean distance between ground truth and predicted center points is calculated for AASCE19 dataset. The ED is simple straight line distance between centers of manually extracted vertebrae and predicted vertebrae. The distance distribution in case of AASCE19 dataset is not normally distributed where we have certain examples in the dataset having relatively large center distances in comparison mean center distance.

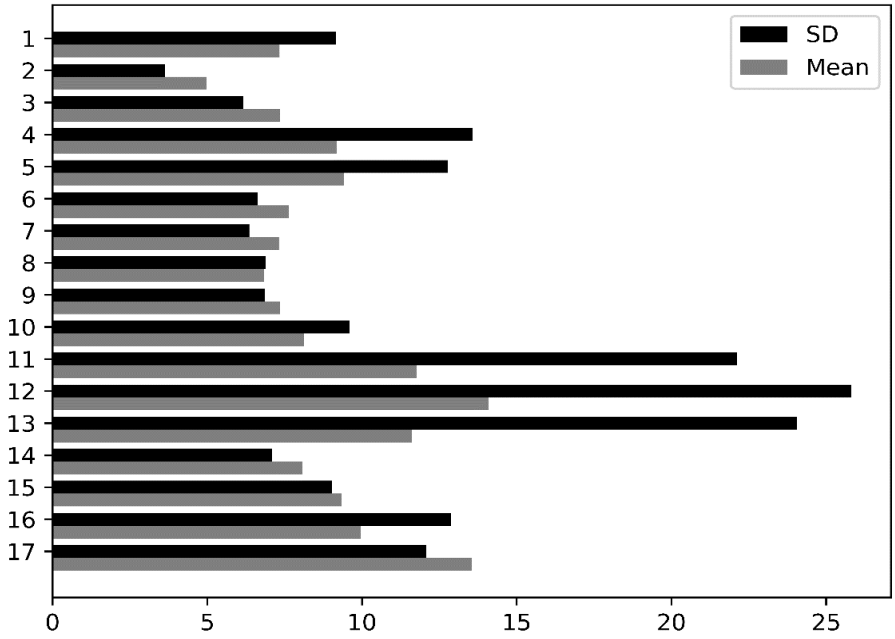

Figure 4-8 Mean and STD of Euclidean distance for Center Points of AASCE19 dataset

This effect can be seen from above figure where we have relatively large STD in comparison to mean for certain vertebrae. In order to show the distribution of distances for different vertebrae, we have also added the box plots as shown in Figure 4-9.

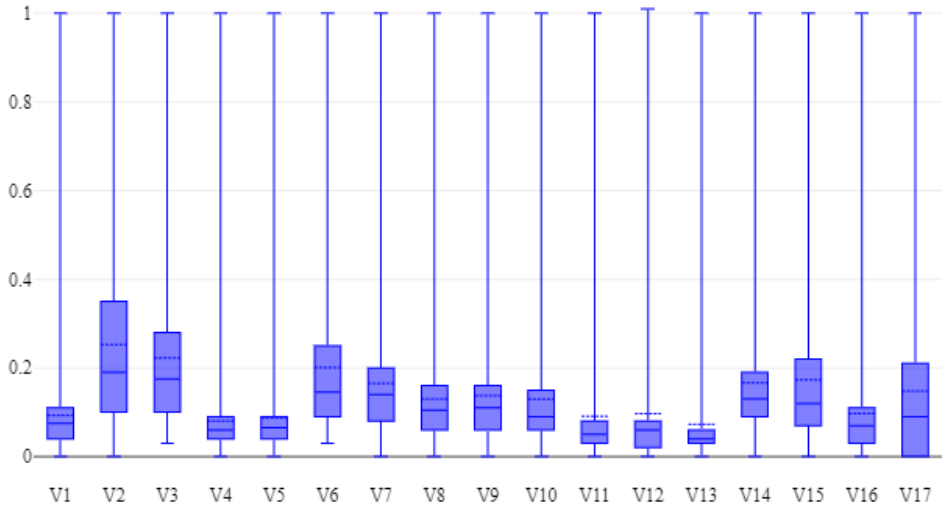

Figure 4-9 Boxplots of all seventeen vertebrae center points of AASCE19 dataset

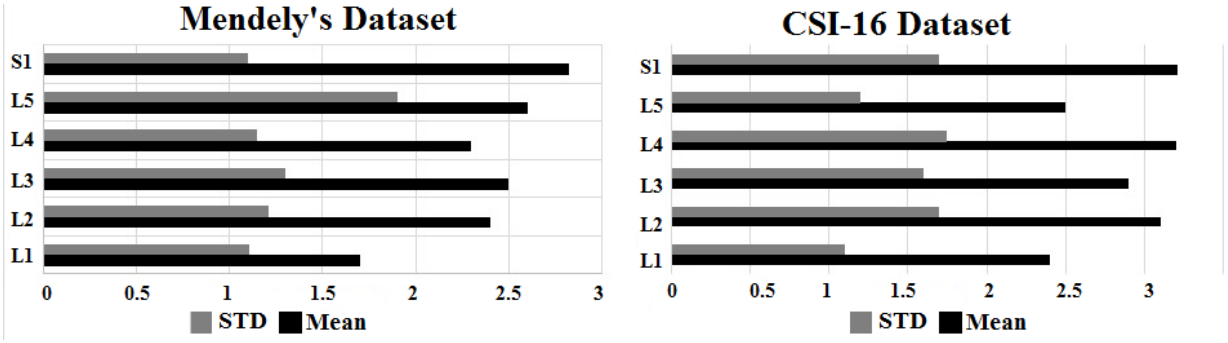

Figure 4-10 Mean and STD of Euclidean distance for center points of Mendeley's and CSI-16 dataset

Similarly, Figure 4-10 shows mean and STD distance error for Mendeley's and CSI16 datasets. It is clear from Figure 4-8 and Figure 4-10 that mean distance between original and predicted vertebrae centers are 2.3 for Mendeley's, 3.7 for CSI16 and, 9.05 for ASSCE19 datasets respectively. The results clearly shows values for each vertebrae; this indicates that the mean values are less as compared to standard deviation.

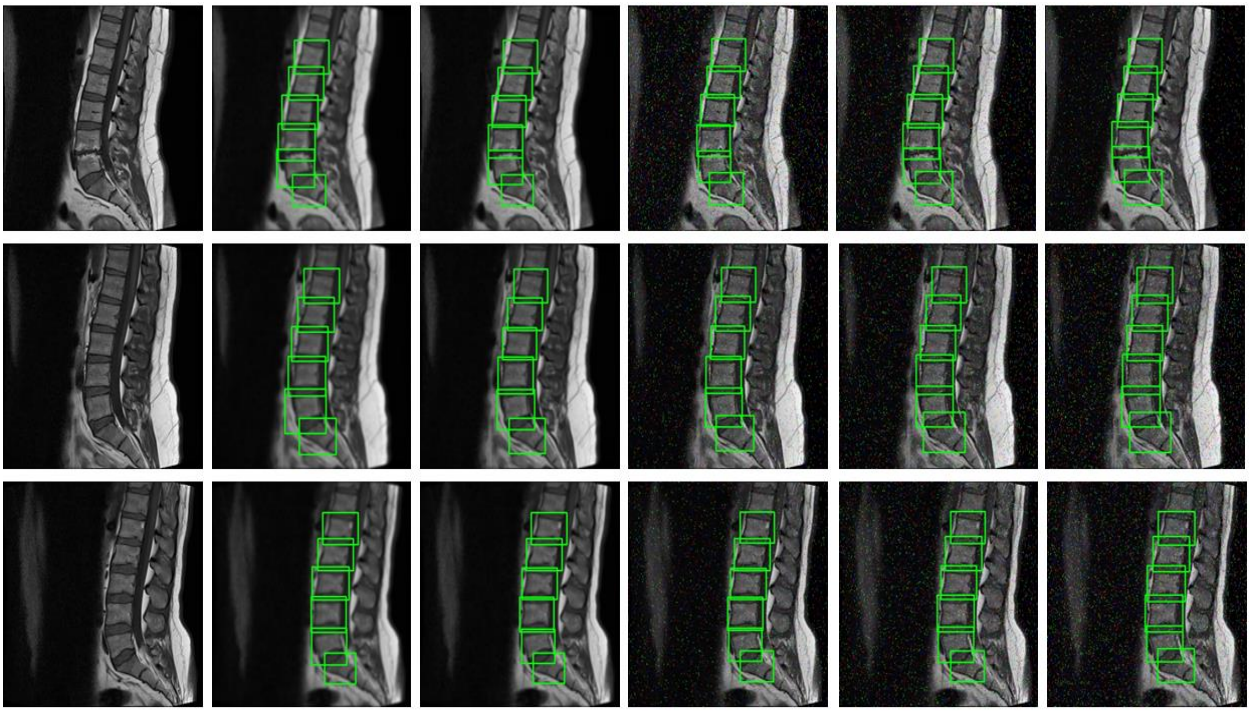

Figure 4-11 Noise based localization results of YOLOv5. From left to right: (a) Original Image, (b) Gaussian noise with sigma 1.5, (c) Gaussian noise with sigma 1, (d), (e) and (f) Salt and Pepper noise with densities 0.02, 0.03 & 0.05

For robust extraction of vertebrae, we aim to utilize robust localization algorithm that work well even in the presence of noise. As the medical imaging modalities have three common types of noises the one being speckle noise, which is basically random fluctuations in the return signal from an object. The second type is technical noise which arises from the difference in scanning procedure; the third one is biological noise which arises in image acquisition such as patient movement during projection causes blurriness in images [85]. To further elaborate robustness of our proposed framework, noise-based results of the YOLOv5s are illustrated in Figure 4-11. We have added Gaussian noise to cater the biological and techno noise and Salt & Pepper noise to address speckle noise for the experimentations. The results clearly show outstanding performance of YOLOv5 architecture.

The effect of noise is also calculated quantitatively for all three datasets and the Table 4-4 shows the mAP results of YOLOv5 on all three datasets with varying noise densities. It is clear from the results that the model shows quite robust results against the addition of noise even with large noise densities.

Table 4-4 Effect of Gaussian noise addition on vertebrae localization in terms of mAP score on AASCE19 and Mendeley's dataset with varying noise densities (d)

#	Datasets	Image Type	mAP			
			d=0.02	**d=0.03**	**d=0.05**	**d=0.07**
1	AASCE19	X-ray	0.94±0.02	0.93±0.025	0.93±0.025	0.90±0.04
2	Mendeley's Data	MRI	0.97±0.03	0.97±0.03	0.96±0.03	0.94±0.05
3	CSI16	CT	0.95±0.03	0.94±0.035	0.94±0.035	0.92±0.05

For the statistical evaluations of the proposed technique, we have conducted Pearson correlation and t-test. Figure 4-12 and Figure 4-13 show that there is high a correlation between original locations of vertebrae and the ones detected through proposed technique. Same is evident through t-test which provided a *p-value* of 0.742×10^{-8}.

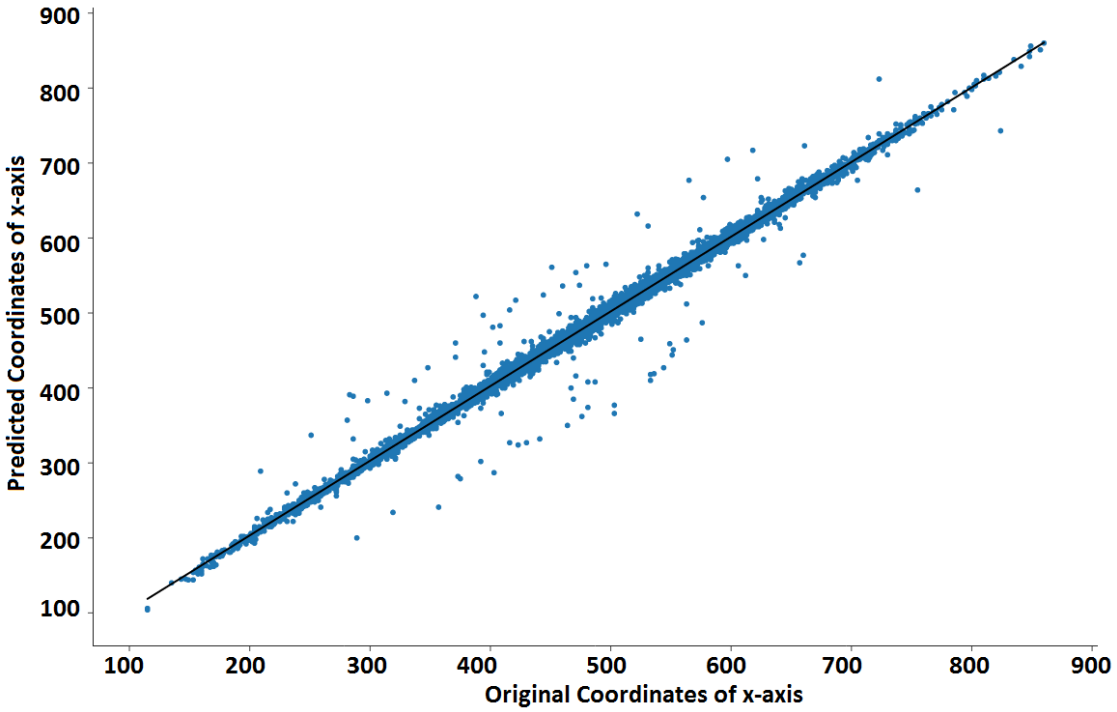

Figure 4-12 Pearson correlation between x coordinates of actual and detected vertebrae

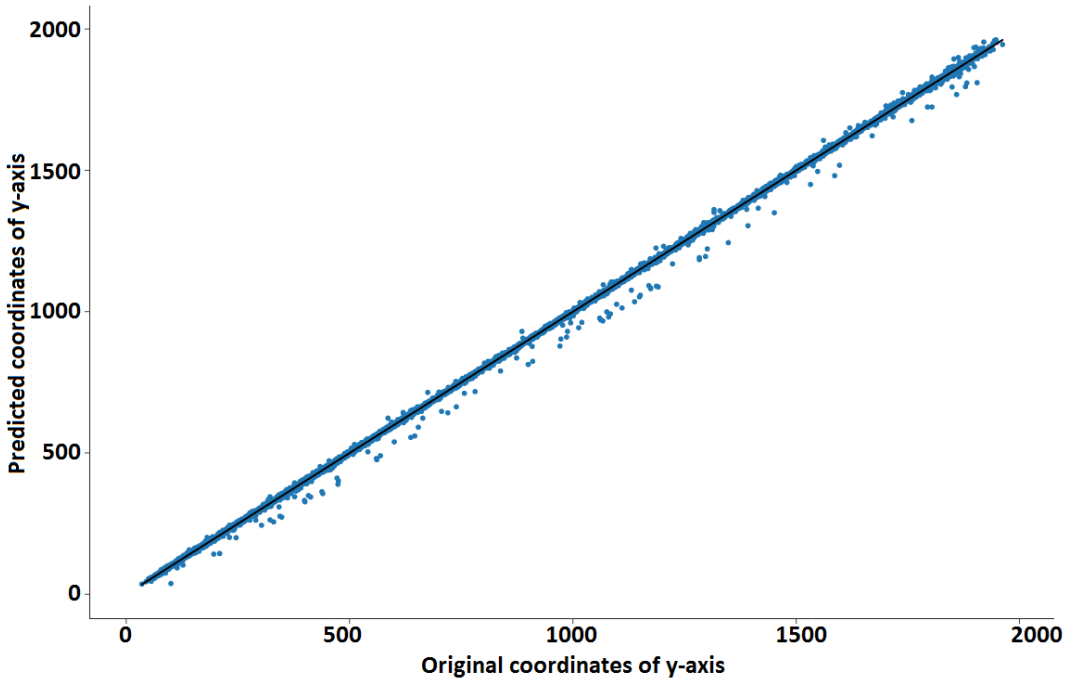

Figure 4-13 Pearson correlation: between y coordinates of actual and detected vertebrae

4.4 Spine Column Segmentation

Meticulous spine column segmentation from medical imaging plays a pivitol role in CAD Systems as it is used to assist clinical specialists for differential diagnoses of spinal diseases such as degenerative disc, Kyphosis, Lordosis, Scoliosis, and spondylolisthesis[12]. Furthermore, it can also be used as an input ingredient for the shape analysis and classification modules. However, bone anatomy in medical imaging has a high contrast rate. But due to unique bone patterns and boundaries of the vertebrae, its identification is considerably a challenging task. To review and evaluate the different segmentation techniques, this section is further divided into multiple CNN techniques. The prominent CNN techniques with their detailed architecture are presented in the following section.

4.4.1 Mask RCNN

Mask RCNN is a deep region-based neural network for object instance segmentation. Instance segmentation, provides correct detection of the objects in an image, later it also perform segmentation of each instance. Therefore, it combination of both object detection and object classification framework. He et al. [86] proposed Mask-RCNN, which is an enhancement of faster RCNN. Fast R-CNN, the whole image is loaded and passed it to several convolutional and max pooling layers which generates a conv feature map. In the second module, instead of selective search like Fast R-CNN, the Faster R-CNN detector uses Region Proposal Network (RPN). The feature map is passed to small RPN in order to produce region proposals. This method introduces a concept of pre-defined anchor boxes of k sizes. These anchor boxes have location and scale relative information about the image. This concept speeds up the process of detection, and it produces output with k number of bounding boxes. Later, ROIAlign trick is used in pooling layer to fix reshaping of bounding boxes, then finally, it uses a fully connected layer to classify objects. Mask R-CNN builds on the Faster R-CNN object detection algorithm by adding a parallel branch for predicting object masks in addition to the bounding boxes. This branch is used to predict the pixel-level segmentation mask for each object instance in the image. The model is trained on a dataset of images and their corresponding object annotations, which include class labels, bounding

[12] Spondylolisthesis is vertebral disease cause back ache to occur due to vertebral bone slips out of alignment.

boxes, and masks. In the first step, it generates a proposals for ROI in the form of a bounding box from the input image. In the second step it refines the bounding box and generate mask at pixel level of the object. All the convolutional layers are of 3×3 size, except the output which is of 1×1 size, deconvolutional layers are of 2×2 size with 2 stride, and activation function ReLU is used in hidden layers. During inference, the model takes an input image and outputs a set of bounding boxes, class labels, and masks for each object detected in the image. This makes Mask R-CNN well-suited for tasks such as instance segmentation, where the goal is to identify and segment each individual object instance in the image. Mask R-CNN has achieved up to the mark performance on several benchmark datasets, including COCO [13](Common Objects in Context) and Pascal VOC[14] (Visual Object Classes). It is widely used in various researches and applications, such as robotics, autonomous driving, and medical imaging.

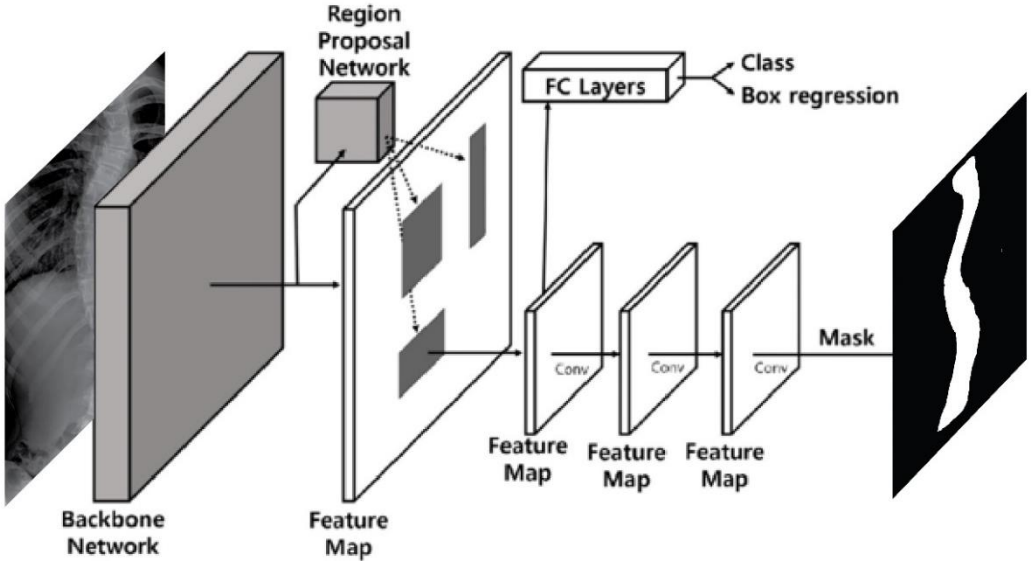

Figure 4-14 Detailed architectural overview of segmentation algorithm Mask RCNN [87]

Figure 4-14 shows the detailed architecture of the Mask-RCNN network and the Table 4-5 shows the list of parameters along with their assigned values in the methodology. In the architecture of

[13] COCO is a huge dataset containing more then 330,000 images with up to 2.5 million object instances labeled across 80 object categories.

[14] Pascal VOC, is an older dataset that was first introduced in 2005 and has since been updated several times. The dataset contains around 20,000 images across 20 object categories.

Mask R-CNN, hyper-parameter tuning is time-consuming as multiple attempts are carried out to manually tune hyper-parameters. A lot of work has been done to find optimal values for, especially for learning rate and momentum. In addition to this, no work has been done to investigate automatic tuning of hyper-parameter tuning.

Table 4-5 Parametric values of Mask RCNN architecture

Parameters	**Values**
Learning Rate	0.001
Weight Rate Decay	0.0001
Momentum	0. 9
Batch Size	1
Number of Iterations	50
Number of anchors	5
Anchor size	[32,64,128,256,512]
RPN Anchor Ratio	[0.5,1,2]
No of Classes	2
Pool Size	7

Other Neural Networks

The literature identified popular segmentation neural networking models for medical image segmentation. From these four of them are selected on basis of their high accuracy. These networks are tested on a dataset a comparative analysis is carried out, and the study results are explained. Figure 4-15 explains the architectures of other neural networks that were opted for comparative study a) FCN for 8, 16 and 32s, (b) SegNet, and (c) U-Net. Input to model indicates the image, whereas Conv indicates the convolution layer in combination with both batch normalization and rectified non-linear functions. The rectanglular labels represent the output after max pooling or the up-sampling method. The symbol "+" indicates concatenation of features.

4.4.2 U-net

The size invariant network accepting all size images is U-Net architecture [88]. As the name explains, the structure of network, it is shaped as U with a total of 23 convolutional layers. The

contracting path of the U-Net architecture helps in extraction of high level features. It consists of several convolutional layers with max pooling operations, which reduces the spatial resolution of feature maps while escalating the no of channels. The left part is contracting, and the right part is an expansion path. The U-Net architecture expansive path involves several up-sampling layers with convolutional layers, which uniformly increase the spatial resolution of the feature maps while decreasing the no of channels. This helps to generate a high-resolution segmentation map that corresponds to the input image. Input image is entered to a block that contains two convolutional layers with kernel of 3x3 size with Adam activation functions, escorted with max pooling. Due to max pooling of 2x2 and stride 2 decreases the size of feature maps, increasing the number of feature channels. Each iteration is concatenated with a parallel side of the expansion iteration which is branched for up sampling. The last layer is of 1x1 size that produces the desired no of classes. This architecture does not have any fully connected layers, and it allows for seamless segmentation. Total four iterations of up-sampling inclusive of 2 blocks of convolution layers accompanied with max-pooling is applied. When the plateau appeared in the model's accuracy, it was stopped for further iterations.

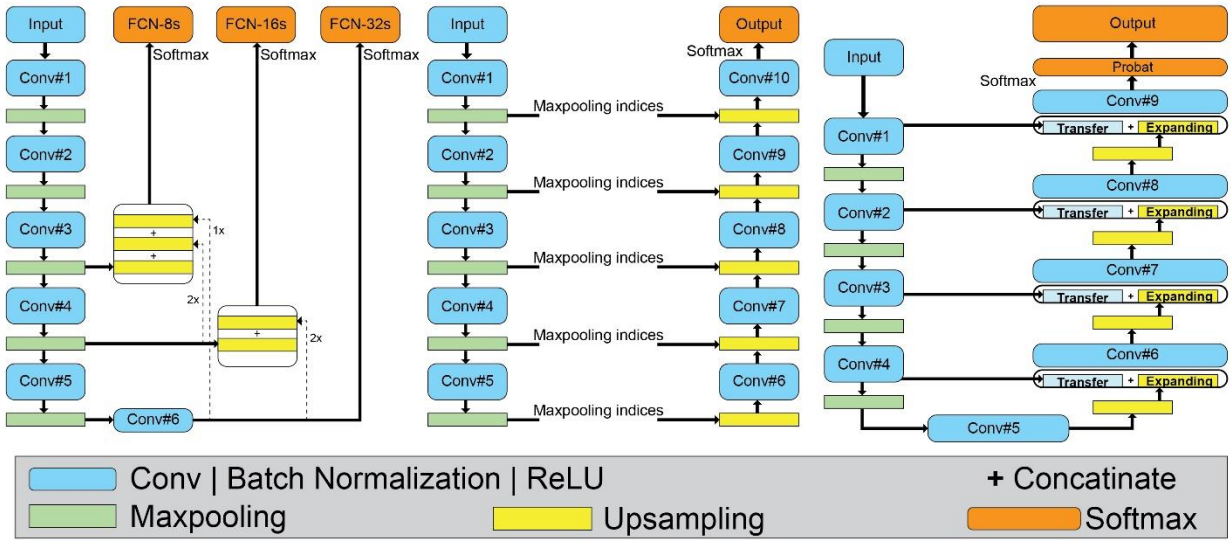

Figure 4-15 Architectures of other Neural Networks. From left to right: (a) FCN for 8,16 and 32s (b) SegNet and (c) U-Net.

4.4.3 FCN

FCN stands for Fully Convolutional Network, which is a deep learning architecture used for image segmentation. FCN [89] is a type of network that utilizes hierarchical features. CNN works with pixel-to-pixel semantic segmentation. The connected layers require input with a fixed size, FCN is introduced to connect CNN. FCN has dense prediction and produces output in the same dimension. It has in total of six convolutional layers of any size, in the initial stage, the dimension remains the same but in the final sixth stage the input size decreases to 1x32 paramount for dense prediction layer along with up-sampling. The pivotal factor for FCN is its size invariant behaviour, but the network is computationally expensive as it has several floating-point operations that are necessary to process. The FCN architecture consists of an encoder network, this part is composed of multiple convolutional and pooling layers, and a decoder network, is composed of multiple up-sampling and convolutional layers. The encoder network extracts high-level features from the input image, while the decoder network converts these features back into a segmentation map with the same spatial resolution as the input image. In addition to the encoder and decoder networks, FCN also includes skip connections that connect corresponding layers between the encoder and decoder networks. These skip connections help to preserve spatial information and fine-grained details that are lost during the down-sampling operations of the encoder network.

4.4.4 SegNet

Badrinarayanan et al. [90] introduced an architecture that was mainly formulated for semantic segmentation. It basically embraces the encoder-decoder framework. In the encoder-decoder architecture there are two major components. The first component is an encoder network that has a deconvolution and an up-sampling layer. The encoder network is composed of several convolutional layers with max pooling, which extracts high-level features from the input image while reducing the spatial resolution of the feature maps. The decoder network then up-samples the feature maps back to the original image resolution using a pooling index obtained during the max pooling operation in the encoder network. One of the unique features of SegNet is that it includes skip connections, similar to U-Net and FCN, which connect corresponding layers between the encoder and decoder networks. However, SegNet uses max pooling indices to guide the up-sampling in the decoder network, which allows it to reconstruct the object boundaries more accurately. Another unique feature of SegNet is that it includes a trainable softmax layer at the end

of the decoder network, which produces a probability distribution over the different classes of the segmentation task.

4.4.5 Experiments and Metrics

To evaluate a standard machine learning model, our predicted results are split into four categories: true positives (TP) rightly identified spine pixels, false positives (FP) spine pixels termed as background, true negatives (TN) rightly identified background pixels, and false negatives (FN) background pixels termed as spine values. To evaluate the set of predicted masks, each predicted mask is compared with each available target mask for a given input. Precision metric (Eq. 4.3) effectively explains the clarity of our positive detections relative to the ground truth.

$$Precision = \frac{TP}{TP+FP} \tag{4.3}$$

The segmentation results among the different neural networks are compared on the bases of Dice Score. The Dice score (Eq 4.4) is mainly used in literature to quantify the performance of segmentation methods. Dice score is a measuring unit of how similar the objects are to the ground truth. The score is calculated by measuring the size of the overlap of the two segmentations and it is divided by the total size of the two objects. The number of true positives is divided by the sum of the numbers of true positives, number of false positives and number of false negatives.

$$Dice\ Score = \frac{2TP}{2TP + FP + FN} \tag{4.4}$$

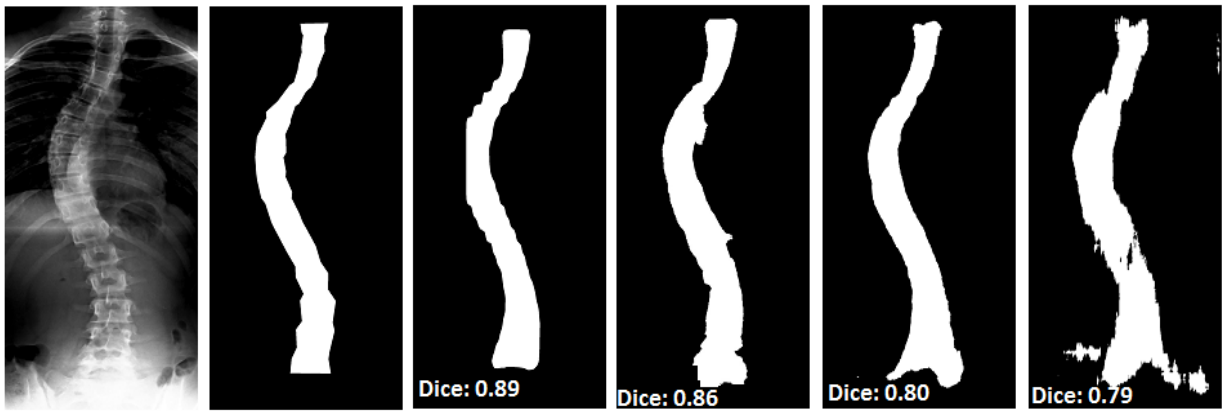

Figure 4-16 Segmentation results. From left to right: a) Original image b) Ground truth c) Mask RCNN d) U-Net e) FCN f) SegNet

The Figure 4-16 shows the original image in (a) and after the manual labelled binary mask is presented in (b). In comparison with the automatic predicted mask after segmentation from different neural network techniques, in (c) to (f), the highest dice score attained is 0.89 by Mask RCNN and the lowest dice with maximum spurs in predicted mask is 0.79 by SegNet.

4.4.6 Results

The comparative analysis of different neural networks has been carried out on AASCE19 dataset and Table 4-6 shows the results. The dice score of Mask RCNN has significant differences from other frameworks. This is due to instance segmentation of Mask RCNN the other neural networks performed semantic segmentation. The low performance of U-Net is because it propagates feature maps in each layer, the depth in learning requires more images in given data for training, the performance might get improved with larger datasets. FCN has scale invariant phenomena which produce better results in comparison with the rest of the semantic networks. The precision score from predicted mask is calculated and is mentioned in the last column of the table.

Table 4-6 Compararison of segmentation results usinf different convolutional neural networks on AASCE19 dataset

	Model	Dice Score	Mask Precision Score
1	**Mask RCNN**	**0.8530 ± 0.09**	**0.8631 ± 0.092**
2	U-Net	0.7852 ± 0.05	0.6776 ± 0.025
3	FCN_8	0.8168 ± 0.03	0.7623 ± 0.032
4	SegNet	0.6590 ± 0.07	0.5639 ± 0.015

In Table 4-7 the results of Mask RCNN applied on all three datasets are illustrated. The highest dice and precision score is for Mendeley's dataset as it has high quality MRI scans, Therefore, the algorithm has produced remarkable predictions of segmented spinal column from the given ground truth.

Table 4-7 Spine segmentation results of proposed network on all three datasets

#	Dataset	Dice Score	Mask Precision Score
1	AASCE19	0.8530±0.09	0.8631±0.09
2	CSI16	0.9601±0.07	0.9674±0.06

3	Mendeley's	0.9713±0.02	0.9789± 0.03

Here, in the Table 4-8 comparison of proposed methodology with the latest state-of-the art techniques from literature is presented. The dice score of proposed technique is higher with other articles in the literature on different datasets.

Table 4-8 Comparison of segmentation results of proposed network with related literature work

#	Author	Method	Image Type	Dice Score
1	Lu et al. [47]	U-Net	MRI	0.93
2	Lessmann et al. [50]	FCN	CT	0.94
3	Liang et al. [54]	DAB-U-Net	MRI	0.91
4	**Proposed**	**Mask-RCNN**	**MRI**	**0.97**

Here in the Figure 4-17 the coloured coded regions are shown to represent the difference is results of each neural network. The white region indicates true positive, green is false negative, blue depicts false positive, and rest of the black area in the image is true negative. The results clearly show that the proposed network has produced good results as compared to other networks.

- White part indicates true positive (A true positive is when the algorithm correctly identifies a pixel or region as belonging to the object of interest)
- Green is false negative (A false negative is when the algorithm incorrectly identifies a pixel or region as not belonging to the object of interest when it does.)
- Blue depicts false positive (A false positive is when the algorithm incorrectly identifies a pixel or region as belonging to the object of interest when it does not.)
- Black area in image is true negative. (A true negative is when the algorithm correctly identifies a pixel or region as not belonging to the object of interest.)

As mentioned earlier, that instance segmentation architecture of proposed network where first the instance is localized and then pixel-wise segmented produces better results. The second-best results are given by FCN with least numbers of spurs in segmented masks. It should be highlighted here that for comparative analysis we have used the default architecture of all networks. These

results might get little improved with some architectural changes and tuning of parameters in the model of network.

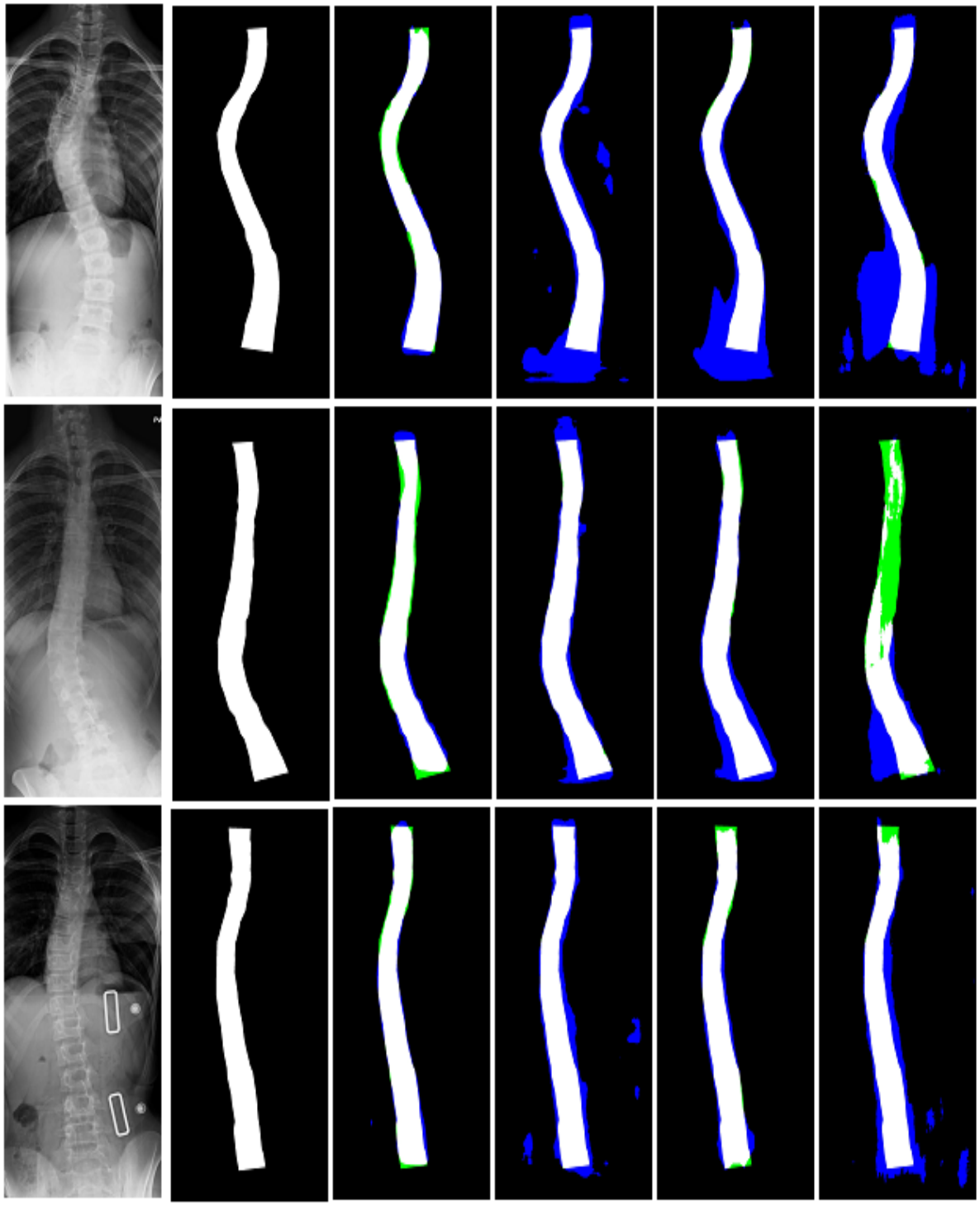

Figure 4-17 The Spine Column Segmentation results. From left to right: a) Original image b) Ground truth c) Mask RCNN d) U-Net e) FCN-8 f) SegNet

4.5 Center Profiling

The localization and segmentation streams have two different types of results. The vertebrae localization has predicted bounding boxes for vertebrae. On the other hand, the segmentation block has delivered whole spine column segmented masks. To proceed further, the calculation of the center point from both resultant images requires two different strategies. These approaches provide the spine center profile, which is a single line curvature pattern.

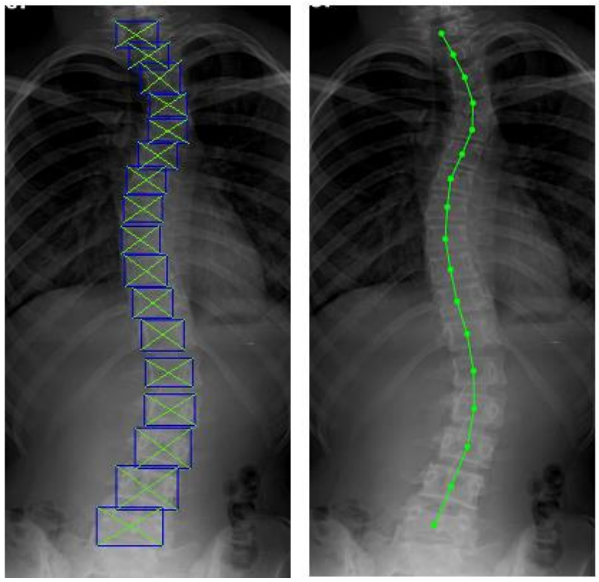

Figure 4-18 Center point and curvature profile extraction from localized vertebrae

After localization of vertebrae, predicted bounding boxes will have corner points with the help of those corners. Figure 4-18 shows that for each bounding box the diagonal ends of the corner points are connected. These diagonal lines intersect at a single point, which is considered the center point of the vertebra. Later, these center points of each vertebra are joined together that produce the curvature of the whole skeleton. On the other hand, spine segmentation masks produced by segmentation block, are passed to the block of morphological thinning. The thinning block which is also termed as skeletonization approach. Morphological thinning is achieved by iteratively removing pixels from the object while maintaining connectivity and topology. The process starts by selecting a structuring element, which is a small binary pattern used to probe the image. The structuring element is then moved throughout the image, and if the pattern of pixels within the structuring element matches a predefined condition, the central pixel is removed. The thinning process is repeated iteratively until no more pixels can be removed without changing the topology

of the object. The result is a skeleton that represents the centerline of the object, which can be used for various applications such as shape analysis, object recognition, and pattern matching. The resultant image is a thin line of the object as shown in Figure 4-19. This gives the tidy curvature center profile that is later used for shape analysis.

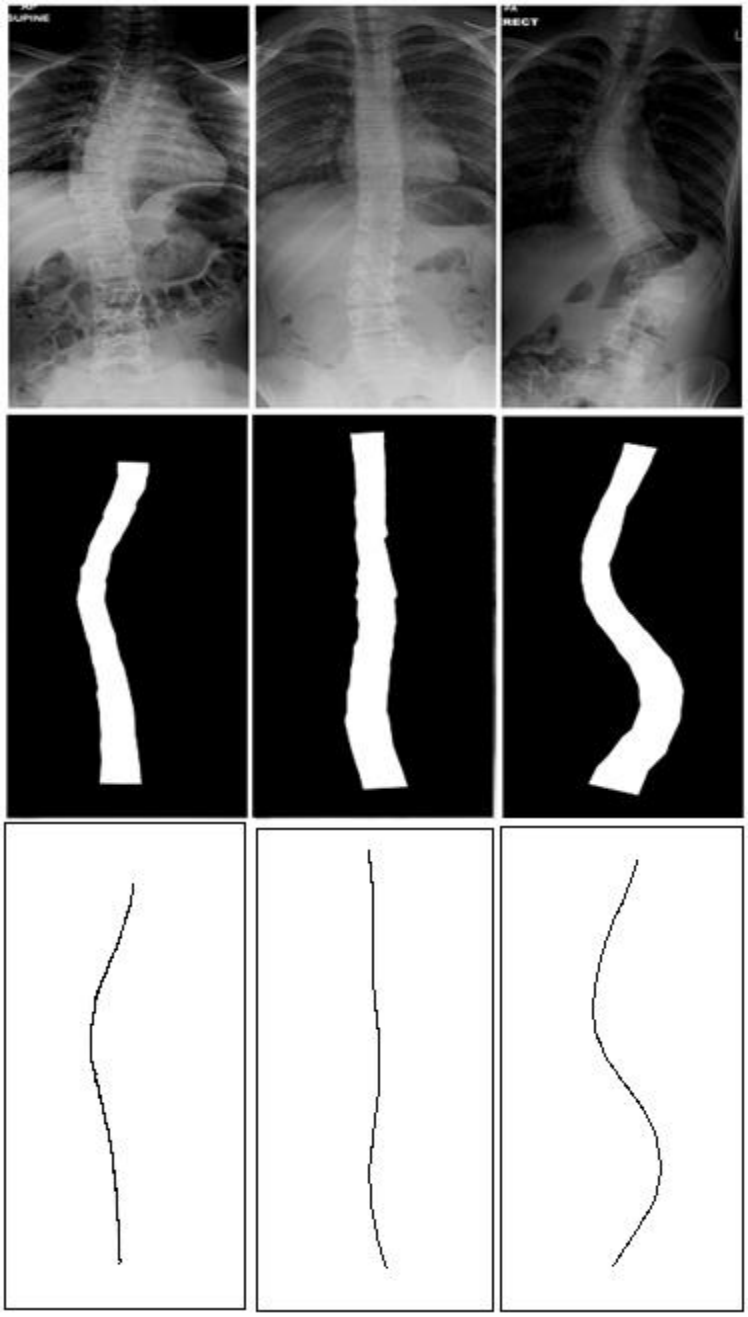

Figure 4-19 Curvature center profile extraction from segmented spine column. From top to bottom: (a) Original image (b) Segmented Mask (c) Morphological thinning

4.7 Discussion

The results indicate the impressive contribution as YOLOv5 approach has localized the vertebrae with mAP reaching up to 94%. The localization results are later utilized for the calculation of center points. The results of center point are analysed through calculation of ED that is shown with its mean and STD values for all points. In segmentation of spinal column, the comparison of standard neural networks is used without any modification in architecture, this shows Mask-RCNN with its crude nature performed better than U-Net, FCN and SegNet. Although the literature shows good results for U-Net and FCN, but those papers have used hybrid and modified versions to refine the segmentation. Here, a point is worth to mention that instead of vertebrae segmentation and spine localization, we have opted for a flip approach of vertebrae localization and spine segmentation. That is why comparative analysis with literature is not relevant here due to the opposite nature of the procedure.

4.6 Summary

In this chapter we have discussed the first module of our proposed methodology to localize vertebrae using an object localization algorithm. Our approach utilized the YOLOv5 framework to extract vertebrae from these locations center points were computed. In parallel to this, for spine segmentation, a comparative study on different architectures of CNN's was analysed and Mask-RCNN produced better results in comparison with FCN, U-Net and SegNet. Mask R-CNN is a two-stage architecture that combines both object detection process along with the semantic segmentation in a single framework. The architecture uses a Region Proposal Network (RPN) framework that identifies object proposals, followed by a mask head that predicts a binary mask for each object proposal. U-Net, on the other hand, is a fully convolutional network (FCN) that uses an encoder-decoder architecture to generate a pixel-wise segmentation mask. Later on, depending upon the distance between center point's evaluations of vertebrae localization is presented and for all CNNs approaches results dice score are presented for comparison with Mask-RCNN. We have also discussed and highlighted curvature profile formulation approaches from both localization and segmentation results. In the next chapter, we present the second module of our proposed framework. The results of module 1 are passed as input for the feature extraction and classification module.

5 Chapter

Spine Column Analysis for Shape and Cobb Angles

This chapter discusses the shape analysis methodology and Cobb estimation for classification of deformities. Same as the methodology split, the chapter is divided into similar partitions and each of them is discussed in detail with inclusion of various steps of the algorithm to be followed. The underlying details of the proposed technique for each block have been explained. The limitations and advantages of proposed method over other approaches have been pointed out with all the necessary information.

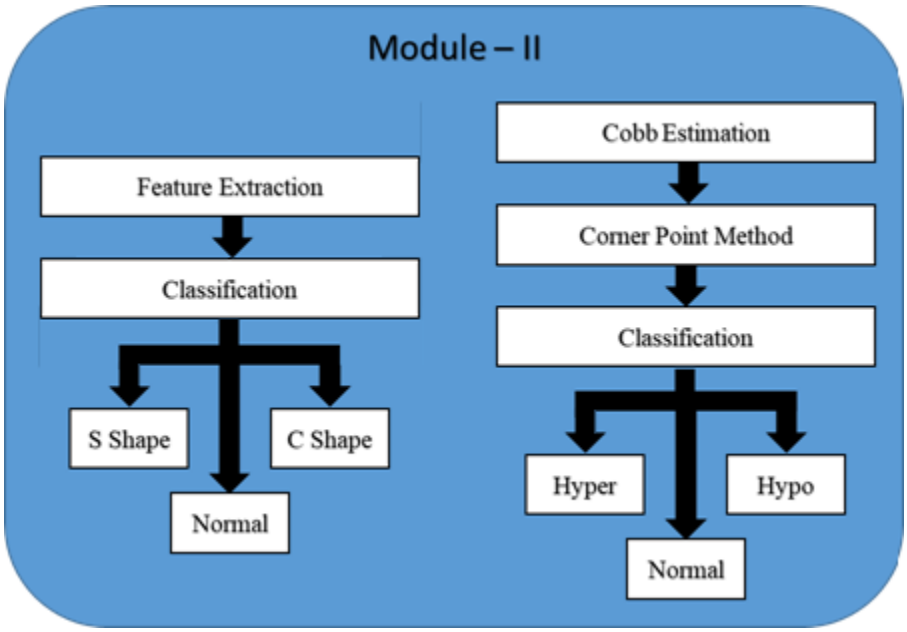

Figure 5-1 Overview of shape analysis and Cobb estimation framework of Module-II

5.1 Overview

Curves in spine are observed with two different views, one is Coronal and the other is Sagittal. In Figure 5-1 the flow of Module II is shown with parallel two blocks. The AASCE19 dataset in the coronal plane is analysed for feature extraction. From these proposed feature sets the classification of scoliosis is carried out classifying the deformity into C-shape and S-shape. Multiple Cobb estimation procedures are evaluated. The other two datasets in the sagittal plane are passed to edge detection and corner estimation block, and after that the corner point Cobb estimation supported the classification of lordosis into hyper, hypo and normal.

5.2 Proposed Framework

The first phase of framework provided two types of results which are fed to this module II. The localization stream has delivered centroids of each vertebra of spinal cord while the segmentation block has produced binary thin center profile for spine column. Both results will be entered as input in the shape analysis and Cobb estimation block. Parallel to each other both blocks work simultaneously; in the shape analysis module the objective is to classify the normal, S and C shape curvature from the images. While the Cobb estimation will present, orientation-based results that will give the severity analysis of disproportionality.

5.3 Shape Analysis

The spine column deformity analysis requires the curvature shape assessment. The classic research of Scoliosis disease describes two major sideways curvature issues in the spinal cord; one is of shape S and other is of shape C. The increase in the severity of disease leads to surgical treatment. The early identification of an abnormal curvature can initiate timely treatment, and it prevents the escalation in the severity. According to the clinical parameters the segregation of the shapes identify the treatment plan of brace styling, massage patterns and exercises. The shape analysis is carried out by feature set formulation. These features will be passed to classifier for classification into C-shape, S- shape and normal [91].

5.3.1 Feature Extraction

Generally, the clinical parameters which have been used up till now are based on angles of curvature, lengths and vertebral anatomical locations. To measure these basic clinical parameters, we proposed feature set to assess the deformity based on the geometrical structure of spine. A group of measuring quantitative features were taken and with empirical evaluations and regressive assessments we identified five specific features that can classify the scoliosis. The center-line spine curvature is evaluated for feature selection processes. Center points of each vertebra are taken from localization module and center-line spinal profile is produced from column segmentation module. Both modules have generated five features by segmentation and three features by localization. ‘Mean Absolute Gradient Magnitude’ and ‘Mean Absolute Gradient Phase’ are generated from center-line spinal profile. ‘Absolute Difference between Max and Min’. Deviated Vertebra Points,

‘Segment-wise Mean’ and ‘Segment-wise Standard Deviation’ are generated from localized vertebra center points. The explanation of feature set is given below [91].

Mean Absolute Gradient Magnitude

The mean absolute gradient magnitude defines the rate of change. It can be positive or negative. For normal, the deviation would be very small. This is because for normal, there should be no (or negligible) change with respect to x axis. For C curve, the magnitude will be a bit more but the magnitude value for the S curve will be higher as compared to normal or C shaped. The equation is given in Eq 5.1 to calculate this value.

$$|G| = \sqrt{\left[G_x^2 + G_y^2\right]} = \sqrt{\left[\left(\frac{\partial f}{\partial x}\right)^2 + \left(\frac{\partial f}{\partial y}\right)^2\right]} \tag{5.1}$$

Mean Absolute Gradient Phase

Along with the magnitude of change, it also tells the direction of change in the image intensities, also referred to as phase. Like our first feature, there would be negligible change in phase angle as well for normal images. Smaller value will be detected for C shaped and the most change in phase will be detected for S shaped curve. The direction of gradient is obtained by Eq 5.2.

$$D = tan^{-1}\left(\frac{G_y}{G_x}\right) \tag{5.2}$$

Absolute Difference between Max and Min Points

For this feature, the whole column absolute max and min points are the extreme points on the x-axis of the image. The difference of those extreme ends with rest of all center points is calculated.

As shown in Figure 5-2 (a), the extreme values for a normal spine on the x axis are not very much deviated from the mean position (shown by a line in the center) hence resulting in a small value. While, for C shaped Figure 5-2 (b) and S shaped Figure 5-2 (c). For the C shaped spines, the deviation found would be on either left or right side of mean. While, for the S shaped spine, the deviation found would be on both sides of the mean.

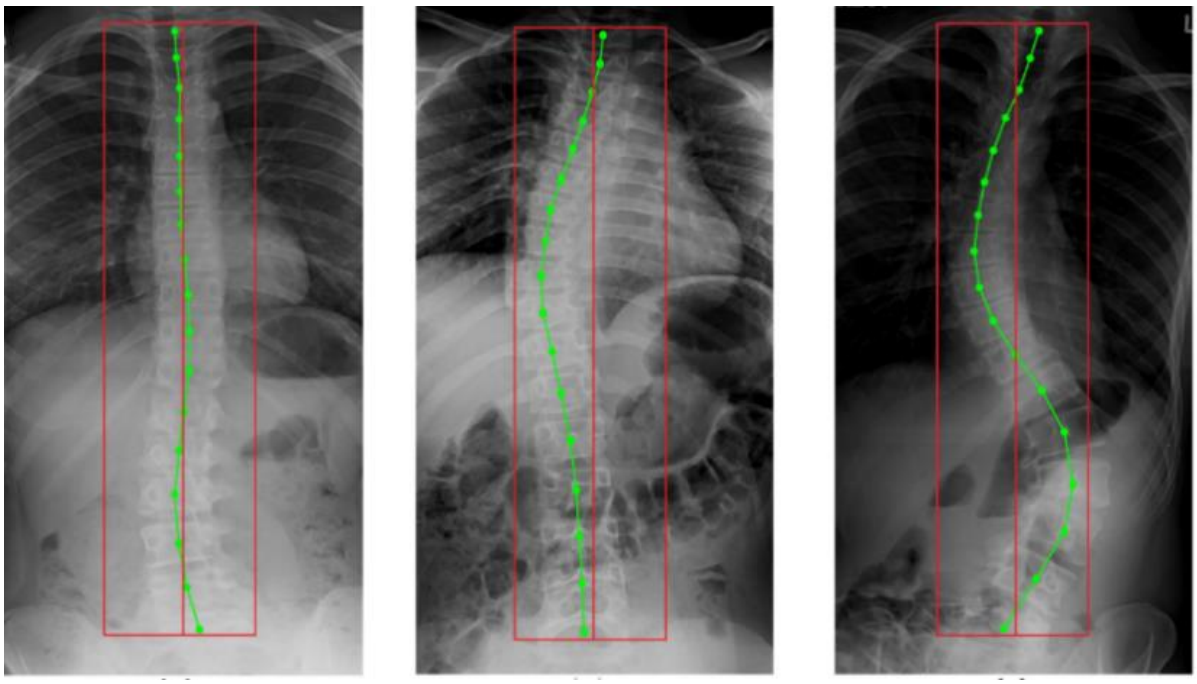

Figure 5-2 Absolute difference between max and min points deviated. From left to right: (a) Normal spine with negligible deviation from mean, (b) C curve shows deviation on one side, (c) S curve shows deviation on both left and right from the mean position

Segment-wise Mean

There are 17 vertebra center points that we have received from vertebra localization module. From these, we have divided them in 4 segments. These segments are from vertebrae 1-4, 5-8, 9-12 and 13-17. We will calculate the same absolute difference of min and max for each segment. The mean is computed from that difference value of all four segments. This will give the variation details at local level. The right side of Figure 5-3 shows how different segments are created from a parent image which is at left side. The values of features will be calculated for each segment.

Segment-wise Standard Deviation

As mentioned above, the description regarding split of segments in vertebral column image. From the absolute difference of min and max for each segment we will calculate the standard deviation for all four segments. This will provide the variation details at local level.

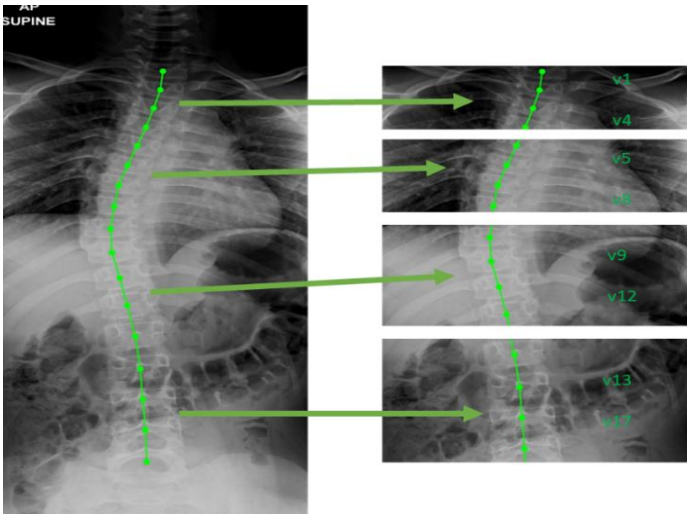

Figure 5-3 Segment-wise division of original image to calculate absolute difference of max and min of each segments

5.3.2 Curvature Classification

The three-class problem is addressed with the help of RF classification. The forest is comprised of multiple decision trees. Samples from data are selected randomly, results prediction is done from each tree, and the best solution is calculated by means of voting of all trees. RF classifier is also termed as Meta estimator that fits several decision trees on different sub-samples of data and utilize averaging to refine the predictive accuracy. It also controls the phenomena of over-fitting. To compare our classifier results, three other classifiers that are Support Vector Machine (SVM), Decision Tree (DT), and k-Nearest Neighbour (kNN) are tested on dataset and result comparison is explained in following section [91].

5.3.3 Experiments and Metrics

To evaluate classification performances, we have used Accuracy that can be calculated by Eq 5.3. The accuracy in percentage is measured from the ratio of the correctly identified subjects to the whole pool of subjects multiplied by 100. Here, TP and TN refers to the cases where the model accurately predicted the positive class as positive and negative class as negative. In the other two scenarios FP is refered to the cases where the model predicted the class as positive, but it was actually negative, and in case of FN the model predicted the class as negative, but it was actually positive.

$$Accuracy = \frac{TP+TN}{TP+FP+TN+FN} * 100\% \quad (5.3)$$

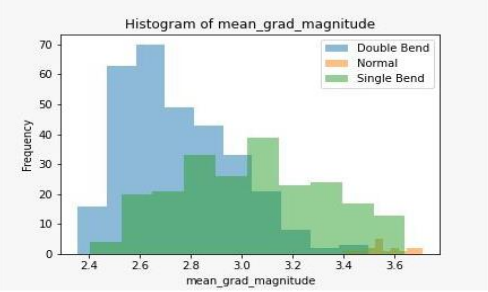

	Double Bend	Normal	Single Bend
Double Bend	0.96	0.00	0.04
Normal	0.00	1.00	0.00
Single Bend	0.11	0.01	0.88

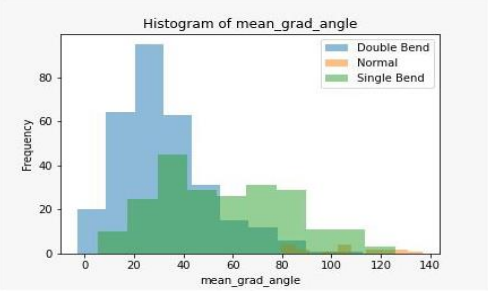

	Double Bend	Normal	Single Bend
Double Bend	0.93	0.00	0.07
Normal	0.00	1.00	0.00
Single Bend	0.10	0.00	0.90

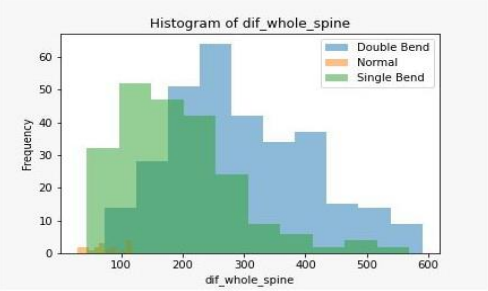

	Double Bend	Normal	Single Bend
Double Bend	0.86	0.00	0.14
Normal	0.00	0.61	0.39
Single Bend	0.22	0.00	0.78

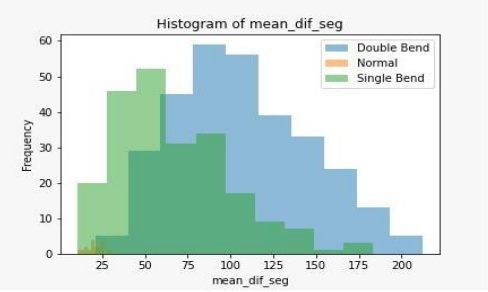

	Double Bend	Normal	Single Bend
Double Bend	0.89	0.00	0.11
Normal	0.00	0.67	0.33
Single Bend	0.23	0.01	0.76

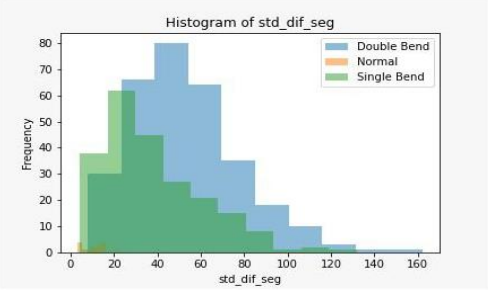

	Double Bend	Normal	Single Bend
Double Bend	0.91	0.00	0.09
Normal	0.00	0.89	0.11
Single Bend	0.12	0.01	0.87

Figure 5-4 Histograms and confusion matrices of the five features used showing how the classes are separable for curvature shape analysis by each respective feature (a) to (e) presented from top to bottom

5.3.4 Results

For classification, we have tested our dataset on four classifiers: kNN, DT, SVM and RF. Figure 5-3 shows the segregation into segments from original image. The working of these five features is shown in Figure 5-4 where separate analysis of them is presented in each row. The confusion matrices are also presented to further elaborate the significance of every feature.

Table 5-1 presents the calculated accuracy of the four-classifier used. Here we can see that the accuracy of RF is found to be better that is 95% than all the others. For kNN, the value of k was empirically set to be 3. DT achieved the second highest accuracy while SVM did not perform very well. The performance of RF is remarkable in comparison with SVM is due to the spread of dataset features. The uneven very irregular decision boundary formation is the major reason to this difference in accuracies [91].

Table 5-1 Accuracy table of results of the four classifiers used

	Model	Accuracy
1	kNN	78.39 ± 0.078
2	DT	92.31 ± 0.02
3	SVM	68.32 ± 0.12
4	**RF**	**94.69 ± 0.03**

KNN	Double Bend	Normal	Single Bend
Double Bend	0.87	0.00	0.13
Normal	0.17	0.44	0.39
Single Bend	0.30	0.00	0.69

SVM	Double Bend	Normal	Single Bend
Double Bend	0.83	0.00	0.17
Normal	0.00	0.00	1.00
Single Bend	0.47	0.00	0.53

DT	Double Bend	Normal	Single Bend
Double Bend	0.93	0.00	0.07
Normal	0.00	0.94	0.06
Single Bend	0.08	0.00	0.91

RF	Double Bend	Normal	Single Bend
Double Bend	0.97	0.00	0.03
Normal	0.00	0.94	0.06
Single Bend	0.09	0.00	0.91

Figure 5-5 Normalized confusion matrices of (a) kNN, (b) SVM, (c) DT and (d) RF presented from left to right, top to bottom

The normalized confusion matrices of all the four classifiers, are presented in Figure 5-5. The performance of RF has slightly increased, as compared with DT with depth of 16 and N_leaves were 93. Random Forest models are known for their ability to handle high-dimensional data and complex relationships between features, making them a good choice for some types of classification and regression tasks. They are also less sensitive to overfitting than some other models, which can be an advantage when working with noisy or incomplete data. On the other hand, kNN with k value set as 3 and SVM with RBF kernel have huge gap of difference in results, with RF. SVM models can be very effective when there is a clear margin of separation between classes, while KNN models can work well when the decision boundaries are not linear.

Table 5-2 Comparison of different image classification models for shape based classification

	Technique	**Accuracy**
1	Efficient-Net B4 Features	89.66%
2	ResNet-16	64.33%
3	DenseNet-121	69.00%
4	VGG-16	58.66%
5	Inception-v3	75.00%

In furtherance to evaluate and compare the performance of our proposed handcrafted features based classification technique with image level classification, we have selected top five of models with the help of literature. These networks are tested on same dataset. The test results in terms of accuracy are shown in Table 5-2. The results clearly indicates that EfficientNet-B4 has performed better from all the other networks. After EfficientNet-B4, results that are given by Inception-v3 are second in line, and have accuracy of 55%. EfficientNet B4 is a larger model compared to Inception-v3. It has more parameters, and its depth and width are optimized using a compound scaling method, which balances the number of parameters and computational cost. EfficientNet B4 has achieved state-of-the-art accuracy on various image classification benchmarks. On basis of speed EfficientNet B4 is also more efficient, with faster training and inference times. However, EfficientNet B4 requires more GPU memory and computational resources during training due to its larger size.

Table 5-3 Comparison of proposed features with deep and hybrid features for classification of scoliosis on basis of shape

	Technique	Accuracy
1	Proposed Features	94.69%
2	Efficient-Net B4 Features	92.79%
3	Hybrid (Deep+Proposed) Features	94.26%

In further elaborate the deep-feature vector extracted from CNN model has 1792 dimensions which has attained an average accuracy of 92.79% in comparison to 94.69% average accuracy by proposed features. We have further experimented by creating a hybrid feature vector through combination of proposed features with deep features and RF classifier which showed comparable results. Table 5-3 shows the results of our proposed methodology compared with deep-features and hybrid feature vector [91].

5.4 Cobb Estimation

Cobb estimation is a method used to measure the degree of spinal curvature in individuals with scoliosis, which is a medical condition characterized by abnormal curvature of the spine. The method is named after John Cobb, who introduced it in 1948. To estimate the degree of spinal curvature using Cobb estimation, two perpendicular lines are drawn on the X-rays of the spine, one on the superior endplate of the most tilted vertebra above the curve, and the other on the inferior endplate of the most tilted vertebra below the curve. The angle between these two lines is then measured, and this angle is used as an indication of the degree of spinal curvature. The angle obtained using Cobb estimation is known as the Cobb angle, and it is used as a standard measure of the severity of Kyphosis, Lordosis, and Scoliosis. However, it has some limitations, such as the reliance on two-dimensional X-rays, which may not accurately reflect the three-dimensional nature of spinal curvature. Additionally, it may be subject to inter-observer and intra-observer variability, as different observers may measure the angle differently.

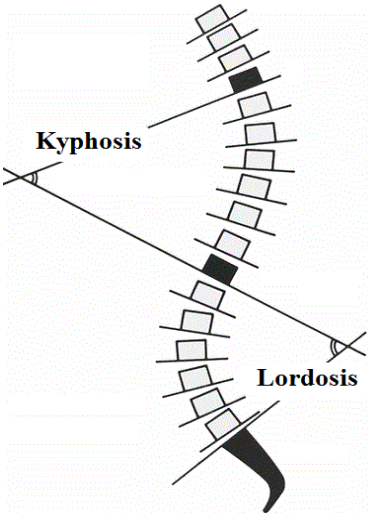

Figure 5-6 Measurement of Cobb angle for Thoracic Kyphosis and Lumbar Lordosis [92]

The four corner points of vertebrae or the predicted bounding boxes can identify height of vertebrae. Standard intervertebral distances that is the distance between consecutive vertebrae at both anterior and posterior sides can also be measured. After computing all types of distances related measurements, angular measurements for orientation are also performed. Figure 5-6 shows Cobb angles calculation for Kyphosis and Lordosis. For the Kyphosis analysis, angle between T4 and T12 is calculated. The Cobb angle is measured from the line drawn through the superior endplate of T, and the other line is drawn through the inferior endplate of T12. The Cobb angle is measured from the angle between intersections of these two lines [86]. Lumbar Lordotic angle is measured between the lines drawn from superior endplate of L1 and superior endplate of S1. Cervical Lordotic angle is measured by connecting the perpendiculars lines dropped from the lower end plates of C2 and C7 [93]. Lordosis is spinal deformity that has inward curvature. The lordosis in lumbar region of spine is divided into two divisions. Hyper Lordosis mainly an excessive inward curve whereas Hypo Lordosis is the lesser curve from normal bend. Figure 5-7 shows the Normal Lumber Bend ranges from 39° to 53° on the other hand Hyper is less than 39° and Hypo is greater than 53°. To evaluate Cobb angles results for Lumbar Lordosis in Hypo and Hyper categories following confusion metrics depicts the results of proposed technique on both datasets.

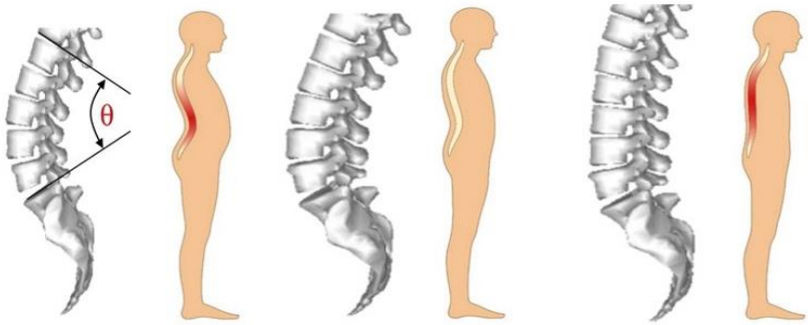

Figure 5-7 Lordosis types on basis of Cobb ranges into (a) Hyper < 39° (b) Normal 39° - 53° (c) Hypo > 53° presented from left to right

Scoliosis is basically titled of vertebrae from its normal position. It is generally classified into three categories: mild where angle is between 10º-24º, moderate where tilt of angle is between 25º-50º and in severe angle is greater than 50º. Levo-scoliosis is the shift of curvature towards the left, and Dextro-scoliosis is the shift of curvature towards the right. The classical approach that is used to determine the Cobb angle for Scoliosis is from the upper and the lower end vertebras of the whole spine. After that, perpendicular line is dropped at the upper and lower end vertebra endplate respectively. The perpendiculars of both endplates, intersect at a certain point. The angle from the intersection point will be Cobb angle [94]. Figure 5-8 shows all three Cobb angle calculation process.

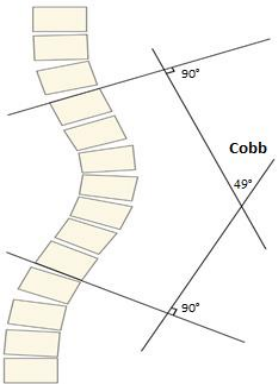

Figure 5-8 Measurement technique of Cobb angle for scoliosis in spine [95]

5.4.1 Corner Point Method

For corner points calculation first, we have to identify the edges of vertebrae. To calculate Cobb angle, corner point information is required. Therefore, after edge detection, corner points are calculated. To increase prominence regarding these edges, the HED[15] edge detection is used. Xie

[15] Holistic- Nested Edge Detection

and Tu in [96] introduced a simple approach of nested network which is able to deliver predictions from multi-scales. Their proposed technique automatically learns the hierarchical features that are difficult to resolve manually in image edge detection. The term holistic, means that belief of interconnect for modeling structured output which aims to predict edges in an image-to-image fashion. The nested term emphasizes refined edge maps that are inherited. They formulated a lone stream of deep network with outputs of various sides. HED is based on a fully convolutional neural network (FCN) architecture, which means that it can handle input images of arbitrary sizes and produces dense edge maps as output. The key innovation in HED is the use of a multi-scale feature fusion strategy, which allows it to capture edges at different scales and resolutions.

HED consists of a base network, which extracts features from the input image, and several side output layers, which produce edge maps at different scales. The side output layers are then combined to produce a final edge map using a weighted average strategy that emphasizes edges at different scales. One unique feature of HED is its holistic approach to edge detection, which means that it aims to detect object boundaries in their entirety rather than individual edges or segments. This is achieved by combining multi-level edge features that capture both fine-grained and coarse-grained structures in the image. Another unique feature of HED is its nested architecture, which means that it has multiple layers of feature fusion and refinement that progressively improve the edge detection performance. The use of multiple layers allows it to capture more complex edge structures and refine the edges detected at lower scales. Figure 5-9 presents the step wise view of Cobb estimation through corner point method.

It is noteworthy point to mention here that the with the help of YOLO we can extract ROI that contains three-star vertebrae L1,L5 and S1 irrespective of any information regarding the orientation of these vertebrae. We have used the simplest and the most popular corner point algorithm presented by Chris Harris and Mike Stephens in 1988 [97]. Thus, Harris corner is applied on the Gaussian smoothed images that produce the corner points. These corner points will facilitate for calculation of Lumbar Lordotic Angle (LLA) and Lumbosacral Angle (LSA). In order to calculate the LLA the angle is calculated between superior endplate of L1 and S1. On the other hand, for LSA, the angle is calculated between inferior endplate of L5 and superior endplate S1. The slope of the lines can be calculated from (Eq 5.4).

$$m_{L5,S1} = \frac{c2_y - c1_y}{c2_x - c1_x} \tag{5.4}$$

Here, m represents the slope, c1 and c2 are corner points with values of x and y axis. The angle measured using the expression given in (Eq 5.5).

$$\theta = tan^{-1} \left/ \frac{m_{L5} - m_{S1}}{1 + m_{L5} m_{S1}} \right. \tag{5.5}$$

m_{L5} and m_{S1} are the slope of inferior endplates of L5 and superior endplate of m_{S1}. The same equations can be used to find the slope and angle for LLA.

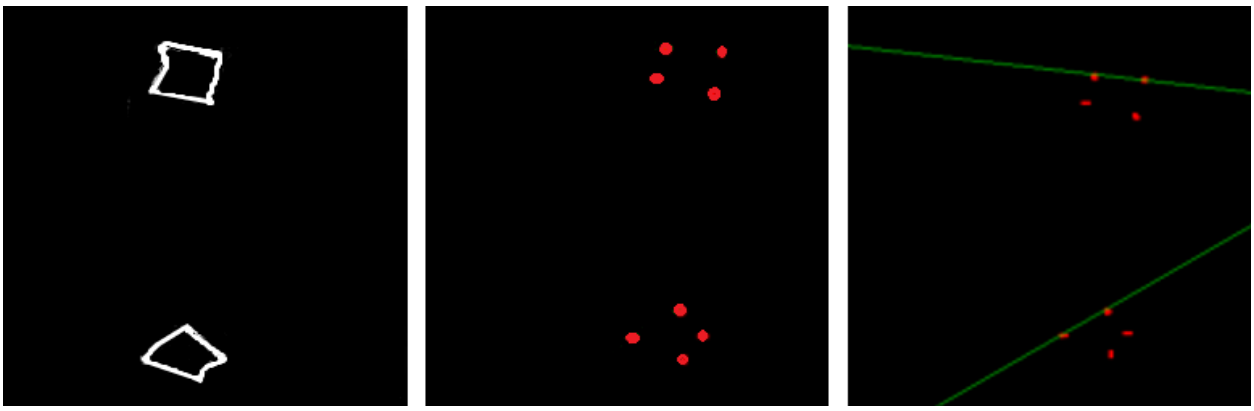

Figure 5-9 Lumbar lordosis Cobb angle calculation from corner point method

5.4.2 Other Methods

In [99], posterior-inferior corners of superior vertebrae are connected to form a straight line that represents the length of lumbar. For remaining in-between vertebrae posterior-inferior corners are joined perpendicularly, and the ratio of sum of lengths of perpendicular lines with the total length of spine measures Ishihara index. The Maximum Distance Method is proposed in [94]. Instead of connecting the posterior corner-points, anterior-inferior corners of superior vertebras and inferior vertebras are joined to form a straight line, representing the lumbar height. After that, maximum orthogonal distance is calculated from straight line, and remaining in-between vertebras distance is measured. The ratio of maximum distance and spine length is then measured. The method proposed by Chen [99], the lines that are connecting centroids of two superior vertebras and the line connecting two inferior vertebras form an angle of intersection is considered as the Cobb angle. Cobb angle of intersection is formed between the tangent lines drawn by connecting

posterior-inferior and posterior-superior, corner-points of two superiors as well as inferior vertebras [99].

Yang et al. presented in [101] AUC[16] technique in this research paper a curvature is formulated by joining the posterior corner points of lumbar vertebrae. Later, superior corner point is drops connecting it to the inferior corner point. AUC method for lumbar lordosis classification, first need to train a binary classification model using a set of labeled data. This labeled data should consist of measurements of lumbar lordosis angle and corresponding labels indicating whether each measurement is normal or abnormal. The enclosed region is measured if the area under the region is less the curvature is set to be deformed [102] and [103].

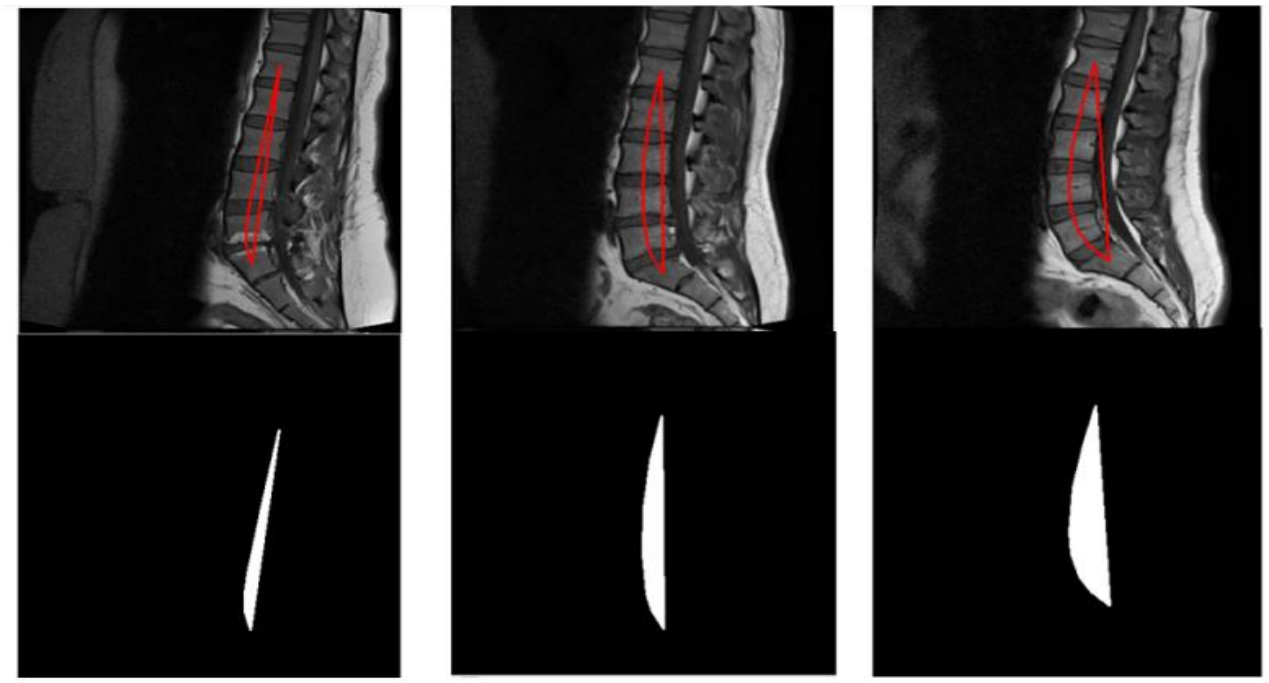

Figure 5-10 Region plot of an image and its respective area. From left to right (a), (b) and (c) represent hypo, normal, and hyper lordosis cases respectively.

These alternate approaches require more complex working and demanding intensive calculation. The [98], [94] and [100] methods described above, involve multiple measurements, whereas the centroid method [99] has intensive calculation, but results seem reliable. The technique is given by Yang et al. [101] require calculations through software-assistance and without using manual

[16] Area Under the curve

methods. The reliability and productivity of these alternate approaches are found to be better than rest of Cobb method. For the purpose of this research thesis, and from clinical perspective modified Cobb angle for curvature assessment are applied in the proposed method. The Cobb angles are calculated using these above discussed approaches.

All the ranges are evaluated with the gold standard ranges the Table 5-4 below explains each range of all diseases.

Table 5-4 Standard Cobb angle chart of ranges for Scoliosis, Kyphosis and Lordosis

Disease	**Cobb Ranges in degree**
Normal Range Scoliosis	0-10 <10 Mild <20 Moderate < 40 severe
Normal Range Lordosis	39-53 Below 39 Hypo Above 53 Hyper
Normal Range Kyphosis	35-42 <45 Hyper <60 Congenital >30 Scheuermann

5.4.3 Experiments and Metrics

To evaluate Cobb estimation, we have used Mendeley's and CSI16 dataset that contains MRI and CT scans. The number of classes defined as hypo-Lordosis, normal and hyper-Lordosis respectively. MAE of angles is used to evaluate estimation result and its value is in degrees. It measures the error difference from actual angle with the predicted one. Low value of ME explains the less error between the ground truth and predicted values (Eq. 5.6).

$$ME = \frac{1}{K}\sum_{l=0}^{k-1}\left|a_{predicted} - a_{original}\right| \quad (5.6)$$

Here, k is the total no of images, $a_{predicted}$ is an angle that is predicted and at the same time $a_{original}$ is the value of an angle in the ground truth.

5.4.4 Results

The proposed automated spine deformity module of classification has MAE and standard deviation of absolute error values for Lumbar Lordotic Angle (LLA) and Lumbo-Sacral Angle (LSA) are presented for Mendeley's dataset in Table 5-5. The same results for CSI16 dataset are presented in Table 5-5. It has correctly identified straight-back (normal) and sway-back (disorder cases). Each image has different curve and area which differentiates the disease.

The performance of proposed method is better as the comer points provide exact location of vertebrae and the calculations of Cobb are near to accurate. The comparison with latest technique have used CenterPoint's and connecting these center points will produce curvature a little difference in deviation in CenterPoint will have significant effect on the AUC [102].

Table 5-5 Mean and standard deviation absolute error of Mendeley's Dataset

MD	Masood et al. 2021 [82]		Proposed Method	
	MAE	Standard Deviation	MAE	Standard Deviation
LLA	1.45°	1.31°	0.29°	0.21°
LSA	1.55°	1.33°	0.38°	0.27°

Table 5-6 Mean and standard deviation absolute error of CSI16 Dataset

CSI 16	Masood et al. 2021 [82]		Proposed Method	
	MAE	Standard Deviation	MAE	Standard Deviation
LLA	1.61°	1.63°	0.38°	0.32°
LSA	1.67°	1.65°	0.49°	0.43°

Normalized confusion matrix shown in Table 5-7 of Lordosis assessment with region area calculation and corner point calculation for Mendeley's dataset. For Mendeley's Dataset, we were able to achieve an accuracy of 76.47% using AUC and 98.04% using the CP method [103].

Table 5-7 Confusion Matrix of Mendeley's dataset of proposed methodology in comparison with latest literature

Masood et al. 2021 [82]	Hypo	Normal	Hyper
Hypo	1.00	0.00	0.00
Normal	0.26	0.63	0.11
Hyper	0.00	0.19	0.81

Proposed	Hypo	Normal	Hyper
Hypo	1.00	0.00	0.00
Normal	0.05	0.95	0.00
Hyper	0.00	0.00	1.00

Normalized confusion matrix shown in Table 5-8 of Lordosis assessment with region area calculation and corner point calculation for CSI16 dataset. For CSI16 Dataset, we achieved an accuracy of 75.00% using AUC and 81.25% using CP method.

Table 5-8 Confusion matrix of CSI16 Dataset of proposed methodology in comparison with latest literature

Masood et al. 2021 [82]	Hypo	Normal	Hyper
Hypo	0.75	0.00	0.00
Normal	0.22	0.78	0.00
Hyper	0.00	0.33	0.67

Proposed	Hypo	Normal	Hyper
Hypo	0.75	0.00	0.00
Normal	0.11	0.89	0.00
Hyper	0.00	0.33	0.67

Table 5-9 shows the comparison of proposed methodology on Mendeley's dataset for Lordosis assessment with latest publication of Masood et al. [82] 2021. The result shows significant difference of 2 degrees in mean error from the proposed methodology.

Table 5-9 Comparison of proposed method with latest literature

	Techniques	Dataset	mAp	Mean Error	
				LLA	LSA
Proposed Methodology	YOLOv5-HED	Mendeley's	0.975	0.29˚	0.38˚
		CSI16	0.952	0.38˚	0.49˚
Masood et al. 2021 [81]	ResNet-U-Net	Mendeley's	-	2.61˚	2.01˚

5.5 Discussion

The grand challenges on this dataset have used Cobb estimation approach restricted the evaluation metric for comparison. Thus, the biggest challenge was to introduce a novel approach for S and C curvature classification for scoliosis. The feature set classification based approach cannot be compared as this approach is not used by any research before. The adequacy for this solution regarding clinical point of view is that the scoliosis is classified into two categories that is S and C shape the treatment pattern might be similar like massage, braces, chiropractic's and physiotherapy. But both curvature shape defines the massage pattern, brace styling and exercises. The convex area of curvature needs to be identified for these treatments. The S shape has two convex which indicate more severe damage in spine. The Cobb estimation is basically the procedure when no further treatment option is left except of surgery. It is basically a pre-operative procedure that is why for early diagnosis of scoliosis and shape based deformity would help in treatment plan for clinical specialist [102].

5.6 Summary

In this chapter, we have explained the second module of our proposed system for the classification of spinal curvature deformities. The method proposed does not depend upon any specific imagining modality. Therefore, our proposed algorithm can objectively assess all the three categories of deformed spine. In this module feature-based classification is presented for scoliosis assessment. Cobb estimation technique is compared with latest state-of-the-art literature attaining the accuracy of 97% and reducing the mean error up to 2 degrees.

6 Chapter

Conclusion and Future Work

This chapter presents the summary of the thesis. The brief discussion with concluding remarks along with the future work to direct the research community, regarding other perspectives in this field.

6.1 Thesis Summary

The research theme for this thesis revolved around an automated system that localizes and segments the spinal cord to assess the deformity of the curvature of the spine. The effectiveness and of reliability this automated system is directly connected with the precision of vertebra localization and spine segmentation, that is later used for extraction of curvature measurements for shape analysis and disproportionality diagnosis. To reach the achieving point of our goal, selection of suitable methodology plan is most important, along with the involvement of multiple datasets with different viewpoints of spine. To contribute to this particular aspect, different imaging modalities with sagittal views, or cervical, thoracic and lumbar spine images are annotated manually. It was a meticulous process involving radiologist involvement for accurate labelling. Extensive detailed exhaustive review of literature was carried out, and research gaps were identified. The research problem was further explored in order to plug solutions in the gaps. As our first phase, a customized vertebral localization, and spine column segmentation, algorithm is proposed based on object detection, and semantic segmentation conventional machine learning and image processing techniques. The second phase addresses the issue of shape analysis of extracted spinal curvature and the Cobb estimation for accurate deformity classification. However, on the other side, the performance metrics of the proposed tailored algorithm were in a lower shade because the literature showed an entirely opposite approaches the segmentation of vertebrae and localization of spine was generalized solution opted by most of research community. In the recent literature, deep learning architectures are extensively used with a lot of modified versions. The aim was to give a different perspective to this research problem, so a novel approach of object detection was incorporated and both shape analysis and Cobb estimation hybrid methods were tested to increase reliability of system. The time-consuming method was manually dataset labelled formulation of aground truth images. Finally, the extracted measurements of spine curvature,

classification methodologies for spinal deformities, clinically termed as Scoliosis, Kyphosis and Lordosis, are assessed and reliable results are produced.

6.1.1 Limitations

Our vertebrae localization algorithm is an object detection algorithm. Since it has not been used before, therefore,comparison of results is a bit challenging. The spine segmentation technique is already compared with relevant approaches. The second phase we have limitations of end plate orientation information for Cobb estimation, we have utilized some variant techniques to calculate the Cobb without this information. Multiple datasets are used so the different orientation sizes of images produce different accuracy in results. To cater for this we have used some approaches to calculate the centroid of vertebrae. Some of the assumptions are made such as the image is upright, and the first and the last vertebrae are somehow detected even for ground truth and predicted results. With half available view in prediction, that is why a threshold is applied to maintain the total count of vertebrae even. Finally, all the methodogies used in this thesis might suffer a little bit when highly irregular shaped vertebra comes at the test time. However, this can be encountered by training the machine learning-based models are on multilple datasets, having both healthy and unhealthy vertebrae. One of our dataset has osteoporosis spine with slight deformed vertebrae. The principal target during this study was to establish a fully automatic multi-modality based image analysis framework, that segregated deform and normal spine curvature. Very less attention was given to recognition of abnormal situations. Moving forward, the proposed solution in a given thesis can be utilized as a starting point, and more emphasis on detection of the complex cases can be a future direction.

6.1.2 Hazardous Impacts

Vertebrae localization is a critical step in analysing spinal deformities using digital spinal images. However, there are potential hazardous impacts associated with this process, which include:

- Radiation Exposure: Spinal images are typically obtained using X-rays or other forms of radiation, which can be harmful in high doses. Multpile times repeated exposure to such radiations during the diagnosis process can increase the risk of cancer and other health problems.

- Misdiagnosis: Incorrect localization of vertebrae can result in misdiagnosis of spinal deformities. This can lead to inappropriate treatment plans and potentially harmful surgical interventions.
- Time-Consuming: Vertebrae localization is a time-consuming process that requires highly skilled professionals with specialized training. This can lead to delays in diagnosis and treatment.
- Patient Discomfort: Patients undergoing spinal imaging may experience discomfort or pain, especially if they are required to hold a specific position for an extended period.
- Cost: The cost of obtaining and analyzing spinal images can be expensive, especially for individuals without adequate insurance coverage.

To minimize these potential hazards, it is important to use appropriate safety measures when obtaining spinal images and to ensure that highly trained professionals perform the vertebrae localization process. Additionally, alternative imaging techniques that do not involve radiation exposure, such as MRI, may be used in some cases.

6.2 Conclusion

To sum up all the work in a nutshell, a huge effort was put into this research thesis, to produce an automated system that assess the spinal images with the same perspective as a neurosurgeon. Moreover, it should be able to evaluate the deformity on the same pattern as done clinically by the doctors in their routine evaluation of subjects, which is carried out through physical examination. The research was able to achieve this said goal by formulating a decision-making tool for the most critical procedures. These are based on spinal measurements, which are normally done manually through laborious techniques. The system regardless of restriction of imaging modality and without restriction of regional segregation in the spine column, all categories are addressed properly. Illumination problems in acquisition are well taken care of. We even added some Gaussian and salt & pepper noise in the images to test the performance. It was observed that our system was able to take care of the noise and the performance matrices were not affected. Adoption of such automated curvature assessment system as proposed in this research thesis, will certainly benefit and save the valuable time of the clinician, as well as provide the confidence to their decision for treatment. Additionally, the thesis also introduced a concept of fully automated classification of severity-based spinal disorders. This was done with shape analysis for Scoliosis

and Cobb estimation was done for Kyphosis and Lordosis. In addition to that, further analysis in S-shape and C-shape segregation was carried out which allowed a deformity to be further classified. Lordosis was further classified as hypo Lordosis and hyper Lordosis. It is important to reiterate the fact that the intended purpose of the proposed research is certainly not to replace or discard the role of the medical specialist. The primary motivation is to aid the medical specialist with robust detection of the deformity along with critical analysis of the curvature and hence provide assistance to the less experienced radiologist in the field. Thus, to introduce a vote of confidence and reliability in their decision that was based on manual diagnosis.

A novelty of our work is that to the best of our knowledge, to date, no work has been done on feature based classification of scoliosis. Thus, our introduced feature-set provides a new direction to the research community where further work can be done and this technique can be explored to further extents. This work was presented in an international conference organized by IEEE where this work was much appreciated and led to winning the best paper award. In addition to this, we further explored additional options in the same problem domain. We compared our results with deep features and it was concluded that hand crafted feature set proposed by us led to a better accuracy than five different deep learning methods used by us. The details of this published paper are available in Appendix A, Conference Publications on page number 90. The abstract of publications are also mentioned in Appendix D.

Before this, clinically deformity was calculated with the help of Cobb angle calculation. To follow the same pattern as that of clinical examination and performing calculations with existing datasets, we calculated the Cobb angles with two different methods of the datasets mentioned in Datasets section on page number 51 for lumber lordosis. This made us form a single framework that is able to perform evaluation upon images of the same subject from sagittal view and coronal plane view. This is also a new trend in the field as no framework can do that to date. To add more value to that, our framework can work upon X-Ray, CT and MRI image modalities.

6.3 Future Work

In this section, extension of this research in the future is discussed. The proposed framework can be extended to other spine diseases. The available datasets may seem sufficient, but for better analysis and to test the reliability of the novel system require more medical images. The work may be extended by using 3D volumetric scans, hence formulating another dataset with different orientations of spine images.

1. Virtual reality (VR) technology can be used to create immersive 3D visualizations of spinal cord images, allowing medical professionals to view the spine from different angles and perspectives. This can enhance the accuracy of diagnosis and treatment planning.
2. The extension of the localization of vertebrae and deformity analysis using digital spinal cord images for accidental patients can have significant implications for emergency medicine and trauma care. Here are some potential ways this technology could be applied:
    - Rapid Diagnosis: Accidental patients with spinal cord injuries require immediate medical attention, and accurate diagnosis is critical. The use of digital spinal cord images for vertebrae localization and deformity analysis can help emergency medical professionals quickly identify the location and severity of spinal cord injuries, allowing for faster and more effective treatment.
    - Treatment Planning: Once a spinal cord injury has been diagnosed, treatment planning becomes critical. The use of digital spinal cord images can help healthcare professionals develop personalized treatment plans that address the specific location and severity of the injury. This can improve patient outcomes and reduce the risk of complications.
    - Follow-up Care: Patients with spinal cord injuries require ongoing follow-up care to monitor their progress and adjust treatment as needed. The use of digital spinal cord images can help healthcare professionals track the healing process and make adjustments to the treatment plan as necessary.
3. The current framework highlights severity level in spinal deformity which can also benefit for diagnosis of:
    - Osteoporosis: It is a condition where bones become weak and brittle, and it can increase the risk of spinal fractures. The technology of vertebrae localization and deformity analysis could be used to detect and monitor changes in the shape and density of vertebrae in patients with osteoporosis.
    - Spinal tumors: Spinal tumors can cause deformities and compress the spinal cord or nerve roots. The technology of vertebrae localization and deformity analysis could be used to locate and measure the size of spinal tumors and to monitor changes in their shape over time.

- Spinal cord injuries: Spinal cord injuries can cause deformities and changes in the shape of the spine. The technology of vertebrae localization and deformity analysis could be used to monitor changes in the shape of the spine and to evaluate the effectiveness of rehabilitation therapies.
- Degenerative disc disease: It is a severe condition where in the vertebral discs in the spine break down over time. The technology of vertebrae localization and deformity analysis could be used to monitor changes in the height and shape of the discs and to evaluate the effectiveness of treatments.
- Detection of arthritis-related changes: Digital spinal images could be used to detect changes in the spine that are indicative of arthritis. This could include changes in the shape or alignment of the vertebrae, as well as the presence of bone spurs or other signs of joint damage.

4. Integration with electronic health records (EHRs): Digital spinal cord images and associated analysis data can be integrated with EHRs, allowing medical professionals to access patient data and images from a centralized location. This can improve collaboration and communication between different healthcare providers.
5. Extending the localization of vertebrae and deformity analysis using digital spinal cord images to a cloud-based system has several advantages. Here are some potential benefits of a cloud-based system for this technology:
    - Accessibility: A cloud-based system allows users to access the technology from anywhere with an internet connection, making it more convenient for medical professionals and patients to access the system. This is especially useful for remote and rural areas where access to medical services may be limited.
    - Scalability: A cloud-based system can easily scale up or down depending on the number of users and the amount of data being processed. This means that the system can handle a large volume of data without the need for expensive hardware upgrades.
    - Collaboration: A cloud-based system allows multiple users to access and collaborate on the same data, making it easier for medical professionals to share information and coordinate care.

- Data security: A cloud-based system can provide enhanced data security measures such as data encryption, user authentication, and access controls, which can help protect patient data from unauthorized access.
- Cost savings: A cloud-based system eliminates the need for expensive hardware and infrastructure, as the system is hosted on remote servers. This can result in cost savings for both medical institutions and patients.

References

[1] R. C. Gonzalez, R. E. Woods, and S. L. Eddins, *Digital image processing using MATLAB*. Pearson Education India, 2004.

[2] ACA, "Back Pain Facts and Statistics", Online [https://handsdownbetter.org/health-and-wellness/back-pain-facts-and-statistics/]. Accessed: 2021-11-23

[3] J. Hartvigsen, M. J. Hancock, Alice Kongsted, Quinette Louw et al. "What low back pain is and why we need to pay attention." The Lancet 391, no. 10137 (2018): 2356-2367.

[4] A. Wu, L. March, X. Zheng, J. Huang, X. Wang, J. Zhao et al. "Global low back pain prevalence and years lived with disability from 1990 to 2017: estimates from the Global Burden of Disease Study 2017." Annals of translational medicine 8, no. 6 (2020).

[5] S. A. Khan, "Situation analysis of health care system of Pakistan: post 18 amendments." Health Care Current Reviews 7, no. 3 (2019): 1-9.

[6] Reporter, "Country has only 120 neurologists" Online [https://www.dawn.com/news/1077118] Accessed: 2021-11-23

[7] F. M. Maynard *et al.*, "International standards for neurological and functional classification of spinal cord injury," *Spinal cord*, vol. 35, no. 5, pp. 266–274, 1997.

[8] Quick Anatomy of Spine Online [https://www.kostindia.org/quick-anatomy-of-the-spine/] Accessed: 2018-11-06

[9] R. S. Snell, *Clinical anatomy by regions*. Lippincott Williams & Wilkins, 2011.

[10] S. A. Goldman, "MSD MANUAL Spinal Cord." Online [https://www.msdmanuals.com/home/brain,-spinal-cord,-and-nerve-disorders/biology-of-the-nervous-system/spinal-cord Accessed: 2018-10-10

[11] Rachel Nall, "A guide to the spinal cord: Anatomy and injuries", https://www.medicalnewstoday.com/articles/326984, accessed: 2021-11-10.

[12] Christopher & Dana Reeve Foundation, "How the spinal cord works", https://www.christopherreeve.org/living-with-paralysis/health/how-the-spinal-cord-works, accessed: 2021-11-10.

[13] "Central Nervous System Stimulants and Depressants." Online [https://pharmacology2011.wikispaces.com/Central+Nervous+System+Stimulants+and+Depressants?responseToken=0fc07ea7d318272406434de5fcd45dfcf] Accessed: 2018-10-10

[14] S. Kemp, “DIGITAL 2018: GLOBAL DIGITAL OVERVIEW.” Online [https://datareportal.com/reports/digital-2018-global-digital-overview] Accessed: 2018-10-01

[15] J. Migala, “9 Surprising Ways Bad Posture Can Mess with Your Health.” Online [https://www.thehealthy.com/osteoporosis/surprising-ways-bad-posture-can-affect-your-health/] Accessed: 2018-10-10

[16] W. J. Kim, Young Dong Song, and Won Sik Choy. "Multilevel thoracolumbar spondylolysis with spondylolisthesis at L4 on L5." Clinics in Orthopedic Surgery 7, no. 3 (2015): 410-413.

[17] T. Y. Tawfq Zyoud, S. N. Abdul Rashid, S. Suppiah, R. Mahmud, Abubakar Kabeer, Rosliza Abd Manaf, and Ezamin Abdul Rahim. "Estimation of body height from spinal length measurements using post-mortem computed tomographic images." The Malaysian Journal of Pathology 42, no. 3 (2020): 423-431.

[18] F. Gaillard, “Normal full length spine MRI. Case study”, Spine Musculoskeletal, Radiopaedia.org, Jan 2010 Accessed: 2018-10-10

[19] M. H. Carstensen, Mashael Al-Harbi, Jean-Luc Urbain, and Tarik-Zine Belhocine. "SPECT/CT imaging of the lumbar spine in chronic low back pain: a case report." Chiropractic & manual therapies 19, no. 1 (2011): 1-5.

[20] A. Gundgurthi, M. K. Garg, Reena Bhardwaj, Sandeep Kharb, Aditi Pandit, Karninder S. Brar, Ravi Kumar, and A. G. Pandit. "Spinal polyostotic fibrous dysplasia in two adults: Does only biopsy unravel the mystery?." Indian Journal of Endocrinology and Metabolism 17, no. 6 (2013): 1108.

[21] A. L. Goldberg and S. M. Kershah, *"Advances in imaging of vertebral and spinal cord injury."* The journal of spinal cord medicine 33, no. 2 (2010): 105-116.

[22] S. Oiseth, L. Jones, E. Maza, "CT image viewing planes", April 2021. Online Available [https://www.lecturio.com/concepts/computed-tomography-ct/]

[23] D. Alexandru, and William So. "Evaluation and management of vertebral compression fractures." The Permanente Journal 16, no. 4 (2012): 46.

[24] P. Trobisch, O. Suess, and F. Schwab. "Idiopathic scoliosis." Deutsches Ärzteblatt International 107, no. 49 (2010): 875.

[25] Dr. Liji Thomas, “Pediatric Spinal Deformities” , Online [https://www.news-medical.net/health/Pediatric-Spinal-Deformities.aspx] Accessed: 2019-12-01

[26] Dr. T. J. Gerhard, “Spine in Motion Chiropractic.” Online [https://www.dreamstime.com/stock-image-scoliosis-different-types-curvatures-caused-image39558961] Accessed: 2020-08-01

[27] Masafumi Machida, Stuart L. Weinstein, and Jean Dubousset, eds. Pathogenesis of idiopathic scoliosis. Springer, 2018.

[28] Lam JC, Mukhdomi T. Kyphosis. In: StatPearls. StatPearls Publishing, Treasure Island (FL); 2021. PMID: 32644371.

[39] P. Pekovic, "Kyphosis and facts.", Online [https://steemit.com/fitness/@petar.pekovic/kyphosis-and-facts-b8381bdfeaece] Accessed: 2020-08-02

[30] Cartwright, Cathy C., and Donna C. Wallace, eds. Nursing care of the pediatric neurosurgery patient. Springer, 2007.Online [https://nursekey.com/spine/#CR77]

[31] Been, Ella, and Leonid Kalichman. "Lumbar lordosis." The Spine Journal 14, no. 1 (2014): 87-97.

[32] Mistovich RJ, Spiegel DA. The spine. In: Kliegman RM, St. Geme JW, Blum NJ, Shah SS, Tasker RC, Wilson KM, eds. Nelson Textbook of Pediatrics. 21st ed. Philadelphia, PA: Elsevier; 2020:chap 699.

[33] M. M. Flint, "Lumbar posture: a study of roentgenographic measurement and the influence of flexibility and strength," *Research Quarterly. American Association for Health, Physical Education and Recreation*, vol. 34, no. 1, pp. 15–20, 1963.

[34] W. Y. Loebl, "Measurement of spinal posture and range of spinal movement," *Rheumatology*, vol. 9, no. 3, pp. 103–110, 1967.

[35] M. H. Mehta, "Radiographic estimation of vertebral rotation in scoliosis," *The Journal of bone and joint surgery. British volume*, vol. 55, no. 3, pp. 513–520, 1973.

[36] M. D. Levine and J. Leemet, "Computer recognition of the human spinal outline using radiographic image processing," *Pattern Recognition*, vol. 7, no. 4, pp. 177–185, 1975.

[37] M. P. Chwialkowski, P. E. Shile, R. M. Peshock, D. Pfeifer, and R. W. Parkey, "Automated detection and evaluation of lumbar discs in mr images," in *Images of the Twenty-First Century. Proceedings of the Annual International Engineering in Medicine and Biology Society*, 1989, pp. 571–572.

[38] P. P. Smyth, C. J. Taylor, and J. E. Adams, "Automatic measurement of vertebral shape using active shape models," *Image and Vision Computing*, vol. 15, no. 8, pp. 575–581, 1997.

[39] Anonymous, "Medical Dictionary." Online [https://tinyurl.com/y5qrkvsr] Accessed: 2020-01-10

[40] J. Fatima, M. Usman Akram, A. Jameel, and A. Muzaffar Syed. "Spinal vertebrae localization and analysis on disproportionality in curvature using radiography—a comprehensive review." EURASIP Journal on Image and Video Processing 2021, no. 1 (2021): 1-23. (IF: 1.789)

[41] M. Brejl and M. Sonka, "Object localization and border detection criteria design in edge-based image segmentation, automated learning from examples," *IEEE Transactions on Medical imaging*, vol. 19, no. 10, pp. 973–985, 2000.

[42] A. Tezmol, H. Sari-Sarraf, S. Mitra, R. Long, and A. Gururajan, "Customized Hough transform for robust segmentation of cervical vertebrae from X-ray images," in *Proceedings Fifth IEEE Southwest Symposium on Image Analysis and Interpretation*, 2002, pp. 224–228.

[43] J. Carballido-Gamio, S. J. Belongie, S. Majumdar, "Normalized cuts in 3-D for spinal MRI segmentation," *IEEE transactions on medical imaging*, vol. 23, no. 1, pp. 36–44, 2004.

[44] Z. Peng, J. Zhong, W. Wee, and J. Lee, "Automated vertebra detection and segmentation from the whole spine MR images," in *2005 IEEE Engineering in Medicine and Biology 27th Annual Conference*, 2006, pp. 2527–2530.

[45] X. Xu, D.-J. Lee, S. Antani, and L. R. Long, "A spine X-ray image retrieval system using partial shape matching," *IEEE Transactions on Information Technology in Biomedicine*, vol. 12, no. 1, pp. 100–108, 2008.

[46] M. Benjelloun and S. Mahmoudi, "Spine localization in X-ray images using interest point detection," *Journal of digital imaging*, vol. 22, no. 3, pp. 309–318, 2009.

[47] T. Klinder, J. Ostermann, M. Ehm, A. Franz, R. Kneser, and C. Lorenz, "Automated model-based vertebra detection, identification, and segmentation in CT images," *Medical image analysis*, vol. 13, no. 3, pp. 471–482, 2009.

[48] E. A. Ribeiro, M. H. Nogueira-Barbosa, R. M. Rangayyan, and P. M. Azevedo-Marques, "Detection of vertebral plateaus in lateral lumbar spinal X-ray images with Gabor filters," in *2010 Annual International Conference of the IEEE Engineering in Medicine and Biology*, 2010, pp. 4052–4055.

[49] M. A. Larhmam, S. Mahmoudi, and M. Benjelloun, "Semi-automatic detection of cervical vertebrae in X-ray images using generalized Hough transform," in *2012 3rd International Conference on Image Processing Theory, Tools and Applications (IPTA)*, 2012, pp. 396–401.

[50] A. Rasoulian, R. Rohling, and P. Abolmaesumi, "Lumbar spine segmentation using a statistical multi-vertebrae anatomical shape+ pose model," *IEEE transactions on medical imaging*, vol. 32, no. 10, pp. 1890–1900, 2013.

[51] R. Korez, B. Likar, F. Pernuš, and T. Vrtovec, "Model-based segmentation of vertebral bodies from MR images with 3D CNNs," *International conference on medical image computing and computer-assisted intervention*, 2016, pp. 433–441.

[52] A. Arif, M. Rehman, K. Knapp, and G. Slabaugh, "Fully automatic cervical vertebrae segmentation framework for X-ray images," *Computer methods and programs in biomedicine*, vol. 157, pp. 95–111, 2018.

[53] D. Shi, Y. Pan, C. Liu, Y. Wang, D. Cui, and Y. Lu, "Automatic localization and segmentation of vertebral bodies in 3d CT volumes with deep learning," in *Proceedings of the 2nd International Symposium on Image Computing and Digital Medicine*, 2018, pp. 42–46.

[54] J. T. Lu *et al.*, "Deepspine: Automated lumbar vertebral segmentation, disc-level designation, and spinal stenosis grading using deep learning," *arXiv preprint arXiv:1807.10215*, 2018.

[55] A. K. Davison, C. Lindner, D. C. Perry, W. Luo, T. F. Cootes, and others, "Landmark localisation in radiographs using weighted heatmap displacement voting," in *International Workshop on Computational Methods and Clinical Applications in Musculoskeletal Imaging*, 2018, pp. 73–85.

[56] S. Kim, W. C. Bae, K. Masuda, C. B. Chung, and D. Hwang, "Semi-automatic segmentation of vertebral bodies in MR images of human lumbar spines," *Applied Sciences*, vol. 8, no. 9, p. 1586, 2018.

[57] F. Rehman, S. I. A. Shah, M. N. Riaz, S. O. Gilani, and R. Faiza, "A Region-Based Deep Level Set Formulation for Vertebral Bone Segmentation of Osteoporotic Fractures," *Journal of digital imaging*, vol. 33, no. 1, pp. 191–203, 2020.

[58] C. H. Chuang *et al.*, "Efficient Triple Output Network for Vertebral Segmentation and Identification," *IEEE Access*, vol. 7, pp. 117978–117985, 2019.

[59] N. Lessmann, B. van Ginneken, P. A. de Jong, and I. Išgum, "Iterative fully convolutional neural networks for automatic vertebra segmentation and identification," *Medical image analysis*, vol. 53, pp. 142–155, 2019.

[60] Y. Chen, Y. Gao, K. Li, L. Zhao, and J. Zhao, "vertebrae identification and localization utilizing fully convolutional networks and a hidden Markov model," *IEEE transactions on medical imaging*, vol. 39, no. 2, pp. 387–399, 2019.

[61] H. Liebl, D. Schinz, A. Sekuboyina, L. Malagutti, M. T. Löffler, A. Bayat, M. E. Husseini, G. Tetteh, K. Grau, E. Niederreiter et al., "A computed tomography vertebral segmentation dataset

with anatomical variations and multi-vendor scanner data," arXiv preprint arXiv:2103.06360, 2021.

[62] S. Liang, H. Liu, C. Chen, C. Qin, F. Yang, Y. Feng, and Z. Lin, "Research on multi-path dense networks for mri spinal segmentation," Plosone, vol. 16, no. 3, p. e0248303, 2021.

[63] J. Liu, C. Yuan, X. Sun, L. Sun, H. Dong, and Y. Peng, "The measurement of cobb angle based on spine x-ray images using multi-scale convolutional neural network," Physical and Engineering Sciences in Medicine, pp. 1–13, 2021.

[64] H. Anitha and G. K. Prabhu, "Automatic quantification of spinal curvature in scoliotic radiograph using image processing," Journal of medical systems, vol. 36, no. 3, pp. 1943–1951, 2012.

[65] T. A. Sardjono, M. H. F. Wilkinson, A. G. Veldhuizen, P. M. A. van Ooijen, K. E. Purnama, and G. J. Verkerke, "Automatic Cobb angle determination from radiographic images," Spine, vol. 38, no. 20, pp. E1256–E1262, 2013.

[66] Andrei C. Jalba, Michael HF Wilkinson, and Jos BTM Roerdink. "CPM: A deformable model for shape recovery and segmentation based on charged particles." IEEE Transactions on Pattern Analysis and Machine Intelligence 26, no. 10 (2004): 1320-1335.

[67] S. Pasha, P. Hassanzadeh, M. Ecker, and V. Ho, "A hierarchical classification of adolescent idiopathic scoliosis: Identifying the distinguishing features in 3D spinal deformities," PloS one, vol. 14, no. 3, p. e0213406, 2019.

[68] A. Jimenez-Pastor *et al.*, "Automated vertebrae localization and identification by decision forests and image-based refinement on real-world CT data," *La radiologia medica*, vol. 125, no. 1, pp. 48–56, 2020.

[69] C. Vergari, W. Skalli, and L. Gajny, "A convolutional neural network to detect scoliosis treatment in radiographs," *International Journal of Computer Assisted Radiology and Surgery*, pp. 1–6, 2020.

[70] B. Adhi Kusuma, "Determination of spinal curvature from scoliosis X-ray images using K-means and curve fitting for early detection of scoliosis disease." In 2017 2nd International conferences on Information Technology, Information Systems and Electrical Engineering (ICITISEE), pp. 159-164. IEEE, 2017.

[71] Y. Pan, Q. Chen, T. Chen, H. Wang, X. Zhu, Z. Fang, and Y. Lu. "Evaluation of a computer-aided method for measuring the Cobb angle on chest X-rays." European Spine Journal 28, no. 12 (2019): 3035-3043.

[72] A. Safari, H. Parsaei, A. Zamani, and B. Pourabbas. "A semi-automatic algorithm for estimating cobb angle." Journal of biomedical physics & engineering 9, no. 3 (2019): 317.

[73] B. Chen, Qiuhao Xu, Liansheng Wang, Stephanie Leung, Jonathan Chung, and Shuo Li. "An automated and accurate spine curve analysis system." IEEE Access 7 (2019): 124596-124605.

[74] R. H. Alharbi Meshal, B. Alshaye, Maryam M. Alkanhal, Najla M. Alharbi, Mosa A. Alzahrani, and Osama A. Alrehaili. "Deep Learning Based Algorithm for Automatic Scoliosis Angle Measurement." *In 2020 3rd International Conference on Computer Applications & Information Security (ICCAIS)*, pp. 1-5. IEEE, 2020.

[75] J. Liu, C. Yuan, X. Sun, Lechan Sun, Hua Dong, and Yun Peng. "The measurement of Cobb angle based on spine X-ray images using multi-scale convolutional neural network." Physical and Engineering Sciences in Medicine (2021): 1-13.

[76] C. Zhang, Jun Wang, Jian He, Peng Gao, and Guotong Xie. "Automated vertebral landmarks and spinal curvature estimation using non-directional part affinity fields." Neurocomputing 438 (2021): 280-289.

[77] J-L Cui, De-Dong Gao, Sheng-Jun Shen, Lin-Ze Wang, and Yan Zhao. "Cobb Angle Measurement Method of Scoliosis Based on U-net Network." (2021).

[78] L. Wang, Cong Xie, Yi Lin, Hong-Yu Zhou, Kailin Chen, Dalong Cheng, Florian Dubost et al. "Evaluation and Comparison of Accurate Automated Spinal Curvature Estimation Algorithms with Spinal Anterior-posterior X-Ray Images: The AASCE19 Challenge." Medical Image Analysis (2021): 102115.

[79] J. Yao, J. Burns, S. Getty, J. Stieger, R. Summers "SpineWeb Collaborative Platform for Research on Spine Imaging and Image Analysis. [Online]. Available http://spineweb.digitalimaginggroup.ca/Index.php?n=Main.Datasets#Dataset_13.3A_xVertSeg_-_Segmentation_and_Classification_of_Fractured_Vertebrae

[80] Accurate Automated Spinal Curvature Estimation MICCAI 2019 Challenge Dataset," AASCE19. [Online]. Available: https://aasce19.github.io/#challenge-dataset

[81] S. Sudirman, A. Al Kafri, F. Natalia, H. Meidia, N. Afriliana, W. Al-Rashdan, M. Bashtawi, and M. Al-Jumaily, Lumbar Spine MRI Dataset," Mendeley's Data, vol. 2, 2019. [Online]. Available: https://data.mendeley.com/datasets/k57fr854j2/2

[82] R. Farhat Masood, H. Taimur, I. Ahmad Taj, M. Asad Qureshi, M. Babar Khan, (2021), \Composite Dataset of Lumbar Spine Mid-Sagittal Images with Annotations and Clinically Relevant Spinal Measurements", Mendeley's Data, V2, doi: 10.17632/k3b363f3vz.2

[83] J. Redmon, S. Divvala, R. Girshick, and A. Farhadi, "You only look once: Unified, real-time object detection," in Proceedings of the IEEE conference on computer vision and pattern recognition, 2016, pp. 779–788.

[84] G. Jocher, K. Nishimura, T. Mineeva, and R. Vilariño, "Yolov5," Coderepository https://github.com/ultralytics/yolov5, 2020.

[85] Huang, Ren-You, Lan-Rong Dung, Cheng-Fa Chu, and Yin-Yi Wu. "Noise removal and contrast enhancement for x-ray images." Journal of Biomedical Engineering and Medical Imaging 3, no. 1 (2016): 56.

[86] S. Ren, K. He, R. Girshick, and J. Sun, "Faster r-cnn: Towards real-time object detection with region proposal networks," Advances in neuralinformation processing systems, vol. 28, pp. 91–99, 2015.

[87] H. Jung, B. Lodhi, and J. Kang. "An automatic nuclei segmentation method based on deep convolutional neural networks for histopathology images." BMC Biomedical Engineering 1, no. 1 (2019): 1-12.

[88] O. Ronneberger, P. Fischer, and T. Brox, "U-net: Convolutional networks for biomedical image segmentation," in International Conference on Medical image computing and computer-assisted intervention. Springer, 2015, pp. 234–241.

[89] J. Long, E. Shelhamer, and T. Darrell, "Fully convolutional networks for semantic segmentation," in Proceedings of the IEEE conference on computer vision and pattern recognition, 2015, pp. 3431–3440

[90] V. Badrinarayanan, A. Kendall, and R. Cipolla. "Segnet: A deep convolutional encoder-decoder architecture for image segmentation." IEEE transactions on pattern analysis and machine intelligence 39, no. 12 (2017): 2481-2495.

[91] J. Fatima, M. Mohsan, A. Jameel, M. Usman Akram, and A. Muzaffar Syed. "Vertebrae localization and spine segmentation on radiographic images for feature-based curvature classification for scoliosis." Concurrency and Computation: Practice and Experience: e7300. (IF: 1.831)

[92] Musculoskeletal Key, "*Posture Analysis in Patients with Spinal Osteoporosis*", Online [https://musculoskeletalkey.com/posture-analysis-in-patients-with-spinal-osteoporosis/]

[93] Unknown, "*2016 A bit on spine mobility from different prespectives*.", Online [https://www.somamovementstudio.com/blog/2016/5/30/nerdilates-a-bit-on-spine-mobility-from-different-perspectives] Accessed: 2019-05-01

[94] S. A. Voutsinas, and G. Dean MacEwen. "Sagittal profiles of the spine." Clinical Orthopaedics and related research 210 (1986): 235-242.

[95] Unknown, "Cobb Angle Measurement", Online [https://scoliosis3dc.com/scoliosis-resources/cobb-angle-measurement/] Accessed: 2019-05-01

[96] Saining Xie, and Zhuowen Tu. "Holistically-nested edge detection." In Proceedings of the IEEE inter-national conference on computer vision, pp. 1395-1403. 2015.

[97] Chris Harris and Mike Stephens. "A combined corner and edge detector." In Alvey vision conference, vol. 15, no. 50, pp. 10-5244. 1988.

[98] A. Ishihara, "Roentgenographic studies on the normal pattern of the cervical curvature." Nihon seikeigeka gakkai zasshi 42, no. 11 (1968): 1033-1044.

[99] Y-L Chen, "Vertebral centroid measurement of lumbar lordosis compared with the Cobb technique." Spine 24, no. 17 (1999): 1786.

[100] D. E. Harrison, R. Cailliet, D. D. Harrison, T. J. Janik, and B. Holland. "Reliability of centroid, Cobb, and Harrison posterior tangent methods: which to choose for analysis of thoracic kyphosis." Spine 26, no. 11 (2001): e227-e234.

[101] B. P. Yang, C. W. Yang, and S. L. Ondra. "A novel mathematical model of the sagittal spine." Spine 32, no. 4 (2007): 466-470.

[102] J. Fatima, A. Jameel, M. Usman Akram, A. Muzaffar Syed, and M. Mushtaq. "Automatic Localization and Segmentation of Vertebrae for Cobb Estimation and Curvature Deformity." INTELLIGENT AUTOMATION AND SOFT COMPUTING 34, no. 3 (2022): 1489-1504. (IF: 3.401)

[103] R. F. Masood, I. A. Taj, M. B. Khan, M. A. Qureshi, and T. Hassan. "Deep Learning based Vertebral Body Segmentation with Extraction of Spinal Measurements and Disorder Disease Classification." Biomedical Signal Processing and Control 71 (2022): 103230.

Appendix A

Publications

Journal Publication

i) **Joddat Fatima,** Mashood Mohsan, Amina Jameel, Muhammad Usman Akram, and Adeel Muzaffar Syed. "Vertebrae localization and spine segmentation on radiographic images for feature-based curvature classification for scoliosis." *Concurrency and Computation: Practice and Experience:* e7300**. (IF: 1.831)**

ii) Malaika Mushtaq, Muhammad Usman Akram, Norah Saleh Alghamdi, **Joddat Fatima**, and Rao Farhat Masood. "Localization and Edge-Based Segmentation of Lumbar Spine Vertebrae to Identify the Deformities Using Deep Learning Models." Sensors 22, no. 4 (2022): 1547. **(IF: 3.576)**

iii) **Fatima, Joddat,** Amina Jameel, Muhammad Usman Akram, Adeel Muzaffar Syed, and Malaika Mushtaq. "Automatic Localization and Segmentation of Vertebrae for Cobb Estimation and Curvature Deformity." *INTELLIGENT AUTOMATION AND SOFT COMPUTING* 34, no. 3 (2022): 1489-1504. **(IF: 3.401)**

iv) **Joddat Fatima,** Muhammad Usman Akram, Amina Jameel, and Adeel Muzaffar Syed. "Spinal vertebrae localization and analysis on disproportionality in curvature using radiography—a comprehensive review." *EURASIP Journal on Image and Video Processing 2021*, no. 1 (2021): 1-23. **(IF: 1.789)**

Conference Publications

i) **Joddat Fatima**, Amina Jameel and M. Usman Akram, "Imaging Modalities for Vertebrae Segmentation and Spinal Deformity Diagnosis: A Review", 5th International Conference on Communication and Computer Engineering from 17 – 19 July 2018 in Melaka, Malaysia

ii) **Joddat Fatima,** Mashood M. Mohsan, Muhammad Umair Qaisar, Muhammad Hamza, Muhammad Zeshan Tahir, and Ghazzal Zaman. "Handcrafted and Deep features based Classification of Scoliosis." In 2022 2nd International Conference on Digital Futures and Transformative Technologies (ICoDT2), pp. 1-6. IEEE, 2022. (BEST PAPER AWARD)

Appendix B

CSI 2016

The 4th International Workshop and Challenge on Computational Methods and Clinical Applications for Spine Imaging is a scientific event focused on the intersection of computer science, medical imaging, and spine health. The workshop and challenge provide a platform for researchers and clinicians to exchange ideas and present their latest research findings on computational methods and clinical applications for spine imaging. The event typically includes keynote lectures, technical presentations, and a challenge competition. The challenge competition involves participants using computational methods to develop algorithms that can automatically detect and quantify spine abnormalities in medical images. The competition provides a platform for researchers to evaluate and compare the performance of their algorithms against those of their peers. The workshop and challenge are aimed at researchers, clinicians, and students working in the fields of computer science, medical imaging, and spine health. The event provides an opportunity for attendees to learn about the latest research developments in the field, exchange ideas, and establish new collaborations.

Contact information: Robert Korez (Robert.korez@fe.uni-lj.si) or Tomaž Vrtovec (tomaz.vrtovec@fe.uni-lj.si) Laboratory of Imaging Technologies University of Ljubljana, Faculty of Electrical Engineering, Slovenia Official website: http://lit.fe.uni-lj.si

AASCE 2019

The MICCAI 2019 Challenge from x-ray images was a scientific challenge organized as part of the Medical Image Computing and Computer Assisted Intervention (MICCAI) conference held in 2019. The challenge aimed to investigate the development of algorithms for semi-automated spine curvature estimation. The challenge alo provide a standard assessment framework using a dataset of x-ray images. The challenge focused on developing algorithms that can accurately estimate the curvature of the spine from X-ray images and correct for any errors that may be present. The nature of such compiition is significant and important for the timely diagnosis and treatment planning of spinal deformities such as scoliosis. This can have a significant impact on a patient's quality of life. Participants in the challenge were provided with a set of training and test images, along with ground truth annotations of the spinal curvature. They were required to develop algorithms that could accurately estimate the spinal curvature and correct for any errors, and were evaluated based on various performance metrics, such as the mean absolute error and the root mean squared error. The challenge provided a valuable opportunity for researchers and practitioners in the field

of medical imaging to collaborate and develop new algorithms and techniques for the accurate and automated estimation of spinal curvature from X-ray images. With the help of from London Health Sciences Center in Canada, in total of 707 spinal anterior-posterior x-ray images for training and testing were collected using EOS medical imaging system.

Organizer were Shuo Li (slishuo@gmail.com), Western University, ON, Canada and Wang (lswang@xmu.edu.cn), Xiamen University, China Dataset is available on the SpineWeb (http://spineweb.digitalimaginggroup.ca/ , Dataset 16)

Mendeley 2019

The third open-access dataset used in our study, having 515 Lumbar Spine MRI scans collected from patients with symptomatic back pain. They have confirmed that all procedures performed are in accordance with the ethical standards of both the United Kingdom and the Kingdom of Jordan and comply with the 1964 Helsinki declaration and its later amendments. The second version of dataset was published in: 3 April 2019 and the contributors are Sud Sudirman, Ala Al Kafri, Friska Natalia, Hira Meidia, Nunik Afriliana, Wasfi Al-Rashdan, Mohammad Bashtawi, Mohammed Al-Jumaily. The Mendeley 2019 Lumbar Spine MRI dataset is a collection of T2-weighted MRI images of the lumbar spine, consisting of 515 cases. The dataset was made publicly available through the Mendeley Data repository in 2019, and it is intended for use in the development and evaluation of algorithms for the automated segmentation of spinal structures. The images were acquired using various protocols and machines, resulting in a diverse set of images with variations in image quality, contrast, and resolution. The dataset includes both sagittal and axial views of the lumbar spine, with each case consisting of multiple slices. The dataset also includes ground truth annotations of the spinal structures, such as the vertebral bodies, intervertebral discs, and spinal canal, which were manually segmented by expert radiologists. These annotations are provided in separate binary masks, one for each structure. The Mendeley 2019 Lumbar Spine MRI dataset is a valuable resource for researchers and practitioners in the field of medical imaging who are interested in developing and evaluating algorithms for the automated segmentation of spinal structures from MRI images. It provides a large and diverse set of images and annotations, allowing for the development and testing of algorithms under various conditions. The data is anonymized and is provided as is. A DICOM viewer maybe necessary to view this dataset. Available at: http://dx.doi.org/10.17632/s6bgczr8s2.2

Appendix C

BIOMISA LAB

In 2013 the BioMedical Image and Signal Analysis (BIOMISA) research group was formed in the Department of Computer and Software Engineering, National University of Sciences and Technology (NUST) College of EME, located in Rawalpindi, Pakistan. The research areas targeted in this lab are: bio-medical signal processing, medical imaging, data analytics, biometrics, artificial intelligence, machine learning & deep learning. The group's research focuses on the development and application of advanced signal and image processing techniques for biomedical applications, including medical image analysis, computer-aided diagnosis, and the analysis of physiological signals such as electroencephalography (EEG) and electrocardiography (ECG). The group also collaborates with clinicians and researchers in the field of medicine to develop innovative solutions to real-world biomedical problems.

Salient Projects Completed:

Some of the projects completed by or lab are:

- EKKO (NEUROTRANSMISSION COGNITIVE THEORY)

The device was developed as a low-cost, portable alternative to traditional echocardiography machines, which can be expensive and require specialized training to operate. The Ekko device was specifically designed to address the lack of access to medical imaging technology in many resource-limited settings, particularly in rural and underserved areas. The device uses artificial intelligence algorithms to generate real-time 2D and 3D images of the heart, allowing healthcare providers to diagnose and monitor various cardiac conditions. Ekko device has received recognition and support from various organizations, including the World Health Organization and the Bill & Melinda Gates Foundation, which provided funding for further development and distribution of the device.

- OCT Image Analysis System for Grading and Diagnosis of Retinal Diseases and its Integration in i-Hospital

Optical coherence tomography (OCT) is a non-invasive imaging technique that uses light waves to generate high-resolution images of the retina, allowing for the early detection and diagnosis of various retinal diseases. However, interpreting and analysing OCT images can be challenging, and requires specialized training and expertise. It is an automated OCT image

analysis system that uses machine learning algorithms to grade and diagnose retinal diseases, such as age-related macular degeneration, diabetic retinopathy, and glaucoma. The system was integrated into a web-based platform called i-Hospital, which allows ophthalmologists to remotely access and analyse patient data, improving the efficiency and accuracy of diagnosis and treatment.

- AL-BASR

It is designed to represent data that accurately captures the state of patient at all times. It is basically an EHR (Electronic Patient Health Record) System that allows to view an entire history of patient. The system is designed to provide a centralized repository for patient health information, allowing healthcare providers to quickly access and share critical data such as medical history, medications, test results, and other relevant information. This system improves the accuracy and efficiency of clinical decision-making, reduce errors and duplication, and enhance the overall quality of care.

- Net-Enabled Retinal Image Analysis its Integration in i-telemedicine system

This project focused on using telemedicine to improve access to eye care, particularly for people living in remote or underserved areas. Net-Enabled Retinal imaging is an important tool for diagnosing and monitoring eye diseases, and telemedicine platforms can potentially enable healthcare providers to remotely access and analyse retinal images, reducing the need for patients to travel to specialized clinics or hospitals.

- Smart-Steth

Smart Steth is combined with a digital stethMic and an android application for diagnosis of Pneumonia. The Smart-Steth device is designed to capture and amplify lung sounds, which can then be analysed by the accompanying Android app to detect signs of pneumonia or other respiratory conditions. By using an air coupled sensor which convert the analog voice signal into digital with advanced signal processing algorithms. Smart-Steth system aims to provide a more accurate and reliable diagnosis of pneumonia compared to traditional auscultation methods.

- Decision Support System for Detection of Glaucoma using Structural and Non Structural Features

  According to estimates from the International Agency for the Prevention of Blindness (IAPB), glaucoma is the second leading cause of blindness in Pakistan, accounting for approximately 16% of all cases of blindness in the country. This project was created to identify early detection of glaucoma. The project was ajoint effort in alliance with Armed Forces institute of Ophthalmology (AFIO). They supported us in data collection annotation and labelling, even trials and validity of algorithms were also conducted by them. The system is designed to be used as a decision support tool for eye care professionals, providing them with objective data and analysis to aid in the diagnosis and management of glaucoma.

Lab Collaborators:

The research group has different academic and industrial collaborators.

Academic Collaborators:

- College of Electrical & Mechanical Engineering
- Center for Advanced Studies in Engineering
- Bahria University

Industrial Collaborators

- Center for Advanced Research in Engineering
- Shifa International Hospital
- Armed Forces Institute of Ophthalmology
- Armed Forces Institute of Radiology & Imaging

With collaborative team of BIOMISA lab in EME College and Dr Muhammad Talha, Consultant Spinal Surgeon and Dr Muhammad Babar Khan Consultant Radiologist at Combined Military Hospital, Rawalpindi assisted us for data annotation and labelling. The Tools used for data annotations and labelling are:

Roboflow:

Roboflow is a computer vision and machine learning platform that allows users to build, train, and deploy computer vision models for a wide range of applications. The platform provides tools and resources to streamline the data preparation process, allowing users to efficiently label and annotate image data, and

transform data into machine-readable formats that can be used to train computer vision models. Roboflow offers support for a variety of popular computer vision frameworks such as TensorFlow, PyTorch, and Keras, and provides pre-built models for common use cases such as object detection, image classification, and segmentation. Roboflow offers a variety of dataset annotation options to help users create high-quality training data for their computer vision models. These annotation options include:

- Bounding Boxes: Users can add bounding boxes around objects in their images to indicate the location of the objects. Bounding boxes are commonly used for object detection and localization tasks.
- Image Segmentation Masks: Users can manually segment objects in their images by creating pixel-level masks. Image segmentation is commonly used for tasks such as semantic segmentation and instance segmentation.
- Keypoints: Users can annotate specific points on objects in their images, such as the corners of a box or the joints of a person. Keypoints are commonly used for pose estimation and human pose estimation.
- Landmarks: Users can annotate specific landmarks on objects in their images, such as the eyes, nose, and mouth on a face. Landmarks are commonly used for facial recognition and tracking.
- Polylines: Users can draw lines or curves around objects in their images. Polylines are commonly used for tasks such as object tracking and boundary detection.

Roboflow also offers automated annotation options, such as object detection and instance segmentation, which can help to speed up the annotation process and reduce the amount of manual labour required.

LabelImg:

LabelImg is an open-source graphical image annotation tool used for object detection and image segmentation tasks in computer vision. It allows users to manually label objects in images with bounding boxes or segmentation masks, which can be used to train machine learning models for object detection or segmentation tasks. LabelImg supports a variety of image formats such as JPEG, PNG, BMP, and TIFF, and allows users to create custom classes and labels for objects in their images. It also offers features such as zooming, panning, and image flipping to make the annotation process more efficient and accurate. However, in general, LabelImg can be used to annotate various types of images including medical images like spine X-rays, CT scans, or MRIs. To use LabelImg for annotating spine images, you would first need to prepare your image dataset, load the images into LabelImg, and create bounding boxes around the

relevant objects of interest (such as vertebral bodies or intervertebral discs). You can then save the annotations in a format compatible with your machine learning framework or library of choice, such as YOLO, TensorFlow Object Detection API, or PyTorch. It is worth noting that annotating medical images can be a challenging task, as the images may contain complex structures and artifacts that can affect the accuracy of the annotation. Therefore, it is important to ensure that the annotations are validated and of high quality before using them to train machine learning models.

Adobe Illustrator:

Adobe Illustrator is a vector graphics software that can be used for a wide range of tasks, including labelling and annotating spine datasets for machine learning applications. Spine datasets are often used in computer vision applications for tasks such as human pose estimation, motion capture, and gait analysis. To label spine datasets in Adobe Illustrator, you can create a new file for each image in the dataset and use the drawing tools to annotate the spine. You can use different shapes and colours to differentiate between different parts of the spine, such as the vertebrae, discs, and nerves. You can also add labels or text to describe the different parts of the spine. Once you have labelled all the images in your spine dataset, you can export the annotations as a JSON or XML file, which can be used to train machine learning models for spine-related tasks. Adobe Illustrator offers many advanced features that can be useful for labelling and annotating spine datasets, such as layers, grouping, and alignment tools, which can help you create accurate and consistent annotations across your dataset. Additionally, you can create custom brushes, symbols, and patterns to speed up your workflow and make your annotations more visually appealing.

Python 3.9 Jupyter Notebook

Python 3.9 Jupyter Notebook is an interactive computing environment that allows users to create and share code, visualizations, and narrative text in a web browser. It is based on the open-source Jupyter project and provides an easy-to-use interface for working with Python 3.9 code. Jupyter Notebook allows users to write and execute Python code in individual cells, which can be run independently or together as a single notebook. It also provides a rich set of features such as code completion, syntax highlighting, and inline plotting, making it a popular choice for data science and machine learning workflows. With Python 3.9, users can take advantage of new language features such as improved type hints, faster performance, and enhanced debugging tools. Additionally, Jupyter Notebook provides seamless integration with popular data science libraries such as NumPy, Pandas, and Matplotlib, allowing users to easily analyse and visualize data. Here are the steps to install Python 3.9 and Jupyter Notebook:

- Go to the official Python website and download the Python 3.9 installer for your operating system.
- Run the installer and follow the instructions to complete the installation process.
- After installation, open a command prompt to type the initial command that will install Jupyter Notebook. The command is “ pip install jupyterlab “
- Once the installation is completed, launch Jupyter Notebook by typing the other command in the command prompt. The command is “ jupyter notebook”
- This will launch the Jupyter Notebook in your default web browser. From here, you can create new notebooks and start coding.
- To stop the Jupyter Notebook server, go back to the command prompt or terminal and press "Ctrl + C".
- That's it! You now have Python 3.9 and Jupyter Notebook installed on your system.

LAB Hardware Resources:

GPU was NIVIDA RTX 2070 with 8 GB RAM

The NVIDIA RTX 2070 is a graphics processing unit (GPU) with 8 GB of RAM. It is designed for use in gaming and professional applications that require high-performance computing capabilities. The RTX 2070 features the NVIDIA Turing architecture, which includes dedicated hardware for real-time ray tracing and artificial intelligence (AI) applications. It has a 1410 MHz base clock speed and a boost clock speed of up to 1620 MHz, making it capable of handling complex graphics-intensive tasks. The GPU also supports NVIDIA G-Sync technology, which synchronizes the display's refresh rate with the GPU's output to eliminate screen tearing and stuttering during gameplay. It has a power consumption of 175 watts and requires an 8-pin power connector for operation. NVIDIA RTX 2070 is a powerful GPU that is well-suited for a wide range of applications, including gaming, 3D rendering, video editing, and machine learning.

NVIDIA GeForce GTX 1060 with 6 GB RAM

The NVIDIA GeForce GTX 1060 is a graphics processing unit (GPU) with 6 GB of GDDR5 memory. It was released in 2016 and is designed for use in gaming and other graphics-intensive applications. The GTX 1060 features NVIDIA's Pascal architecture, which includes improvements in performance and power efficiency over previous generations. It has a base clock speed of 1506 MHz and a boost clock speed of up to 1708 MHz, making it capable of running most modern games at high settings. The GPU has a memory bandwidth of 192 GB/s and a memory speed of 8 Gbps, which allows it to quickly transfer data between

the GPU and the CPU. It has a power consumption of 120 watts and requires a 6-pin power connector for operation. NVIDIA GeForce GTX 1060 is a powerful mid-range GPU that offers excellent performance for gaming and other graphics-intensive applications. While it may not be able to handle the most demanding games at ultra-high settings, it is still capable of running most modern games at high or medium settings with good frame rates.